TECHNISCHE UNIVERSITÄT DRESDEN

HLD.

Direct Measurements
of the Magnetocaloric Effect
in Pulsed Magnetic Fields

Dissertation
zur Erlangung des akademischen Grades
Doctor of Philosophy
(Ph. D.)

vorgelegt von

Mahdiyeh Ghorbani-Zavareh
geboren am 21.03.1984 in Isfahan, Iran

Helmholtz-Zentrum Dresden-Rossendorf
Institut Hochfeld-Magnetlabor Dresden

Fachrichtung Physik
Fakultät Mathematik und Naturwissenschaften
der Technischen Universität Dresden
2016

Tag der Einreichung: 14.01.2016
Tag der Verteidigung: 23.05.2016

1. Gutachter: Prof. Dr. Joachim Wosnitza
2. Gutachter: Prof. Dr. Oliver Gutfleisch

To my parents,
my husband Ali,
my younger brother Hossein,
and my grandparents.

Abstract

The present thesis is devoted to the investigation of the magnetocaloric effect (MCE) by direct measurements in pulsed and quasi-static magnetic fields as well as by analyzing specific-heat data taken in static magnetic fields. The emphasis is on the direct measurement of the adiabatic temperature change ΔT_{ad} in pulsed magnetic fields, because the pulsed-field data allow for an analysis of the sample-temperature response to the magnetic field on a time scale of ~ 10 to 100 ms, which is on the order of typical operation frequencies ($10 - 100$ Hz) of magnetocaloric cooling devices. Besides extending the accessible magnetic-field range to beyond 70 T, the short pulse duration provides nearly adiabatic conditions during the measurement.

In this work, the magnetocaloric properties of various types of solids are investigated: Gadolinium (Gd) with a second-order transition, $Ni_{50}Mn_{35}In_{15}$ with multiple magnetic transitions, and $La(Fe,Si,Co)_{13}$ compounds with first- and second-order transitions, depending on the Co concentration.

The adiabatic temperature change of a polycrystalline Gd sample has been measured in pulsed magnetic fields up to 70 T and also in quasi-static fields up to 2 T. A very large adiabatic temperature change of $\Delta T_{ad} \approx 60$ K is observed near the Curie temperature ($T_C = 294$ K) for a field change of 70 T. In addition, we find that this maximum temperature change grows with $H^{2/3}$.

We have studied the MCE in the shape-memory Heusler alloy $Ni_{50}Mn_{35}In_{15}$ by direct measurements in pulsed magnetic fields up to 6 and 20 T. The results obtained for 6 T pulses are compared with data extracted from specific-heat experiments. We find a saturation of the inverse MCE, related to the first-order martensitic transition, with a maximum adiabatic temperature change of $\Delta T_{ad} = -7$ K at 250 K and a conventional field-dependent MCE near the second-order ferromagnetic transition in the austenitic phase. Our results disclose that in shape-memory alloys the different contributions to the MCE and hysteresis effects around the martensitic transition have to be carefully considered for future cooling applications.

Finally, a comparative study of the magnetic and magnetocaloric properties of $La(Fe,Si,Co)_{13}$ alloys is presented by discussing magnetization, ΔT_{ad}, specific-heat, and magnetostriction measurements. The nature of the transition can be

changed from first to second order as well as the temperature of the transition can be tuned by varying the Co concentration. The MCE of two samples with nominal compositions of $LaFe_{11.74}Co_{0.13}Si_{1.13}$ and $LaFe_{11.21}Co_{0.65}Si_{1.11}$ have been measured in pulsed magnetic fields up to 50 T. We find that $LaFe_{11.74}Co_{0.13}Si_{1.13}$ with a first-order transition ($T_C = 198$ K) shows half of the net MCE already at low fields ($2 - 10$ T). Whereas the MCE of $LaFe_{11.21}Co_{0.65}Si_{1.11}$ with second-order transition ($T_C = 257$ K) grows gradually. The MCE in both compounds reaches almost similar values at a field of 50 T. The MCE results obtained in pulsed magnetic fields of 2 T are in good agreement with data from quasi-static field measurements. The pulsed-field magnetization of both compounds has been measured in fields up to 60 T under nearly adiabatic conditions and compared to steady-field isothermal measurements. The differences between the magnetization curves obtained under isothermal and adiabatic conditions give the MCE via the crossing points of the adiabatic curve with the set of isothermal curves. For $LaFe_{11.74}Co_{0.13}Si_{1.13}$, a $S - T$ diagram has been constructed from specific-heat measurements in static fields, which is used to extract the MCE indirectly. Magnetostriction measurements are carried out for two compounds in both static and pulsed magnetic fields. For $LaFe_{11.74}Co_{0.13}Si_{1.13}$, the strain shows a sharp increase. However, due to cracks appearing in the sample an irreversible magneto-volume effect of about 1% is observed in pulsed magnetic fields. Whereas for $LaFe_{11.21}Co_{0.65}Si_{1.11}$ the data show a smooth increase of the sample length up to 60 T, and a 1.3% volume increase is obtained. We also find that magnetizing the latter sample in the paramagnetic state is tightly bound to the volume increase and this, likewise for the former sample, gives the main contribution to the entropy change.

Contents

1 Introduction

The magnetocaloric effect (MCE) is defined as the thermal response (heating or cooling) of a magnetic substance when a magnetic field is applied or removed. This phenomenon was discovered by the French and Swiss physicists Weiss and Piccard in nickel for which a heating effect of about 0.5 K/T was observed [1, 2]. In 1926, Debye [3] and 1927, Giauque [4] independently suggested that one should be able to achieve ultra-low temperatures using cooling via adiabatic demagnetization. In 1933, Giauque and MacDougall [5] put this idea in to practice and experimentally demonstrated the first operating adiabatic demagnetization refrigerator that reached 0.25 K. Giauque was awarded the Nobel Prize in physics for his work on magnetic refrigeration in 1949. Between 1933 and 1997, a number of advances in the utilization of the MCE for cooling were reported [6, 7, 8, 9]. However, two significant breakthroughs happened in 1997. The first one was a notable achievement by Zimm *et al.* [10], who proved magnetic refrigeration is a viable and competitive cooling technology in the region near room temperature with potential energy savings of up to 30%. The second one was the discovery of the giant MCE in $Gd_5(Si_2Ge_2)$ [11]. These two events attracted interest from scientists and companies worldwide who started developing new kinds of materials usable at room temperature and magnetic-refrigerator designs.

In the following, tremendous efforts have been made to find alternative technologies to replace the conventional gas-compression/expansion technique for cooling applications. Higher-efficiency cooling and environmental-friendly magnetic refrigeration based on the magnetocaloric effect have initiated intensive research activities. Besides its practical application, MCE studies can give an extra insight in the nature of magnetic phase transitions [8, 12].

So far, most MCE studies have been done by calculating the isothermal entropy change, ΔS_{iso}, based on indirect methods. However, for first-order phase

transitions with thermal and magnetic hysteresis, $|\Delta S_{iso}|$ easily could be overestimated, thus additional considerations should be applied [13]. Direct measurements, besides giving directly the adiabatic temperature change, ΔT_{ad}, which is one of the important parameters for magnetic refrigeration, are preferable and closer to the actual process used in applications. Nondestructive pulsed-field facilities have typical pulse lengths of $\sim$10 to a few 100 ms, which match the targeted operation frequency of magnetic refrigerators, $10-100$ Hz [14]. Besides extending the accessible magnetic field range to beyond 70 T, the short pulse duration provides nearly adiabatic conditions during the measurement. Thus, direct MCE measurements in pulsed magnetic fields provide the opportunity to investigate the dynamics of the MCE in a suitable frequency range.

The aim of this thesis was to precisely measure ΔT_{ad} in pulsed magnetic fields under actual process conditions used in applications. To achieve this aim, three different types of solids including gadolinium, $Ni_{50}Mn_{35}In_{15}$, $LaFe_{11.74}Co_{0.13}Si_{1.13}$, and $LaFe_{11.21}Co_{0.65}Si_{1.11}$ were investigated.

Gadolinium is the most common magnetocaloric material for magnetic refrigeration near room temperature. Gd transforms from the paramagnetic to the ferromagnetic state at T_C (between 289 and 295 K) with a second-order phase transition. Its magnetocaloric properties are rather good, $\Delta T_{ad} \approx 5.5$ K for a change of the applied magnetic field from 0 to 2 T. Although the implementation of Gd in commercial magnetic refrigeration devices is not expected, it is widely used as reference material when considering different magnetocaloric material candidates for a magnetic-refrigeration design. In this work, we study the MCE in a Gd sample by direct magnetocaloric measurements in pulsed and in static magnetic fields.

Heusler-type Ni-Mn-In magnetic shape-memory alloys are among the most interesting candidates with first-order magnetostructural transitions in terms of their magnetocaloric properties [15]. $Ni_{50}Mn_{35}In_{15}$ exhibits on cooling a paramagnetic to ferromagnetic transition around 315 K, followed by a first-order structural transition from a cubic high-temperature phase to a low-temperature monoclinic phase around 246 K, the so-called martensitic transition. A conventional MCE is observed around the ferromagnetic transition in the austenitic phase. Additionally, an inverse MCE is present around the martensitic first-order transition leading to a decrease in the sample temperature with increasing

field. In this work, we study the MCE in a $Ni_{50}Mn_{35}In_{15}$ sample by direct magnetocaloric measurements in pulsed magnetic fields and by analyzing specific-heat data taken in static magnetic fields.

Among the promising magnetocaloric materials, $La(Fe,Si)_{13}$-based compounds are most attractive candidates [16, 17, 18]. They show a large magnetocaloric effect and have been widely studied in quasi-static magnetic fields from the perspective of fundamental research and practical applications. The adiabatic temperature change ΔT_{ad} and the Curie temperature T_C of $La(Fe,Si)_{13}$ alloys can be widely adjusted by small additions of other elements such as H or Co. The addition of Co also alters the nature of the magnetic phase transition from first to second order. Therefore, it is of great interest to investigate the MCE dependence on alloying $LaFe_{13-x}Si_x$ showing a change in the nature of the transition. From this point of view, we investigated two compositions: $LaFe_{11.74}Co_{0.13}Si_{1.13}$ and $LaFe_{11.21}Co_{0.65}Si_{1.11}$. The first alloy demonstrates a very pronounced first-order transition at 198 K whereas the second one exhibits a second-order transition at 257 K. In this work, a comparative study of the magnetic and magnetocaloric properties of $LaFe_{11.74}Co_{0.13}Si_{1.13}$ and $LaFe_{11.21}Co_{0.65}Si_{1.11}$ is presented by measuring the magnetization, directly the MCE, and magneto-volume effects in both pulsed and static magnetic fields, as well as the specific heat in static fields.

The current thesis is organized as follows: In chapter 2, I first review some theoretical aspects of the MCE, different ways (direct and indirect) to determine the MCE, as well as properties of magnetic refrigeration and promising magnetocaloric materials for future applications. This is followed by a detailed experimental descriptions of magnetocaloric measurements techniques in pulsed fields and also a short overview of other experimental techniques used in this thesis, including magnetization, magnetostriction, and specific-heat measurements. Finally, the results and discussions for the samples considered in this research (i.e., gadolinium, $Ni_{50}Mn_{35}In_{15}$, $LaFe_{11.74}Co_{0.13}Si_{1.13}$, and $LaFe_{11.21}Co_{0.65}Si_{1.11}$) are presented in chapters 4, 5, 6, and 7, respectively.

2 Magnetocaloric effect

2.1 Thermodynamics of magnetocaloric materials

The physical origin of the MCE is the result of entropy changes arising from the coupling of the magnetic spin system of the solid to the applied magnetic field. In general, all magnetic materials exhibit magnetocaloric effects.

The total entropy, S_{tot}, of a magnetic material at constant pressure is the sum of the magnetic, S_M, lattice, S_{lat}, and electronic, S_{elec}, entropies,

$$S_{tot}(H,T) = S_M(H,T) + S_{lat}(H,T) + S_{elec}(H,T). \tag{2.1}$$

In most cases, the lattice and electronic entropies are basically independent of the magnetic field H (for magnetocaloric materials near room temperature), while the magnetic entropy strongly depends on H. As illustrated in Fig. 2.1, an applied field usually will tend to align the disordered magnetic moments and thus decrease the entropy of the magnetic system, $\Delta S_M < 0$. When the magnetic field is applied isothermally ($T = \text{const.}$), the total entropy decreases due to the reduction in the magnetic contribution, $\Delta S_{tot} < 0$. For an adiabatic process the total entropy of the system remains constant ($S_{tot} = \text{const.}$), so the combined lattice and electronic entropies must increase by $\Delta(S_{lat} + S_{elec}) = -\Delta S_M$ in order to fulfill the condition $\Delta S_{tot} = 0$. The increase of the lattice entropy causes the rise in temperature of the sample, $\Delta T_{ad} > 0$. Conversely, when the field is removed the spins tend to randomize, so the magnetic entropy increases and the lattice entropy and the sample temperature decrease. Therefore, both the adiabatic temperature change, ΔT_{ad}, and the isothermal magnetic entropy change, ΔS_M, are characteristic values of the MCE.

Isothermal process: $\Delta S_T = S(T, B) - S(T, 0) < 0$

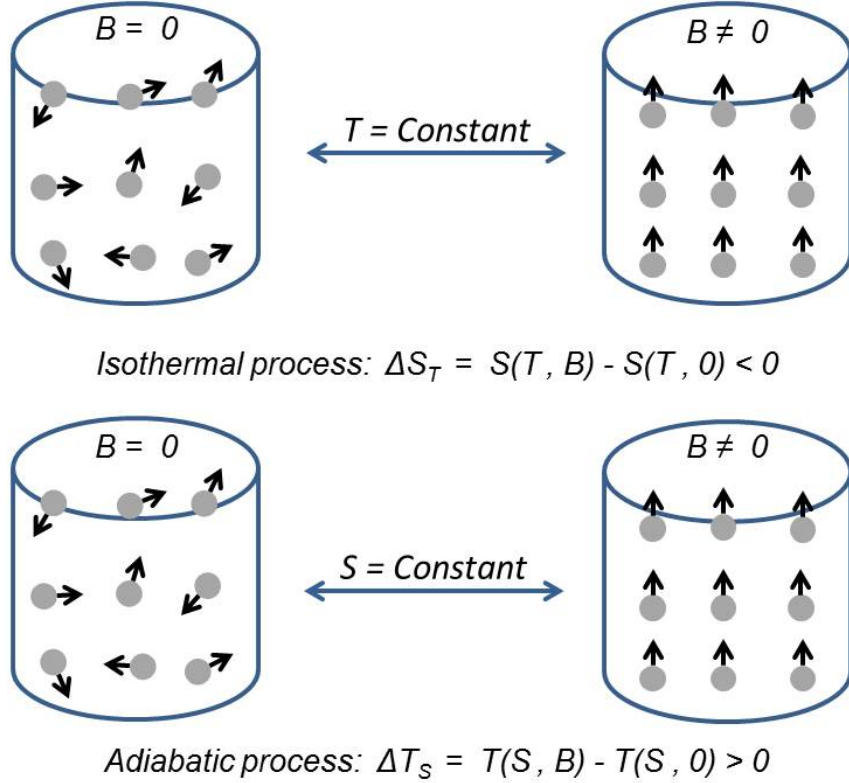Adiabatic process: $\Delta T_S = T(S, B) - T(S, 0) > 0$

Figure 2.1: *Schematic of the two basic processes of the magnetocaloric effect when a magnetic field is applied or removed in a paramagnetic system: the isothermal process ($T = const.$), which usually leads to a negative entropy change ΔS_M, and the adiabatic process ($S = const.$), which gives a positive change in temperature ΔT_{ad}. Taken from Ref. [19].*

Figure 2.2 illustrates the schematic of the thermodynamics of the MCE in a ferromagnet near its Curie temperature (T_C). The total entropy is shown for an applied magnetic field, H_1, and for zero field, H_0, together with the magnetic and non-magnetic (lattice and electronic) entropy parts separately.

In classical thermodynamics, a system (a phase) is characterized by a set of thermodynamic parameters associated with the system. These parameters include macroscopic properties, such as pressure (P), temperature (T), and Gibbs free energy (G). Let us consider what would happen if a certain amount of heat dQ is introduced to the system. The heat will not only increase the temperature of the system (i.e., increase its internal energy by dU) but will also
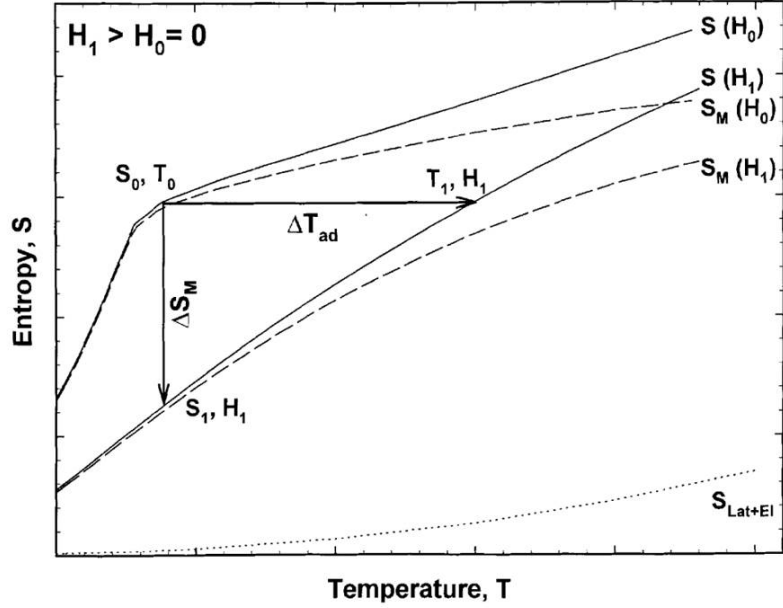
Figure 2.2: *The S-T diagram illustrating the MCE. Solid lines display the total entropy in two different magnetic fields ($H_0 = 0$ and $H_1 > 0$), dotted line shows the electronic and lattice contributions to the total entropy (non-magnetic), and dashed lines show the magnetic entropy in the two fields. The horizontal arrow shows ΔT_{ad} and the vertical arrow shows ΔS_M, when the magnetic field is varied from H_0 to H_1. Taken from Ref. [7].*

enable the system to perform some work, $dW = pdV$, on its environment and finally the magnetization may decrease due to the added heat, $-\mu_0 H dM$ [20].

Therefore, the thermodynamic state of the system is given by:

$$dQ = dU + pdV - \mu_0 H dM. \tag{2.2}$$

For a reversible process, the second law of thermodynamics says that

$$dQ = TdS, \tag{2.3}$$

and then by rearranging the terms in Eq. (2.2) and using Eq. (2.3) , the change in internal energy for a magnetic material is expressed by:

$$dU = TdS - pdV + \mu_0 H dM. \tag{2.4}$$

Since the internal energy contains the term TdS and the entropy is a parameter difficult to control, it is more convenient to express the energy of the system in a form that uses parameters such as T, p, and H. Accordingly, the Gibbs free energy can be defined as:

$$G \equiv U + pV - TS - \mu_0 HM. \tag{2.5}$$

By taking the differential of Eq. (2.5) and inserting the internal energy, dU, from Eq. (2.4), the Gibbs free energy can be expressed as

$$\begin{aligned}
dG &= dU + pdV + Vdp - (TdS + SdT) - (\mu_0 HdM + \mu_0 MdH) \\
&= TdS - pdV + \mu_0 HdM + pdV + Vdp - TdS - SdT - \mu_0 HdM - \mu_0 MdH \\
&= -SdT + Vdp - \mu_0 MdH.
\end{aligned}$$

$$\tag{2.6}$$

Hence, we obtain

$$S = -\left(\frac{\partial G}{\partial T}\right)_{p,H} \tag{2.7}$$

and

$$M = -\frac{1}{\mu_0}\left(\frac{\partial G}{\partial H}\right)_{p,T}. \tag{2.8}$$

From an elementary theorem of calculus, two mixed second partial derivatives of G with respect to T and H are equal. So, the relation between the temperature derivative of the magnetization and the field derivative of the entropy is given by the Maxwell relation:

$$\begin{aligned}
\frac{1}{\mu_0}\left(\frac{\partial S}{\partial H}\right)_{p,T} &= -\frac{1}{\mu_0}\frac{\partial}{\partial H}\left(\frac{\partial G}{\partial T}\right)_{p,H} \\
&= -\frac{\partial}{\partial T}\left(\frac{1}{\mu_0}\frac{\partial G}{\partial H}\right)_{p} \\
&= \left(\frac{\partial M}{\partial T}\right)_{p,H}.
\end{aligned} \tag{2.9}$$

By integrating both sides and rearranging the terms in Eq. (2.9), the isothermal magnetic entropy change under varying magnetic field, $\Delta H = H_F - H_I$, is given by

$$\Delta S_M(T, \Delta H) = \mu_0 \int_{H_I}^{H_F} \left(\frac{\partial M}{\partial T} \right)_{p,H} dH. \tag{2.10}$$

This equation indicates that the magnetic entropy change is proportional to the derivative of the magnetization with respect to temperature at constant field and to the field variation.

The differential of the total entropy, $S_{tot}(H, T)$, can be written as

$$dS = \left(\frac{\partial S}{\partial T} \right)_{p,H} dT + \left(\frac{\partial S}{\partial H} \right)_{p,T} dH. \tag{2.11}$$

On the other hand, the heat capacity, C_x, where x is the constant parameter, is defined as

$$C_x = \left(\frac{\partial Q}{\partial T} \right)_x, \tag{2.12}$$

by using the second law of thermodynamics, $dQ = TdS$, the heat capacity can be represented as

$$C_x = T \left(\frac{\partial S}{\partial T} \right)_x. \tag{2.13}$$

Considering an adiabatic process ($dQ = TdS = 0$) and by using above Maxwell relation (Eq. (2.9)) and Eq. (2.13), the temperature change due to a change in magnetic field is expressed as

$$dT = -\mu_0 \frac{T}{C_{p,H}} \left(\frac{\partial M}{\partial T} \right)_{p,H} dH. \tag{2.14}$$

Now, the adiabatic temperature change is obtained by integrating Eq. (2.14), from the initial field H_I to the final field H_F

$$\Delta T_{ad}(T, \Delta H) = -\mu_0 \int_{H_I}^{H_F} \frac{T}{C_{p,H}} \left(\frac{\partial M}{\partial T} \right)_{p,H} dH. \tag{2.15}$$

By analyzing Eqs. (2.10) and (2.15), some general information about the behavior of the MCE in solids with a second-order phase transition can be achieved [7]:

➤ For both paramagnetic and simple ferromagnetic materials, the magnetization decreases at constant field with increasing temperature, i.e., $(\partial M/\partial T)_H < 0$. Thus for positive magnetic field change, $\Delta H > 0$, $\Delta T_{ad}(T, \Delta H)$ is positive while $\Delta S_M(T, \Delta H)$ is negative.

➤ For ferromagnetic materials, since $|(\partial M/\partial T)_H|$ is maximum at T_C, $|(\Delta S_M(T, \Delta H)|$ displays a peak at T_C.

➤ Although it is not straightforward from Eq. (2.15) (due to the heat capacity anomaly near T_C), $\Delta T_{ad}(T, \Delta H)$ in ferromagnets shows a peak at T_C. The MCE is gradually reduced both below and above T_C [21].

➤ For the same $|(\partial M/\partial T)_H|$, $\Delta T_{ad}(T, \Delta H)$ will be larger at higher temperatures and also when the heat capacity is lower.

➤ For paramagnetic materials, $\Delta T_{ad}(T, \Delta H)$ is considerable only at temperatures close to zero, when the small value of $|(\partial M/\partial T)_H|$ is compensated by a vanishing heat capacity.

It should be noted that certain magnetic systems show a stable ferromagnetic state with large net magnetization at high temperature and a stable anti-ferromagnetic state with small magnetization at low temperatures. In this case the magnetic material exhibits a positive magnetic entropy change ($\Delta S > 0$) and a negative adiabatic temperature change ($\Delta T < 0$) when a magnetic field is applied, i.e., a so-called inverse MCE. For example, the inverse MCE in Heusler-type Ni-Mn-In magnetic shape-memory alloys originates from a first-order structural transition from an antiferromagnetic martensite phase to the ferromagnetic austenite phase. Here an inverse MCE is leading to a decrease in the sample temperature with increasing the field (see chapter 5).

2.2 Measurement of the magnetocaloric effect

2.2.1 Direct measurements

Direct methods for determining the MCE are always based on the measurement of the initial (T_I) and final (T_F) temperatures of the material while varying the external magnetic field from an initial (H_I) to a final value (H_F) under adiabatic conditions. Then, the difference between T_F and T_I gives $\Delta T_{ad}(T)$, for a given T_I and $\Delta H = H_F - H_I$.

The temperature change of the sample can be monitored using contact, i.e., a sensor in direct thermal contact to the sample (suitable for strong magnetic fields and large temperature changes) [22, 23, 24], or non-contact techniques, i.e., a technique based on the thermoacoustic principle. A sample with a periodically changing surface temperature induces exponentially decaying pressure waves which can be detected by a sensitive microphone (suitable for weak magnetic fields and small differences in temperature) [7, 25].

To perform direct measurements of the MCE, a sufficiently fast magnetic-field change is required to ensure adiabatic conditions. Two common ways to accomplish this are: (1) measurements on fixed samples by changing the magnetic field (i.e., charging/discharging the magnet) [23] and (2) by moving the sample in and out of a constant magnetic field [24]. When electromagnets are used, the magnetic field strength is usually limited to less than 2 T. When the sample or the magnet are moved, permanent or superconducting magnets are usually employed, witch limits the magnetic field range to $0.1 - 10$ T [7].

It is worth to point out that in this thesis the MCE has been measured directly using a contact technique (a thermocouple is glued to the sample surface) in pulsed magnetic fields up to 70 T where the magnetic field rate is up to 2000 T/s. The technique is described in chapter 3.

The accuracy of direct measurement techniques is usually within the $5 - 10\%$ range [7, 22, 23, 24, 25] and depends on the errors in thermometry, setting of the magnetic field, the quality of the thermal insulation of the sample (in case of a giant MCE, it becomes a critical source of errors because it can disrupt the adiabatic conditions), the quality of the compensation scheme to eliminate the effect of the ultrafast changing magnetic field (dB/dt contributions) on the

temperature sensor reading [7].

2.2.2 Indirect measurements

Different from the direct MCE measurements, which only give the adiabatic temperature change, indirect techniques allow: (1) the calculation of both $\Delta T_{ad}(T)$ and $\Delta S_M(T)$ from an experimentally measured heat capacity and (2) the calculation of $\Delta S_M(T)$ from magnetization measurements [7].

Most of the MCE studies are based on magnetization measurements and calculated $\Delta S_M(T)$. A series of isothermal magnetization curves have to be measured as a function of magnetic-field for different temperatures. $\Delta S_M(T)$ can be calculated by numerical integration of Eq. (2.10). The accuracy of $\Delta S_M(T)$ calculated from magnetization data depends on the accuracy of the magnetic moment determined as well as the temperature and magnetic-field measurements. Therefore, due to the numerical integration and replacing the exact differentials in Eq. (2.10) (dM, dT, and dH) by the measured variations ($\Delta M, \Delta T$, and ΔH), the error using this technique is in the range of $3 - 10\%$ [7, 26].

The most complete characterization of the MCE is provided by measuring the heat capacity as a function of temperature in constant magnetic fields, $C(T)_H$. The entropy of a magnetic solid can be calculated by using Eq. (2.13) as:

$$S(T)_{H_I} = \int_0^T \frac{C(T)_{H_I}}{T} dT + S_{0,H_I}$$

$$S(T)_{H_F} = \int_0^T \frac{C(T)_{H_F}}{T} \, dT + S_{0,H_F}, \tag{2.16}$$

where S_{0,H_I} and S_{0,H_F} are the zero-temperature entropies. In a condensed system $S_{0,H_I} = S_{0,H_F}$ [27]. Therefore, both $\Delta T_{ad}(T)$ and $\Delta S_M(T)$ can be obtained by $\Delta T_{ad}(T) \approx [T(S)_{H_F} - T(S)_{H_I}]$ and $\Delta S_M(T) \approx [S(T)_{H_F} - S(T)_{H_I}]$, respectively [7, 28, 29].

The accuracy of $\Delta S_M(T)$ and $\Delta T_{ad}(T)$ measurements calculated using heat-capacity data depends on the accuracy of the $C(T)_H$ measurements and data processing (Eq. 2.16) because both are small differences between two large quantities, i.e., temperatures and total entropies [7].

2.3   Magnetic refrigeration

Currently, there is a great deal of interest in utilizing the MCE as an alternate technology for refrigeration both at ambient and cryogenic temperatures. Magnetic refrigeration is a new, more environmentally friendly, efficient and less costly cooling technology. The pre-1996 refrigerator used to contain chlorofluorocarbon (CFC) gases which damage the earth's ozone layer. They were replaced by hydrofluorocarbon (HFC) which is, however, still a greenhouse gas 10,000 times more harmful than CO_2. On the other side, magnetic refrigerators use magnetic materials as refrigerants (usually in a form of spheres or thin sheets) and common heat transfer fluids (e.g. water, air, ethanol or helium gas) with no ozone-depleting and/or global-warming effects [19]. Figure 2.3 shows conventional (top) and magnetic refrigeration (bottom) schematically.

The first successful room-temperature magnetic refrigerator was built in the Ames Laboratory at the university of Iowa [30]. It uses permanent magnets to generate the magnetic field (1.5 T) and two beds containing gadolinium (Gd) spheres with water as the heat-transfer fluid. The cooling efficiency of the best proof-of-principle magnetic refrigerator (operating with Gd as the refrigerant) reaches 60% of the theoretical limit (Carnot efficiency) [7, 8, 10, 12]. Whereas the efficiency of the most efficient commercial gas-compression refrigerators is only about 40% of the Carnot efficiency [31].

Conventional and magnetic-refrigeration cycles use different physical effects for cooling. The four basic steps of a conventional gas compression/expansion refrigeration process are demonstrated in Fig. 2.3 (top). When a gas is compressed (2) its temperature increases, but if it is cooled first and then let to expand (3), its temperature decreases to a much lower value than the starting temperature (4). This principle is used by household refrigerators and air conditioners. The steps of a magnetic-refrigeration process are analogous [see Fig. 2.3 (bottom)]. When a magnetic material is magnetized in adiabatic condition an increase in temperature results (b). Then, if the material is cooled while the magnetic field is kept constant (c) and then demagnetized (d), its temperature decreases accordingly [32].

The heating and cooling that occurs in the latter process is based on the MCE. Thus, magnetocaloric materials are at the heart of every magnetic refrigeration
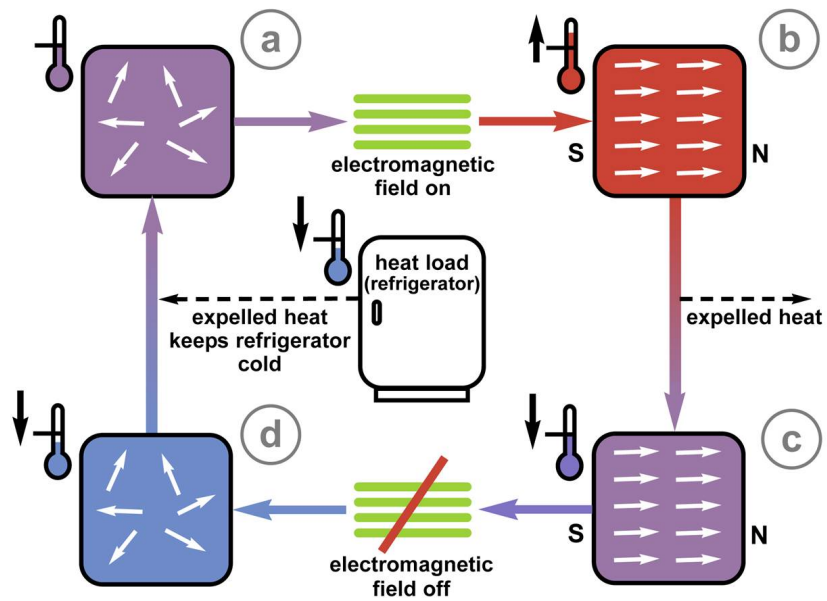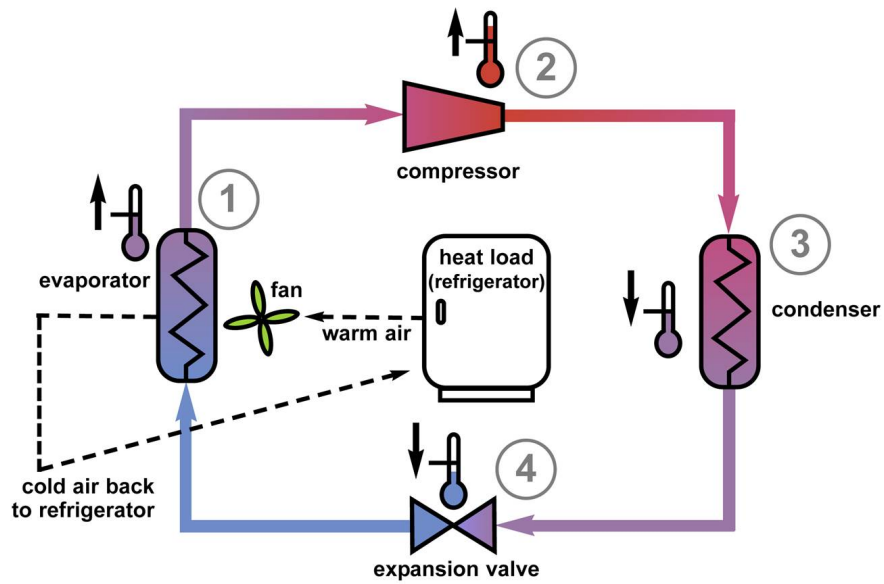
Figure 2.3: *Comparison between conventional (top) and magnetic refrigeration (bottom). Taken from Ref. [32].*

[33]. A large MCE is needed for high cooling power. However, with some magnetocaloric materials, a high efficiency is reached only at high magnetic fields of about 5 T. Therefore, tremendous efforts have been made to search for new magnetic materials displaying larger MCE at lower fields, $\sim$2 T, that can easily be generated by permanent magnets [31].

Suitable magnetocaloric materials will be discussed in more detail in the following section.

2.4 Magnetocaloric materials

In general, magnetocaloric materials are classified into two groups based on the nature of the magnetic phase transition, first-order magnetic-transition (FOMT) or second-order magnetic-transition (SOMT) materials [34]. Since the phase transition happens at the Curie temperature (T_C), the magnetization changes rapidly ($\partial M/\partial T$), and according to the Maxwell relation [Eq. (2.10)] a maximum MCE is expected in this region. How the transition takes place, determines the difference between first-order and second-order materials and, therefore, the MCE value [33]. Figure 2.4 shows schematically the temperature dependence of the magnetization and specific heat for second-order and first-order materials. For a SOMT, the magnetization changes smoothly around T_C [Fig. 2.4(a)], while a sharp magnetization drop is observed in the temperature-induced FOMT [Fig. 2.4(b)]. In a FOMT, the magnetic and the crystal sublattice couple and both undergo a transition, which is accompanied by structural deformation. Whereas for a SOMT only the spin system is changed under the transition. Another important difference between FOMT and SOMT is visible in the specific heat [Fig. 2.4(c,d)]. In SOMT, the specific heat shows a peak-like shape for small fields. The anomaly becomes broader and its maximum is reduced with increasing magnetic field without any remarkable shift in the peak temperature. However, for a FOMT, the specific heat is sharply peaked and the peak position shifts significantly with increasing magnetic fields but the maximum does not change drastically [33].

The properties that determine an optimum material for application may vary with the refrigeration system and desired temperature. On the basis of theoret-
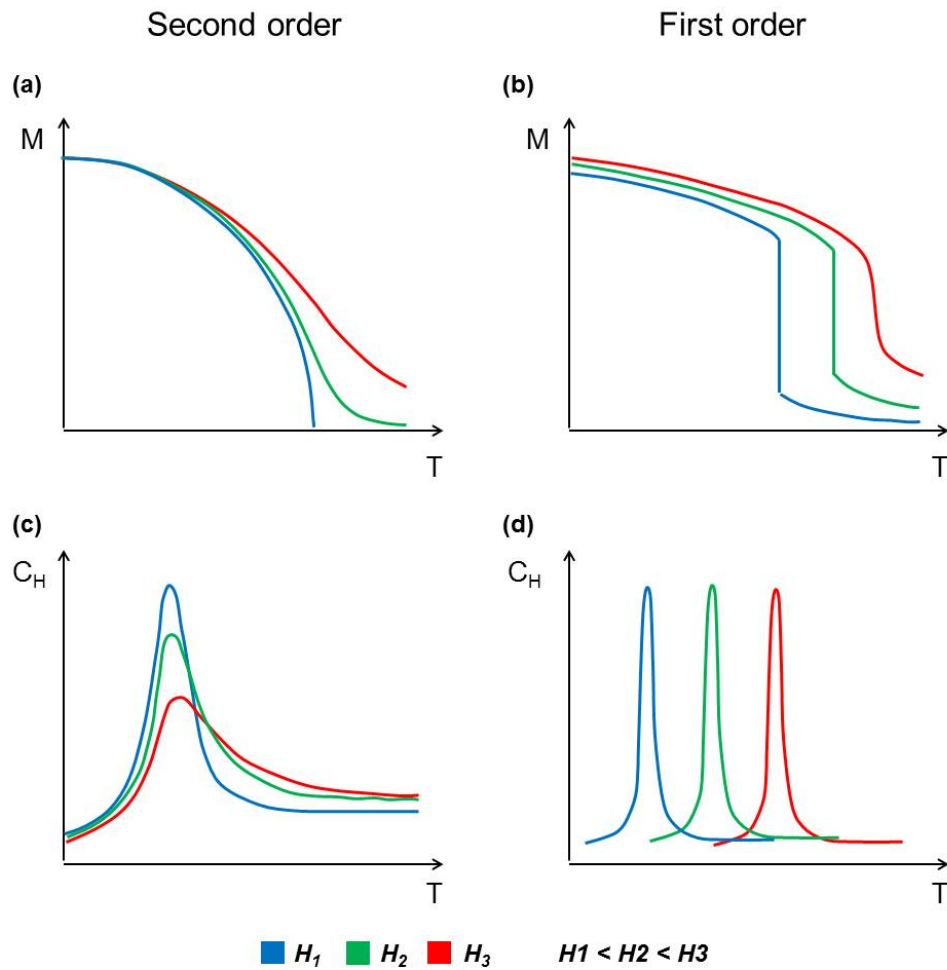
Figure 2.4: *Schematic of the temperature dependence of the magnetization and heat capacity in different magnetic fields for second-order (left) and first-order (right) materials. Taken from Ref. [33].*

ical consideration and the nature of the MCE one can list the following criteria for optimum room-temperature magnetocaloric materials [20, 30, 35] :

✔ Large ΔS_M and ΔT_{ad}

✔ Little to no thermal or magnetic hysteresis

✔ Temperature range of good performance: $40 - 50$ K
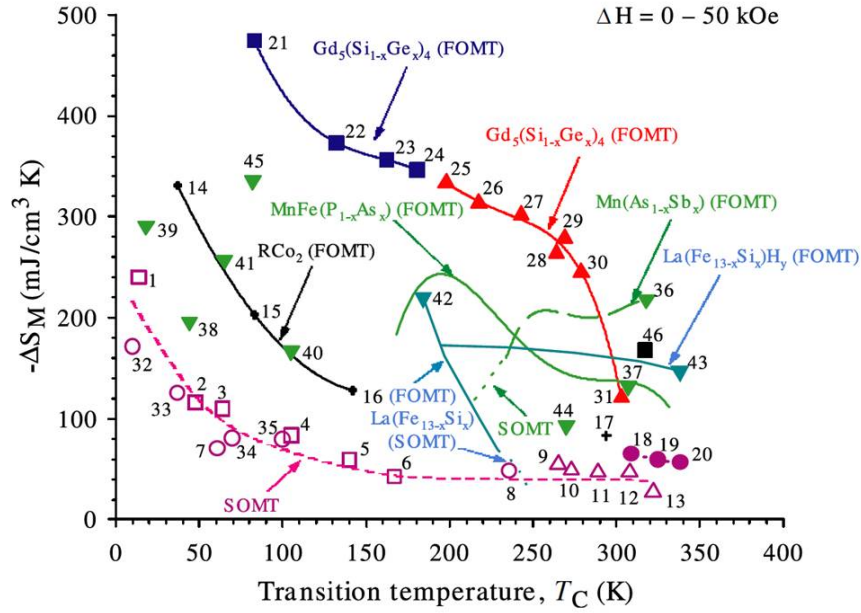
✔ Little to no thermal expansion/contraction

Figure 2.5: *Isothermal entropy change ΔS_M as a function of Curie temperature for a magnetic field change of 5 T for different families of magnetocaloric materials. Pure Gd is seen with caption number 17 marked with a cross symbol. Taken from Ref. [36].*

✔ Low fabrication costs

✔ Large-scale production

✔ Appropriate electrical resistivity to minimize eddy currents

✔ Appropriate thermal conductivity

✔ Low toxicity

✔ Stability (low brittleness, solubility and corrosion)

Since the discovery of the giant MCE in $Gd_5(Si_2Ge_2)$ [11], the search for magnetocaloric materials for room-temperature magnetic refrigeration has attracted much attention. A number of other material families have been found to exhibit giant MCE [37], such as MnAs and $MnAs_{1-x}Sb_x$ compounds [38], $La(Fe_{1-x}Si_x)_{13}$ alloys and their hydrides $La(Fe_{1-x}Si_x)_{13}H_y$ [39, 40], $MnFeP_{0.45}As_{0.55}$ and related

MnFeP$_x$As$_{1-x}$ alloys [31, 41, 42, 43], Ni$_{0.5}$Mn$_{0.5-x}$Sn$_x$ and NiMn-based ferromagnetic shape-memory alloys [15, 44, 45].

Figure 2.5 shows a compilation of some of the most investigated magnetocaloric materials in a plot of ΔS_M versus transition temperature for magnetic-field changes of 5 T. It is obvious that the maximum ΔS_M in FOMT materials is significantly higher than e.g. that of Gd. The giant MCE in these materials arises from magnetic-field-induced magneto-structural transformations (it is either a structural distortion or just a volume expansion without changing the symmetry). This leads to hysteresis losses and fatigue which are critical issues on the search for suitable materials for magnetocaloric-cooling devices. Note, most prototype magnetic refrigerators use pure Gd as refrigerant, which is a SOMT material.

In this thesis, the magnetocaloric properties of Gd, Ni$_{50}$Mn$_{35}$In$_{15}$, LaFe$_{11.74}$Co$_{0.13}$Si$_{1.13}$ and LaFe$_{11.21}$Co$_{0.65}$Si$_{1.11}$ are investigated.

3 Experimental

3.1 Introduction

All pulsed magnetic-field measurements reported in this thesis have been carried out at the Dresden High Magnetic Field Laboratory (Hochfeld-Magnetlabor Dresden, HLD) in the Helmholtz-Zentrum Dresden-Rossendorf (HZDR). A high-power, 50 MJ modular capacitor bank with charging capability up to 24 kV and producing a maximum electric power of $P_{max} \approx 5$ GW is employed to energize the pulsed magnets at the HLD [46, 47]. The magnets are installed in individual pulse cells and electrically separated from each other. The pulsed magnets are immersed in liquid nitrogen to cool the magnets down to 77 K to reduce the ohmic resistance which prevents damaging the magnet and increases the magnet life time. Currently, a number of pulsed-field magnets serve as user magnets at the HLD (see Fig. 3.1) [48, 49].

Two small magnets (magnet C and D) operate with 1.44 MJ total energy and provide pulsed magnetic fields between 53 and 60 T and pulse durations between 25 and 70 ms in bores of 20 mm (magnet C) and 24 mm (magnet D). A 70 T/8.5 MJ magnet (magnet A) produces field pulses of about 150 ms duration in a 24 mm bore. A world-record field of 91.4 T was reached in 2011 by using a 9.5 MJ dual-coil magnets with 16 mm bore [49].

Various experimental techniques are available at the HLD such as electrical transport, magnetization, ultrasound, magnetic resonance and magnetocaloric measurements.

Direct measurements of the magnetocaloric effect in pulsed magnetic fields, besides giving the adiabatic temperature change, ΔT_{ad}, which is one of the most important parameters for magnetic refrigeration, are straightforward and closer to the actual process used in applications. The nondestructive pulsed-field
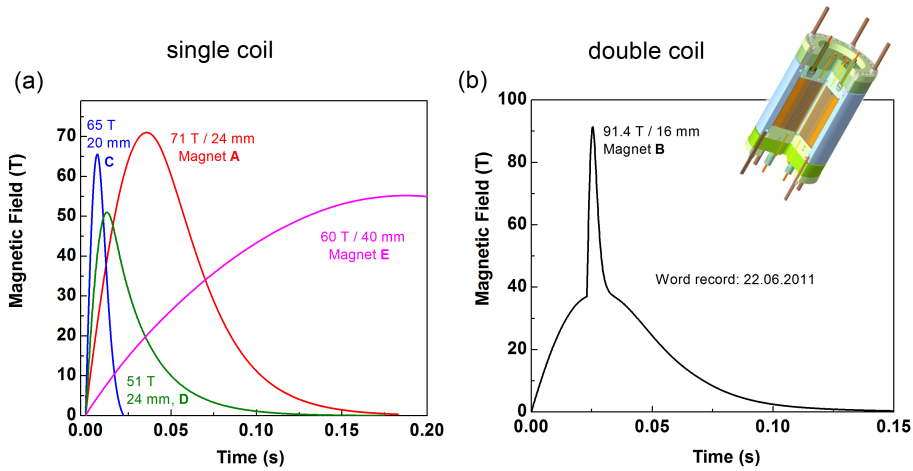
Figure 3.1: *Time dependences of the magnetic fields obtained with different pulsed magnets operational at the HLD. (a) Magnet C is a 1 MJ pulsed magnet with a 20 mm bore. Magnet A and magnet D are 8.5 MJ and 1.5 MJ magnets, respectively, with 24 mm bores. Magnet E is a 43 MJ long-pulse magnet with a 40 mm bore. (b) Magnet B is a dual-coil 9.5 MJ magnet with a 16 mm bore. Taken from Ref. [49].*

magnets in the HLD have typical pulse lengths of 10 to a few 100 ms, which match the targeted operation frequencies of magnetic refrigerators, $10 - 100$ Hz [14]. In addition to extending the accessible magnetic field range to beyond 70 T, the short pulse duration provides nearly adiabatic conditions during the measurement. Therefore, the direct MCE measurements in pulsed magnetic fields provide the opportunity to investigate the dynamics of the MCE in a suitable frequency range.

Some other measurements which are reported in this thesis such as DC magnetization, quasi-static magnetocaloric effect and DC magnetostriction measurements were carried out at the Faculty of Material Science, Darmstadt University of Technology (TU Darmstadt).

In this chapter the experimental method for measuring the magnetocaloric effect in pulsed fields and also a short overview of other experimental techniques used in this work are described.

3.2 Direct measurements of the magnetocaloric effect

3.2.1 Magnetocaloric measurement in pulsed magnetic fields

From the experimental point of view, three essential components are needed to carry out a magnetocaloric measurement: the magnet supplying the magnetic field, a cryostat to cool down (or heat) the sample, and an appropriate thermometer to measure the temperature response of the sample. Especially under the extreme conditions of pulsed magnetic fields each component should work properly together.

In all of the magnetocaloric measurements in this study, we used home-built experimental set-ups. Figure 3.2 shows (a) the schematic drawing of the pulsed-field experimental set-up containing cryostat, magnet, sample holder, and electronic connections and (b) pictures of both sides of the sample holder together with the brass cylinder (local heater) as part of the sample holder. As usual for pulsed-field experiments, all materials and wirings were chosen in order to minimize eddy currents. The electrical wiring on the sample holder were rigidly attached to the G10 rod (1.5 m length). The widest part of the sample holder had an outer diameter smaller than 11 mm [see Fig. 3.2(b)]. The sample holder was enclosed in a thin-walled stainless-steel shield and centered by spacers which were made from PEEK[1]. The sample space inside the shield was evacuated to provide adiabaticity. The assembly was inserted into a helium-4 (^{4}H) bath cryostat.

The accurate and reliable measurement of the magnetic field, H, is a crucial requirement for any pulsed-field measurement. Measuring the induction voltage in a calibrated pick-up coil is the most common method. A pick-up coil consists of one or more turns of wire wound around a definite area on a scale of a few mm^2 [50]. The induced voltage is proportional to the time derivative of the enclosed magnetic flux, $U_{ind}(t) \propto d\Phi/dt \propto dB(t)/dt$, where B is the magnetic flux density. Our pick-up coil is made up of 15 turns (single layer) of 60 μm

---

[1]Polyether ether ketone (PEEK) is a semicrystalline thermoplastic with excellent mechanical and chemical resistance properties that are retained to high temperatures.
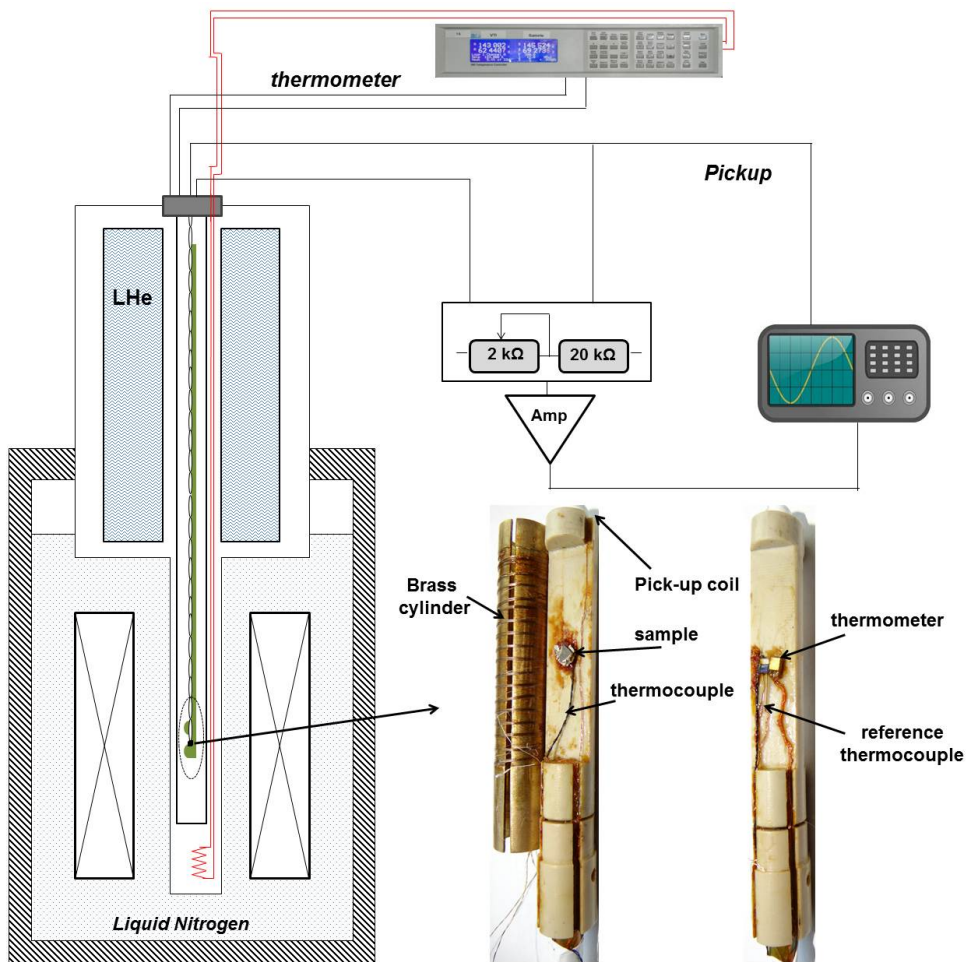
Figure 3.2: *(a) Schematic drawing of the experimental set-up for MCE measurements in pulsed magnetic fields. (b) Pictures of both sides of the sample holder together with the brass cylinder.*

isolated copper wire and located at the end of the sample holder. The induced voltage is recorded by a digital oscilloscope, Yokogawa DL750 (or DL850) with a sampling rate of up to 1 MHz. The digitized data are stored and later integrated numerically to determine the magnetic field as a function of time.

The sample holder is equipped with a local heater [see Fig. 3.2(b)]. In order to homogenize the local temperature, the heater body is made of a thin-wall (0.5 mm thick) brass cylinder, with a longitudinal slit. The latter prevents eddy currents. Manganin wires (50 μm diameter) wrapped around the heater body in bifilar manner, are used as heating element. For the experiment, the heater is positioned around the sample space to ensure uniform temperature distribution. The electrical contacts are made via copper wires. If the sample size is comparable to the inner diameter of the heater body, it is exposed to the radial temperature gradient. The accurate sample temperature is defined by correcting the probe thermometer by the thermocouple reading taken prior to the pulsed.

The system temperature is controlled by using a Lake Shore Model 340 Temperature Controller with PID regulation in conjunction with a local heater and a PT100 thermometer.

The temperature of the sample is measured with a differential copper-constantan thermocouple (see Fig. 3.3). One leg of the thermocouple (sample junction) is sandwiched between the two equally sized plates of the sample which are then glued together with a small amount of silver epoxy (EPO-TEK H20E). This is done to ensure good thermal contact and to decrease the heat loss between the measuring junction and the sample. The other leg (reference junction) is used to measure the temperature inside the sample holder (reference temperature) and detection of a possible influence of the magnetic field on the thermocouple voltage. The sample and reference thermocouple junctions are located at equal height on either side of the sample holder and are, therefore, subject to the same magnetic field.

The thermocouples were calibrated in a Quantum Design PPMS system using melting ice as a reference. Figure 3.4 shows the resulting calibration curve of the temperature as a function of voltages. In case of a small MCE the conversion procedure is rather straightforward. One can take the derivative of $\Delta T/\Delta V$ at the corresponding abscissa and multiply it by the measured ΔV to obtain ΔT.
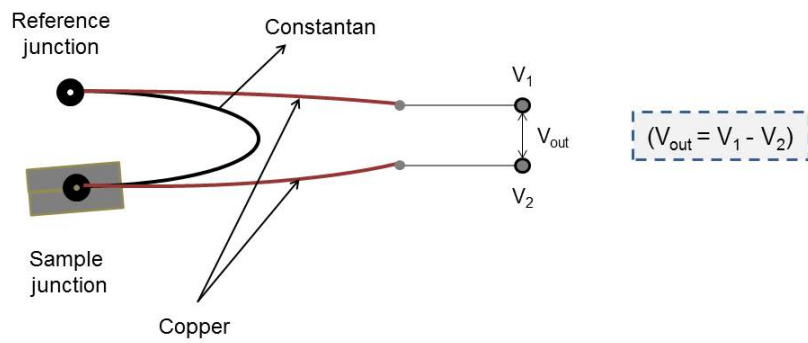
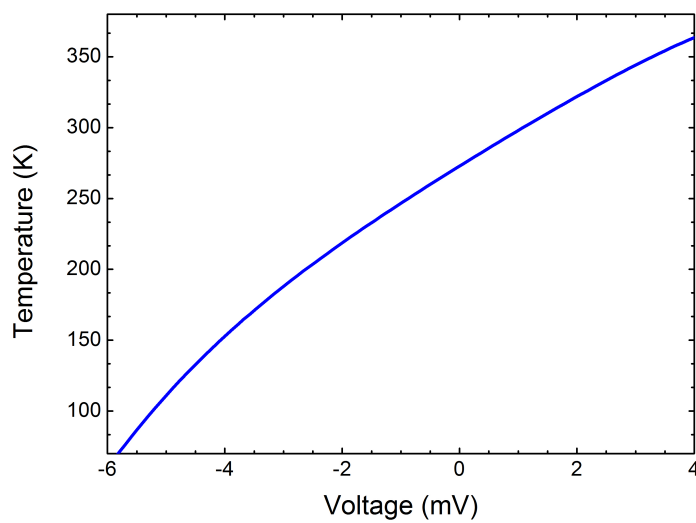Figure 3.3: *Schematic drawing of the differential copper-constantan thermo-couple.*

Figure 3.4: *The calibration plot for the used 25 μm diameter copper-constantan thermocouple (T-type).*

In case of larger temperature changes the conversion is done by the following procedure. For the calibrated thermocouple both $V(T)$ and $T(V)$ are defined, for example in form of polynomials. Given the initial temperature T_i we obtain the corresponding voltage V_i. This value is increased by the measured ΔV. From the inverse dependence $T(V)$ the final temperature T_f is obtained, and then ΔT is defined as $T_f - T_i$.

Although MCE measurements in pulsed magnetic fields provide adiabatic conditions during the measurement and extending the accessible magnetic field range (going beyond 70 T), it is limited by the challenging thermometry in the short pulse duration [23, 51]. This is firstly because any small loop in the thermocouple wiring picks up a very large spurious voltage (dB/dt), even though the thermocouple wires were thoroughly twisted. Anyway, the component of the magnetocaloric effect (ΔV) can be smaller than that of the dB/dt voltage induced in the wiring. To prevent the influence of this interference, an additional compensation circuit was used. The compensation signal from the pick-up coil [see Fig. 3.2(a)], which measures the magnetic field, was passed through a voltage divider and a proper part of it was taken and subtracted from the thermocouple signal. The advantage of the compensation scheme is demonstrated in Fig. 3.5, where the time dependence of the thermocouple signal without compensation (light blue curve) is shown together with that after compensation (dark blue curve). The curves were obtained by using polycrystalline Gd specimen at liquid-nitrogen temperature ($\sim$77 K). It should be noted that Gd has a small positive magnetocaloric effect around 77 K which can be seen as the small maximum in the dark blue curve.

Besides the compensation, averaging between positive and negative pulses (the MCE does not depend on the direction of the field) allows to extract the desired temperature-dependent part of the voltage signal.

Therefore, with the help of the compensation scheme and averaging method, we have been able to nearly eliminate the influence of dB/dt on our experimental results.

After the compensation, the thermocouple signals are amplified by a factor of 10 to 100, and conditioned by a low-noise voltage amplifier (FEMTO-DLPVA). The time-dependent thermocouple signal, $\Delta V(t)$, is recorded by a digitizer and later converted to $\Delta T_{ad}(t)$ by using the thermocouple calibration (see Fig. 3.4)
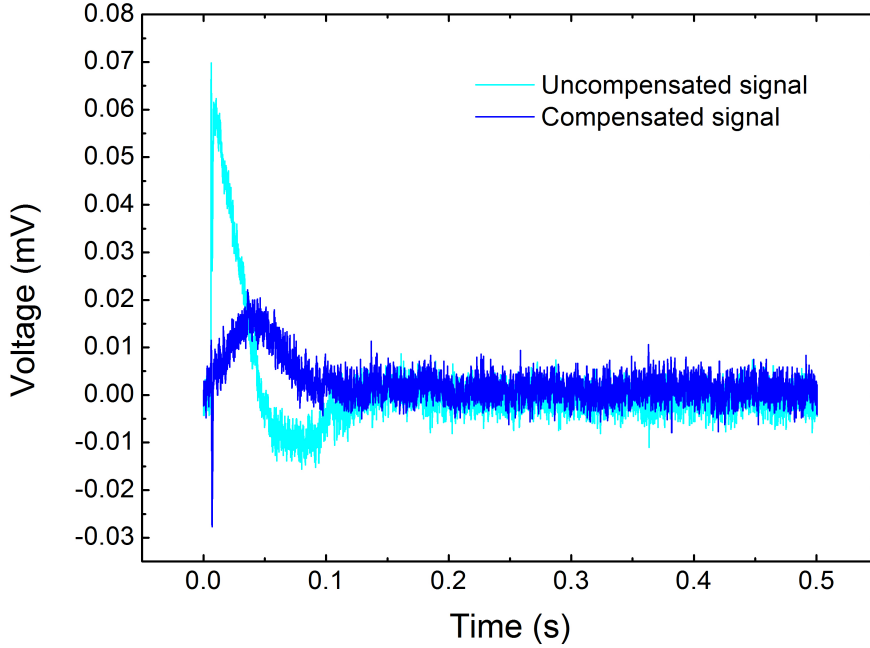
Figure 3.5: *Time dependence of the thermocouple signal without compensation (light blue) and after compensation (dark blue).*

A Matlab program is written to perform the conversion from mV to K.

Figure 3.6 shows the time dependences $\Delta T_{ad}(t)$ for a polycrystalline Gd sample at 285 K recorded during the application of pulsed fields, together with the corresponding pulse profiles. Gd is widely used for testing prototype devices for MCE measurements, since Gd has a large magnetocaloric effect with T_C close to room temperature. The first $\Delta T(t)$ curve was taken in magnet D which generates magnetic-field pulses up to 50 T with a rise time of $\sim$13 ms [Fig. 3.6(a)]. The sample-temperature change was measured using a thermocouple made out of 70 μm diameter wires. It can be seen from Fig. 3.6(a) that in this measurement the heat transfer between the sample and the thermocouple was too slow, so the measured temperature was delayed and did not correspond to the real temperature of the sample. This delay results in an apparent open loop of ΔT as a function of field [inset of Fig. 3.6(a)].

Conversely, the adiabatic MCE data for Gd do not show any sign of hysteretic
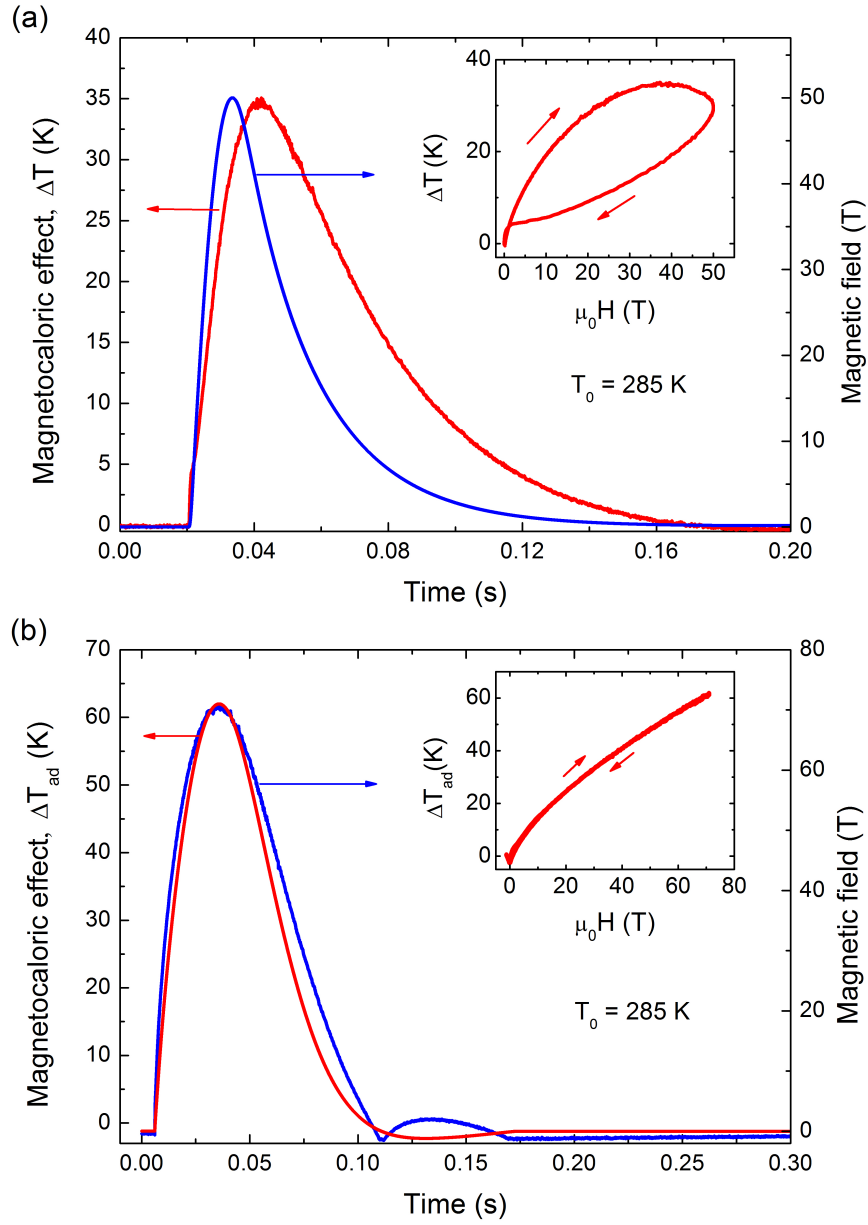
Figure 3.6: *Time dependences of the adiabatic temperature change at (a) 50 T and (b) 70 T, measured in pulsed magnetic fields, for gadolinium at 285 K. The field profile is also indicated (right axis). The insets show the corresponding field dependence of ΔT_{ad}.*

behavior as in the case of the fully adiabatic MCE measurement [Fig. 3.6(b)] for which no loop in $\Delta T(H)$ is observed.

The second $\Delta T_{ad}(t)$ curve [Fig. 3.6(b)] was taken in magnet A, a 70 T magnet with about 30 ms rise time. Here, a thermocouple made of 25 μm diameter wires was used for monitoring the sample temperature. The sample temperature perfectly follows the pulsed-field profile and no delay between the position of the maximum of the pulse and the maximum in $\Delta T_{ad}(t)$ is observed. The thermocouple responses (ΔT_{ad}) upon increasing (heating process) and decreasing (cooling process) field coincide with each other, which confirms that this measurement is fully reversible [see inset of Fig. 3.6(b)]. Furthermore, we do not see any sign of eddy-current heating, since after the magnetic pulse the sample reaches again the starting temperature.

Therefore, taking advantage of the fast field-sweep rate and using a very thin thermocouple (to obtain the quick response), we are able to measure adiabatic MCEs in pulsed magnetic fields.
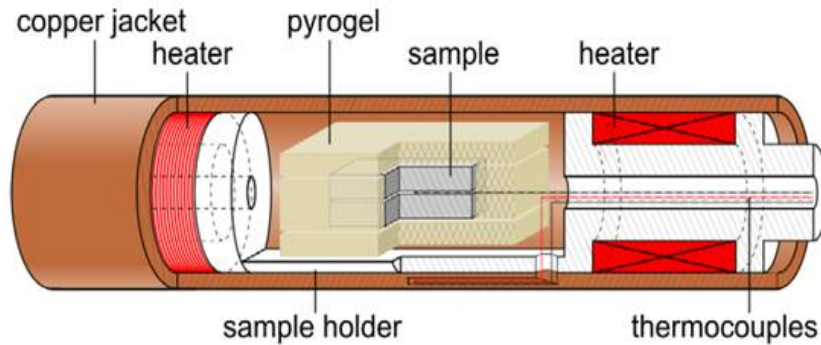
Figure 3.7: *Schematic drawing of the cell for measuring the adiabatic temperature change. Taken from Ref. [52].*

3.2.2 Magnetocaloric measurements in quasi-static field

Direct measurements of the adiabatic temperature change, ΔT_{ad}, in quasi-static fields were performed in a home-built experimental setup in TU Darmstadt. The magnetic field was produced by a permanent-magnet set-up (Halbach type) which consists of two cylinders rotating in opposite directions. The magnetic field was changed in the bore center from 1.93 T to -1.93 T at a rate of about 1 T/s, fast enough to ignore the heat losses from the sample to the environment during the measurement. The temperature changes of the sample were measured using a copper-constantan thermocouple (T-type) with accuracy better than ± 0.01 K. The thermocouple junction was placed between the two equally sized sample pieces (approximate size $4 \times 2 \times 1$ mm) and fixed by a thermo-conductive silver-based UHV (Ultra High Vacuum) glue to increase the thermal contact between the thermocouple and sample. A resistive electric heater was attached to the sample holder and the target temperature was approached without overheating/undercooling during the measurements. A passive adiabatic shield (made from a thin silver film and pyrogel) was used in order to minimize the heat exchange between the sample and the sample holder [52, 53]. The schematic drawing of the measurement cell is shown in Fig. 3.7.

The sample holder was placed inside a vacuum chamber connected to a pump providing pressure down to $\sim 10^{-6}$ mbar. The chamber was placed in the bore of the magnet and immersed into liquid nitrogen.
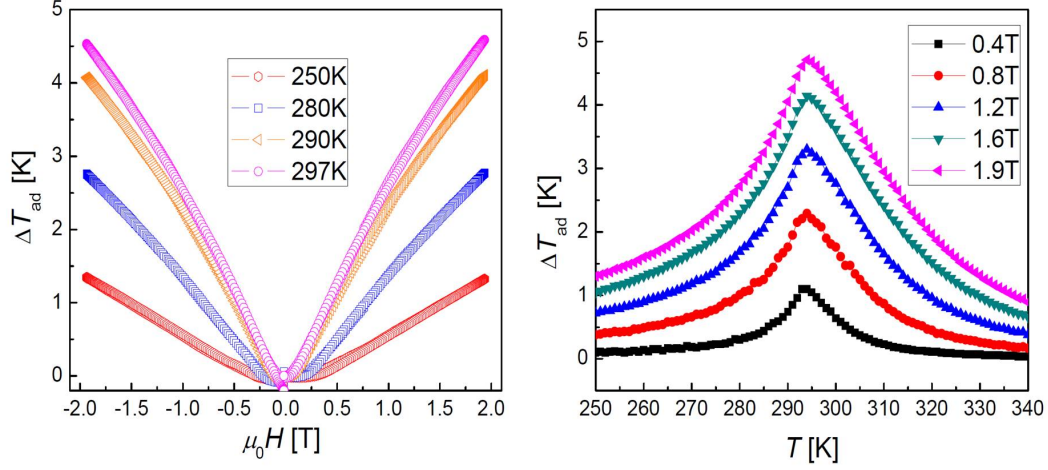
Figure 3.8: *Field and temperature dependence of the adiabatic temperature change in polycrystalline Gd in the vicinity of the Curie temperature for a field change of 1.93 T. Field sweep rate is 1 T/s. Taken from Ref. [52].*

After stabilization of a desired temperature, ΔT_{ad} was measured as a function of magnetic field. The field was changed in the following sequence: $0 \text{ T} \rightarrow +1.93 \text{ T} \rightarrow 0 \text{ T} \rightarrow -1.93 \text{ T} \rightarrow 0 \text{ T}$. The signals from the thermocouple and a Hall probe were amplified and collected using an analog-to-digital converter (at a sampling rate of 1000 points/s) [52, 53].

Figure 3.8 shows the measured data for a polycrystalline Gd sample. Upon increasing the magnetic field the temperature changed from T to $T + \Delta T_{ad}$ (heating process), the sample temperature decreases by the same amount, i.e. $-\Delta T_{ad}$, when reducing the magnetic field. The latter confirms that this measurement is fully reversible [52, 53].
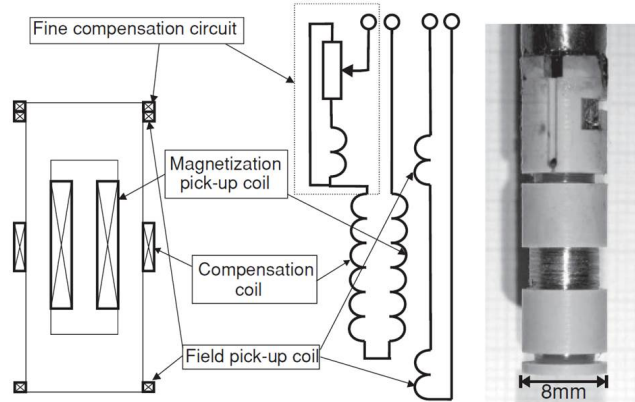
Figure 3.9: *Pickup-coil system used in the pulsed-field magnetometer with (left) the principal sketch, (middle) the electrical scheme, and (right) a picture of the original set up. Taken from Ref. [54].*

3.3 Magnetization measurements

3.3.1 Adiabatic magnetization in pulsed fields

The magnetization in pulsed magnetic fields was measured by use of the induction method. We employed a pick-up coil surrounding the sample (see Fig. 3.9), which consists of 1200 turns of 40 μm copper wire wound around a 3.2 mm diameter sample space and is 5 mm long [54]. Since the coil was placed in a varying magnetic field, it should be connected to a another coil to be compensated in order to measure magnetization, M, instead of the induction, dH/dt [55]. Several arrangements of the compensated pick-up coil system are possible. It was found that a coaxial geometry is best suited as it is less sensitive to the field gradient and vibrations [54]. The compensation coil was wound around a ∼6.8 mm diameter. A small remaining uncompensated voltage due to the temperature-dependent contribution was further reduced at each temperature by using an additional coil (fine-compensation circuit).

The magnetic field was measured by two pick-up coils. These coils were connected in series and placed equal distances above and below the magnetization pick-up coil (see Fig. 3.9) [54]. The signals from the pick-up coils (dH/dt), were

digitized, stored, and later integrated numerically. The pick-up-coil signal was calibrated by measuring the well-known magnetization curve of MnF_2, which exhibits a temperature-independent spin-flop transition at 9.27 T [54].

The sample was placed in the center of the pick-up coil system, by using a properly designed top-loading system. The determination of the magnetization of each sample involves two separate measurements. First, the pick-up signal with the sample in the coil is measured at a desired temperature. Second, the background (without sample) is recorded under identical conditions. The magnetization of the sample is obtained by subtracting the background from the first signal. The absolute value of the magnetization was calibrated by a low-field magnetization measurement, obtained by use of commercial devices in static fields [54].

The magnetization measurements were performed in pulsed magnetic fields up to 60 T. The total pulse duration of the field was about 25 ms with a rise time of about 7 ms.
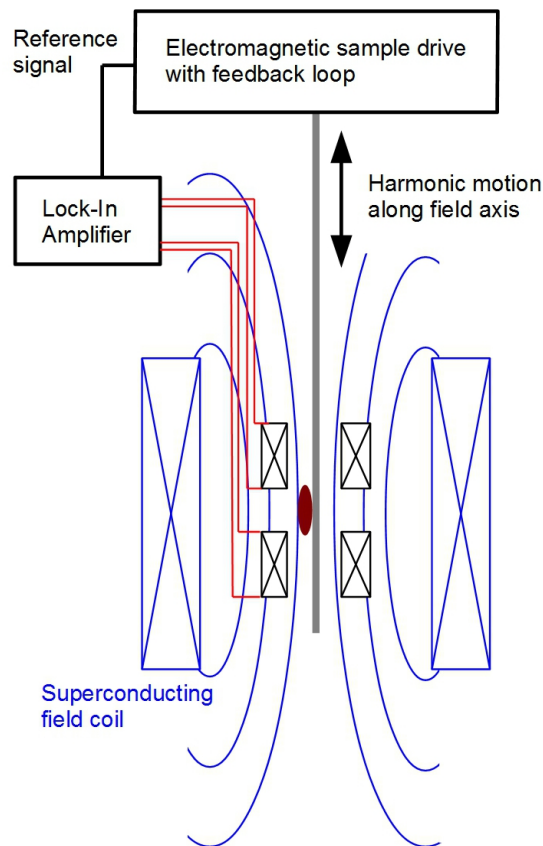
Figure 3.10: *Sketch of a vibrating sample magnetometer (VSM). Courtesy of Dr. M. Uhlarz.*

3.3.2   Isothermal magnetization in DC field

The DC magnetization measurements have been performed by use of a vibrating sample magnetometer (VSM), manufactured by Quantum Design. The VSM uses a technique based on Faraday's law of induction. The sample is mechanically oscillating inside an inductive pick-up-coil system. Typically, the vibration is created by a motor or piezoelectric actuator. The flux change caused by vibrating the sample induces a voltage in the pickup coils, which is proportional to the magnetic moment of the sample. A schematic drawing of a typical VSM is shown in Fig. 3.10. In this technique, the sample is mounted in a polypropylene holder that snaps into a brass trough [56].

The VSM here is capable of measuring magnetization value in the range of 2.5×10^{-5} to 5 emu in the temperature range from 1.9 to 400 K and in the field
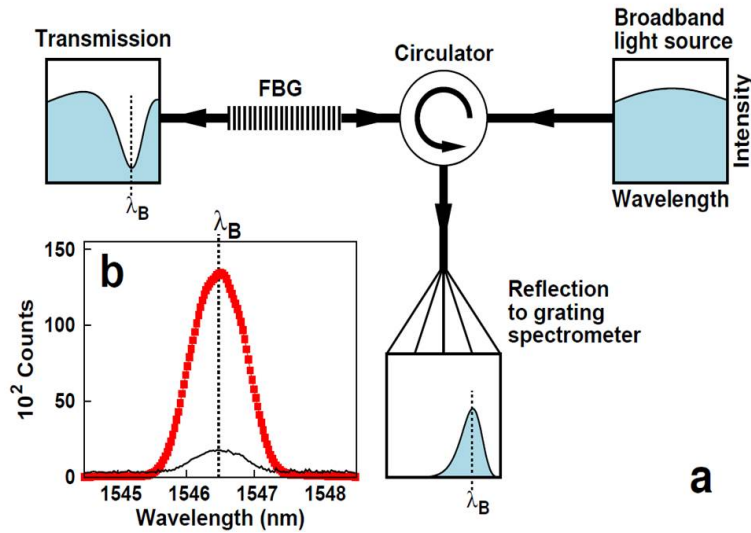
Figure 3.11: *(a) Optical circuit for fiber Bragg grating (FBG) measurements. Each box shows the light spectra in the circuit schematically. (b) A typical reflection spectrum of the FBG at 5.4 K in zero field (red curve). The black curve is the r.m.s. noise (gain by 100). Taken from Ref. [57].*

range from -14 T to 14 T.

3.4 Magnetostriction measurements

3.4.1 Magnetostriction in pulsed fields

The magnetostriction measurements in pulsed magnetic fields were performed by using an optical-fiber strain gauge bonded to the surface of the sample with cyanoacrylate epoxy. The strain gauge is a 1 or 2 mm long fiber Bragg grating (FBG) with a peak reflectivity at 1550 nm. The transmission of the sample strain to the fiber is estimated to be in the range $70 - 90\%$. The sample elongation is converted to a reflectivity-peak shift, which was registered by a high-resolution grating spectrometer with a camera operating at 47 kHz, providing a resolution of better than 10^{-6} in relative elongation. For a detailed description of this technique see reference [57]. The optical circuit is illustrated in Fig. 3.11(a) and a typical reflection spectrum for a 2 mm FBG is shown in
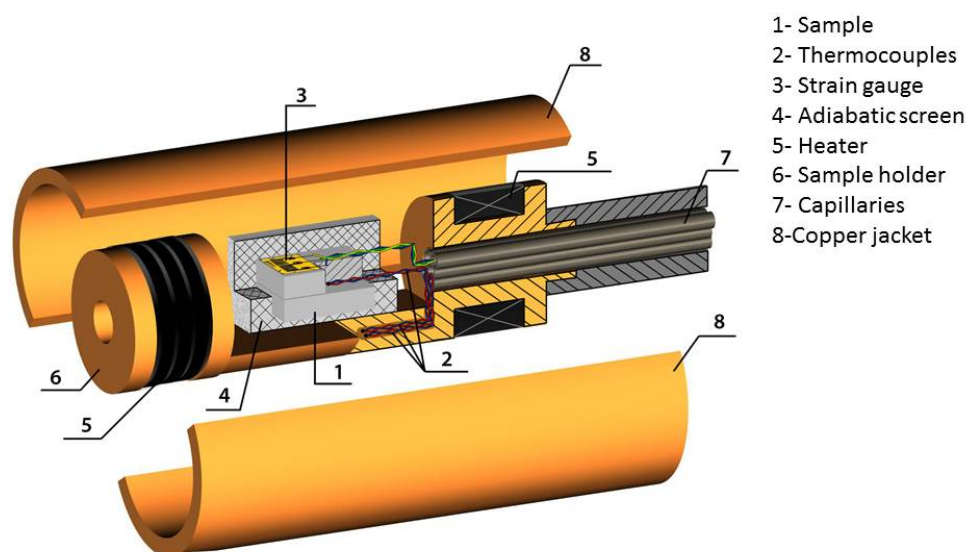
Figure 3.12: *Schematic drawing of the striction measurement cell. Provided by K. P. Skokov.*

Fig. 3.11(b).

The strains were measured in pulsed magnetic fields up to 60 T with a rise time of about 7 ms and a total pulse duration of 25 ms.

3.4.2 Isothermal magnetostriction in DC fields

The magnetostriction and thermal-expansion measurements in quasi-static fields were performed by using commercial strain gauges SK-06-030TY-350 (Vishay) bonded on the sample surface with M-bond 610 adhesive. For better accuracy the strain gauge was connected to a Wheatstone bridge. The voltage-fed Wheatstone bridge was compensated before each measurement. Depending on the resistance change occurring in the strain gauges (due to the sample-length change) a corresponding voltage change of the bridge circuit was recorded by a DL750 oscilloscope.

3.5 Specific-heat measurements

Heat-capacity measurements were performed in a Quantum Design physical property measurement system (PPMS). The PPMS heat-capacity puck with thermal connections to sample and sample platform is shown schematically in Fig. 3.13. The sample is mounted on the platform typically by using a thin layer of Apiezon N grease. The platform is equipped with a heater and thermometer which are attached to its bottom side. The electrical and thermal connections of the platform are provided by thin platinum wires. The PPMS uses a cryopump in order to provide high vacuum during the measurements, so the thermal conductance between the sample platform and thermal bath is only supplied via the wires [58]. Note, to prevent the sample from being detached from the platform in magnetic fields instead of grease GE varnish was used.

The most commonly applied methods to determine the heat capacity are heat-pulse techniques. For the heat-capacity measurement used here, a heat pulse of rectangular shape is applied to the sample platform and its temperature response is obtained as shown in Fig. 3.14. The data analysis is done by means of a single-tau method, when the sample is in good thermal contact with the platform. However, the latter is not always provided, so a two-tau method is
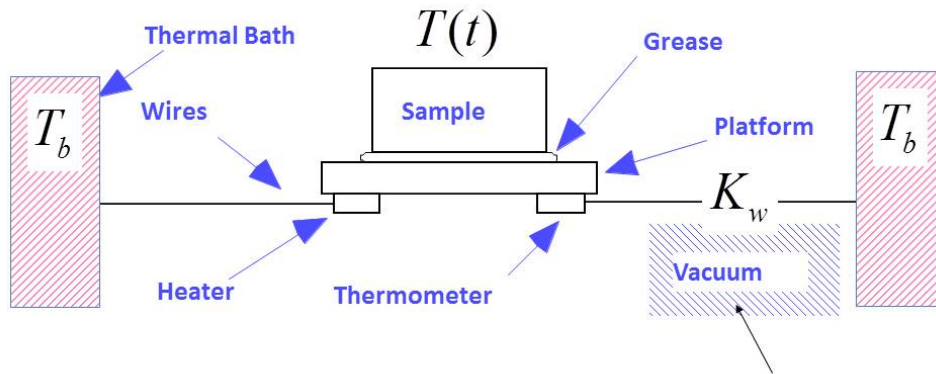

Figure 3.13: *Schematic of the thermal connections to sample and sample platform for the PPMS heat-capacity option. K_W is the thermal conductance of the supporting wires that attach the platform to the thermal bath and T_b is the thermal-bath temperature. Taken from Ref. [58].*
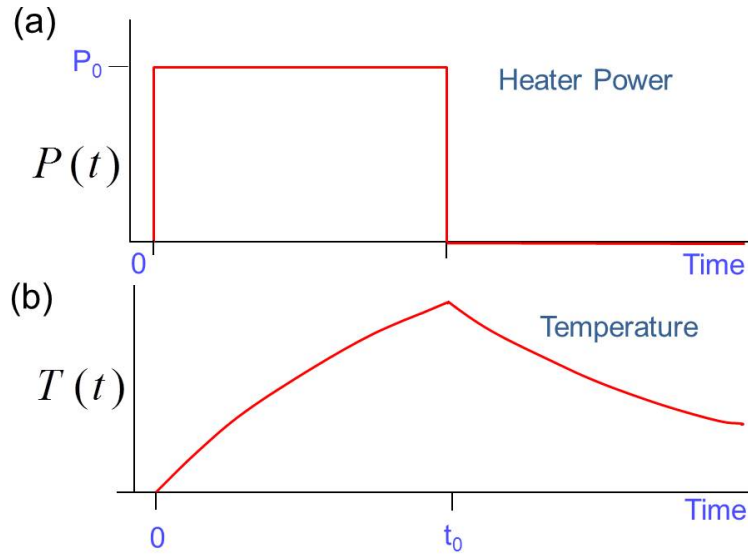
Figure 3.14: *(a) A heat pulse of a rectangular shape is applied to the sample platform between $t = 0$ and t_0. (b) The temperature response of the sample platform. Taken from Ref. [59].*

used, where accurate fits are performed for the heat flow between the platform and thermal bath (τ_1) and the heat flow between the platform and the sample (τ_2) [58, 59].

Although these techniques are widely used, a first-order transition is known for being a challenge for heat-capacity measurements. Since the transition shows a sharp peak in the heat capacity, many standard techniques cannot give a precise value around the transition region. For example, for finite heat pulses, the resolution diminishes around the peak (the resolution is determined by the temperature change, see Fig. 3.14). On the other hand, a first-order transition is usually accompanied by thermal hysteresis, so heating the sample with very small heat pulses instead of driving the sample through the transition keeps the sample in the mixed state i.e., a not well-defined state.

To overcome this problem, we employed a long heat-pulse technique for the transition region along with a slope analysis. The details of the technique are explained as follows: In first approximation, the platform temperature as a

function of time obeys the equation [58]

$$C_{tot}(T)\frac{dT(t)}{dt} = P(t) - K_W[T(t) - T_b],\qquad(3.1)$$

where C_{tot} is the total heat capacity of the sample and platform, $C_{tot} = C_S + C_P$.

If we consider the heating and cooling curves separately [see Fig. 3.14(b)] and assume the same $C_P(T)$ for them, Eq. (3.1) is written as [60]:

$$C_{tot}(T)\frac{dT_h(t)}{dt} = P_h - K_W[T(t) - T_b]\qquad\text{(heating)},\qquad(3.2)$$

$$C_{tot}(T)\frac{dT_c(t)}{dt} = P_c - K_W[T(t) - T_b]\qquad\text{(cooling)}.\qquad(3.3)$$

Then, by solving Eqs. (3.2) and (3.3) simultaneously, C_{tot} is given by

$$C_{tot}(T) = \frac{P_h - P_C}{dT_h(t)/dt - dT_c(t)/dt}.\qquad(3.4)$$

The PPMS software uses Eq. (3.4) to fit the relaxation data (obtained from large temperature rises, up to 30%) and gives a whole series of heat-capacity values during heating and cooling. It must be noted that, because of the poor coupling between the sample and platform in our measurements, only the heating curves were used for fitting. The two-tau method was employed to calculate the heat capacity outside the transition region.

The heat capacity of the sample was determined by two separate measurements. First, the heat capacity of the platform plus the GE-varnish was measured, so-called the addenda heat capacity, C_P. Second, the sample heat capacity plus the addenda, C_{tot}, was measured. Finally the heat capacity of the sample was determined by $C_S = C_{tot} - C_P$.

4 Magnetocaloric effect in gadolinium

4.1 Introduction

Since the discovery of the magnetocaloric effect and later its potential applications, tremendous efforts have been made to utilize this alternative technology to replace the conventional gas compression/expansion technique for cooling applications [10, 36]. When Brown in 1976 demonstrated that by applying a regenerative cooling cycle a significant temperature gradient can be accomplished near the transition temperature of a ferromagnet, he used Gd [61]. He was able to attain a temperature difference of 47 K between the hot (46 ℃) and cold (−1 ℃) end of a magnetic refrigerator by subjecting Gd metal to 50 consecutive magnetization-demagnetization cycles using a magnetic field change from 0 to 7.5 T in combination with a water-ethanol (80% water and 20% ethanol alcohol) regenerator [30, 36]. Whereas the adiabatic temperature change in Gd at 7.5 T is only $\Delta T_{ad} \approx 14$ K, (see Fig. 4.1) which is three times smaller than the achieved temperature difference [62].

Following this success of the proof of principle for magnetic refrigeration, many prototypes have been built and nearly all of them used Gd as a magnetic refrigerant. Although the implementation of Gd in commercial magnetic refrigeration devices is not expected, it is widely used in test devices [63, 64, 65] due to its easy implementation and large magnetocaloric effect with T_C close to room temperature [66].

Gd is a rare-earth metal that crystallizes in the hexagonal close packed (hcp) structure [67]. It forms Gd^{3+} ions with the electron configuration [Xe] $4f^7$. Therefore, it has the large spin angular momentum $S = 7/2$, (which provides
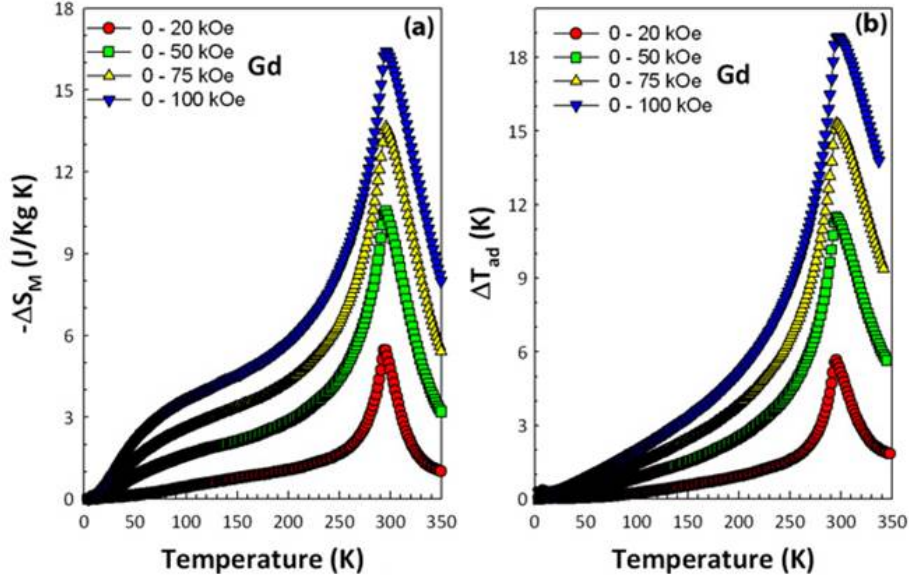
39

Figure 4.1: *(a) The isothermal entropy and (b) adiabatic temperature change of polycrystalline gadolinium for four different field changes. Taken from Ref. [62].*

quite large magnetic moment). The orbital angular momentum is zero ($J = L + S = 7/2$). Due to the lack of orbital angular momentum, it does not show a single-ion anisotropy. Gd transforms from the paramagnetic to the ferromagnetic state at T_C with a second-order phase transition. It remains in the ferromagnetic state down to liquid-helium temperatures [68]. According to literature data, the Curie temperature ranges between 289 and 295 K [69, 70].

So, with a Curie temperature close to room temperature, little to no anisotropy, negligible magnetic-hysteresis losses and, more importantly, a large magnetocaloric effect, Gd has become the benchmark against which most newly found magnetocaloric materials are compared. ΔT_{ad} is ∼5.5 K for a change of the applied magnetic field from 0 to 2 T [20, 62].

In this chapter, we report on the $\Delta T_{ad}(H, T)$ dependences of polycrystalline Gd in the vicinity of T_C determined by means of direct measurements in pulsed magnetic fields (up to 70 T) and quasi-static fields (up to 2 T). In addition, we demonstrate that the maximum temperature change ΔT_{ad} is proportional to $H^{2/3}$.

4.2 Magnetocaloric effect in Gd

The temperature dependences of the adiabatic temperature change, ΔT_{ad}, measured in quasi-static magnetic fields for a polycrystalline Gd sample are shown in Fig. 4.2(a). ΔT_{ad} becomes larger for increasing applied magnetic fields (between 0.4 and 1.9 T), and the MCE is largest at T_C ($\approx$ 294 K). Figure 4.2(b) displays the field dependence of the dynamic temperature change for several different initial temperatures around T_C and for a maximum field change of 1.9 T. The field-sweep rate was $\sim$1 T/s. Here, an increase in the sample temperature is observed upon the application of a magnetic field (conventional MCE). Note that the magnetization (heating process) and demagnetization (cooling process) curves nearly coincide confirming that this measurement is reversible (adiabatic condition).

Figure 4.3(a) shows the adiabatic temperature change determined from direct measurements in pulsed magnetic fields (red symbols) and in quasi-static fields (blue symbols) for field changes of 6.5 T and 2 T, respectively. At the Curie temperature, the maxima of ΔT_{ad} are 4.7 and 13 K, respectively, which are slightly smaller than 5.8 and 13.8 K reported by Dan'kov *et al.* [70] for the same magnetic field changes. It should be noted that the MCE value in Gd strongly depends on the impurity of the sample and the different values reported are mainly caused by different sample qualities [70]. The pulsed-field MCE data were taken in pulsed magnetic fields with field rates up to 200 T/s, which is about 200 times faster than the measurements done in quasi-static fields. However, Fig. 4.3(b) demonstrates that the short pulse time is not detrimental for the response time of the thermocouple and, similar to the quasi-static measurement, the MCE is reversible.

The MCE for the polycrystalline Gd sample was also measured in pulsed magnetic fields up to 70 T for some selected temperatures around T_C [see Fig. 4.4(a)]. The maximum value of ΔT_{ad} is found to be almost 60 K around T_C. We can only compare our results with two available papers by Kihara *et al.* [51] and Kohama *et al.* [71]. They used pulsed magnetic fields up to 55 T to measure the MCE[1] in single-crystalline Gd and obtained a maximum of $\Delta T_{ad} \approx$ 60 K [51].

---

[1]To monitor the sample temperature change, they used a thin-film thermometer which was grown directly on the sample surface [51]

The different values measured for ΔT_{ad} should be mainly due to the different sample quality (we used polycrystalline Gd).

Figure 4.4(b) shows the field dependence of the dynamic temperature change for pulsed fields up to 70 T with a field-sweep rate of 2000 T/s . This is about 2000 times faster than the measurement in quasi-static fields, nevertheless the excellent adiabatic conditions in these measurements are confirmed by the coinciding up- and down-sweep data. It can be seen that the MCE is nearly equal for temperatures above T_C (e.g. at 294, 299, and 305 K).
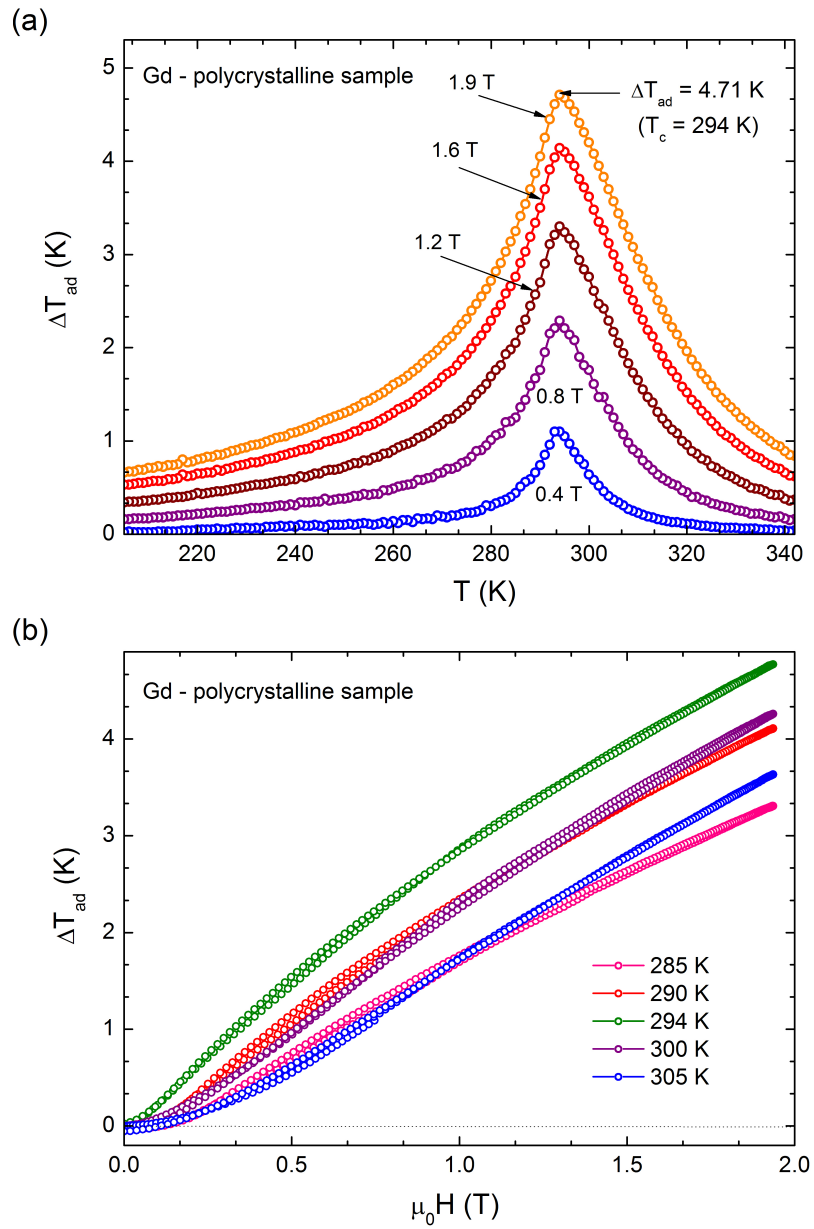
(a)

(b)

Figure 4.2: *The adiabatic temperature change,* ΔT_{ad}, *as a function of (a)
temperature and (b) magnetic field, for Gd measured in quasi-static fields
up to 1.9 T. Data taken at TU Darmstadt by K. P. Skokov.*

(a)

(b)

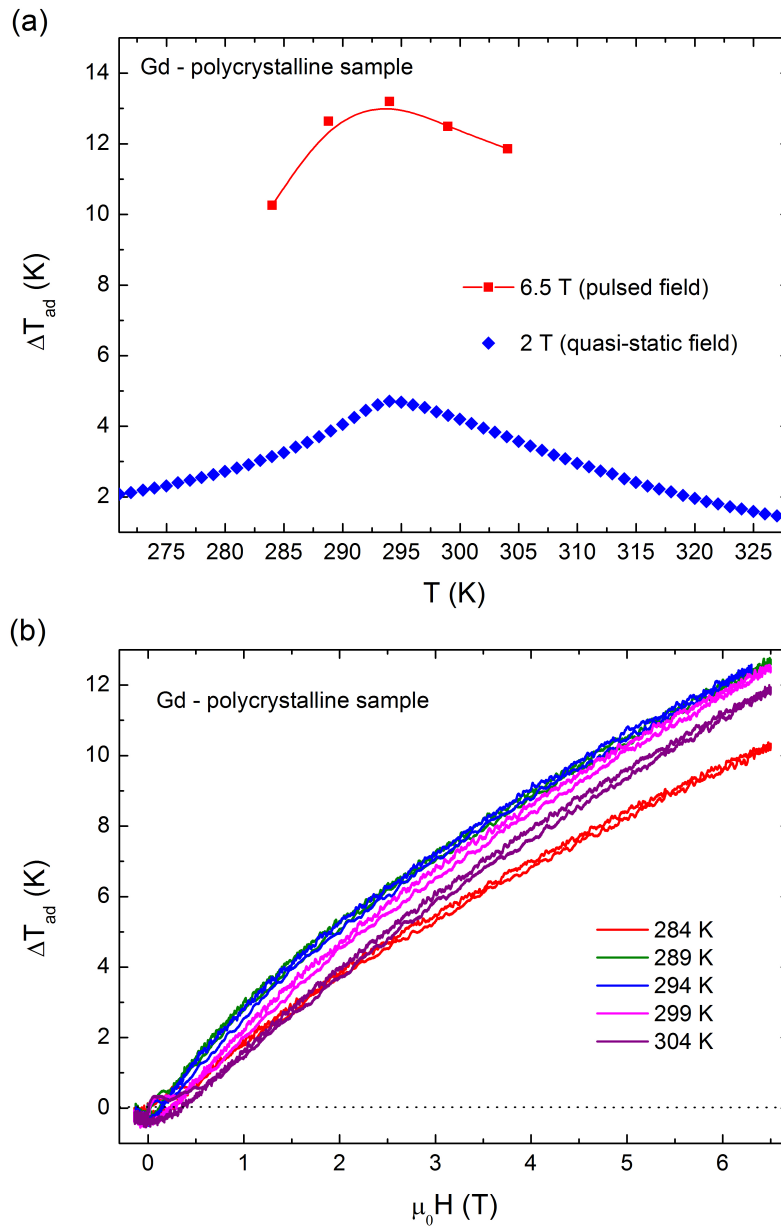Figure 4.3: *(a) Comparison of ΔT_{ad} for Gd measured in pulsed magnetic fields of 6.5 T (red symbols) and in quasi-static fields of 1.9 T(blue symbols). (b) Field dependence of ΔT_{ad} for a pulse-magnetic-field change of 6.5 T.*
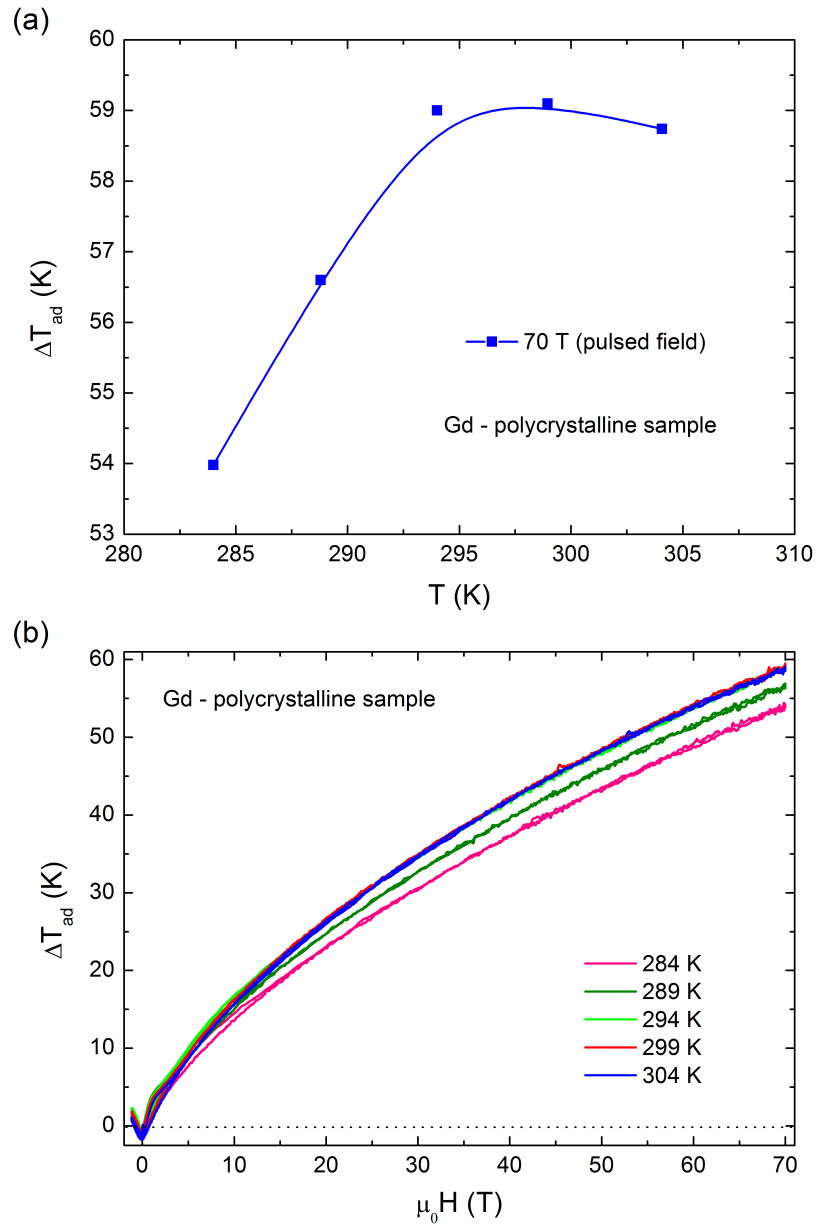
Figure 4.4: *The adiabatic temperature change, ΔT_{ad}, as a function of (a) temperature and (b) magnetic field for Gd measured in pulsed magnetic fields of 70 T.*

4.3 Magnetic-field dependence of the maximum adiabatic temperature change

As mentioned previously, one of the important quantities for the evaluation of the MCE is the adiabatic temperature change, ΔT_{ad}. In simple ferromagnets, the temperature dependence of ΔT_{ad} reaches its highest value near the Curie point T_C [36, 72, 73]. When considering only ferromagnets with a second-order phase transition at T_C, the temperature dependence of ΔT_{ad} shows a caret-like shape [36]. Besides, by changing the magnetic field H, ΔT_{ad} increases vertically around T_C while the shape is not affected by H [see Fig. 4.2(a)]. The height of this peak, $(\Delta T_{ad})_{max}$ grows with H with some field dependence discussed below [74]. Considerable effort has been devoted in finding the exact field dependence [75, 76, 77]. In 1984, Oesterreicher *et al.* [78] used a mean-field theory and found the relation $(\Delta T_{ad})_{max} \propto H^{2/3}$. However, in reality this simple relation between $(\Delta T_{ad})_{max}$ and H does not hold, but contains some extra terms [79, 80]. Remarkable progress in this field was made by Romanov *et al.* in 1997 [81] and later on by Amaral *et al.* in 2008 [82], who used Landau's theory of second-order phase transitions. By that, the following expression was obtained [74, 77, 80]:

$$(\Delta T_{ad})_{max} = \alpha \left(\frac{H}{4b} \right)^{2/3} - \frac{\alpha^2}{18b} \Delta T_C, \qquad (4.1)$$

where α and b are positive parameters independent of temperature or H and ΔT_C is the distribution width of transition temperatures around T_C.

It seems obvious that the above relation is valid only for a limited range of magnetic fields. For example, it fails for small fields, because in the limit $H \to 0$, $(\Delta T_{ad})_{max}$ must vanish. Also, it predicts an unlimited growth as $H \to \infty$ while $(\Delta T_{ad})_{max}$ has an upper limit [80].

However, more recently Lyubina *et al.* [80] also based on Landau's theory for second-order phase transitions for Eq. (4.1) showed that

$$(\Delta T)_{max} = A(H + H_0)^{2/3} - AH_0^{2/3} + BH^{4/3}, \qquad (4.2)$$

where A and B are intrinsic material constants, while H_0 is an extrinsic parameter determined from the purity and homogeneity of the sample. The last term,

$BH^{4/3}$, is needed at higher fields to account for incipient saturation.

In order to verify Eq. (4.2) experimentally for Gd, we plotted the adiabatic-temperature-change data at $T_C \approx 294$ K, shown already in Fig. 4.4(b), against $H^{2/3}$ (see Fig. 4.5). For not too small magnetic fields an approximate version of Eq. (4.2) can be used to describe the data, namely [74]:

$$(\Delta T)_{max} = A(H^{2/3} - H_*^{2/3}),\qquad (4.3)$$

where A and H_* are fit parameters. Note, from Eq. (4.2) follows, $\Delta T_{ad} \propto H$ for H being small.

The plot of the Gd data in Fig. 4.5 shows that the data perfectly follow the $H^{2/3}$ dependence and even for magnetic fields up to 70 T the $H^{4/3}$ term is not needed. The slight deviation at low fields is mainly caused by switching noise at the beginning of the pulsed field. The parameters A and H_* can be easily found from the fit yielding

$$A = 3.48 \text{ K}\mu_0^{2/3}\text{T}^{-2/3}, \qquad H_* = -0.03,$$

which is in good agreement with literature data ($A \approx 3.83 \text{ K}\mu_0^{2/3}\text{T}^{-2/3}$) [74]. A is an intrinsic property of the material, whereas H_* is determined by impurities or inhomogeneities of the material and H_* should go to zero for an ideal material.
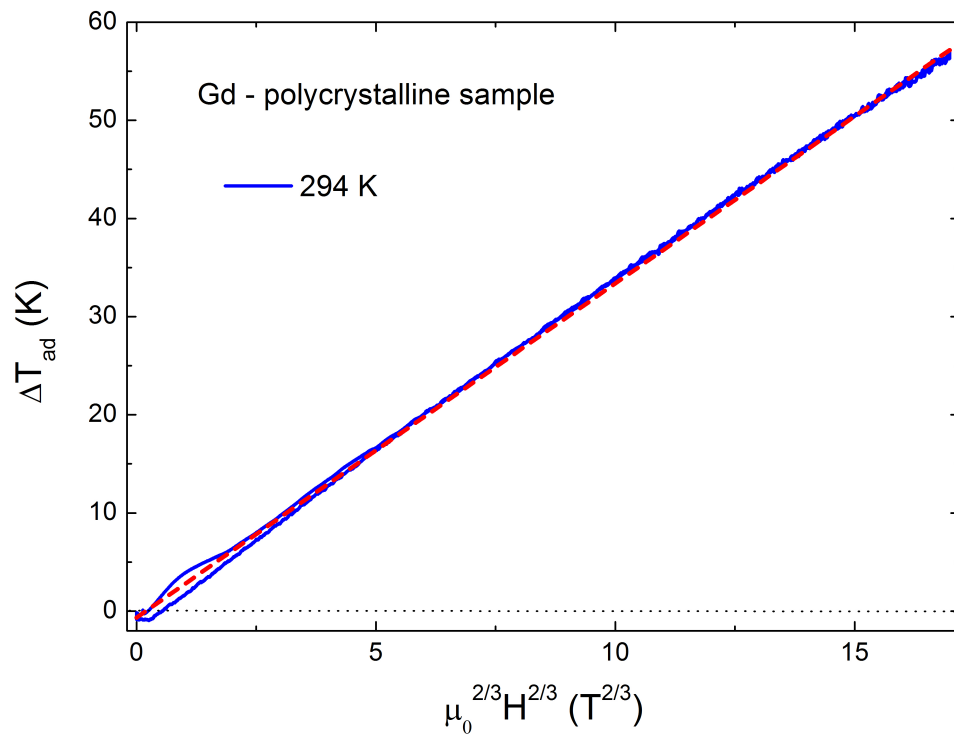
Figure 4.5: *Magnetic-field dependence of the adiabatic temperature change for Gd. The red dashed line is a fit using Eq. (4.3).*

4.4 Summary

In summary, we have investigated the magnetocaloric properties of a polycrystalline gadolinium sample by means of MCE measurements in pulsed and quasi-static magnetic fields, providing the temperature and field dependence of the adiabatic temperature change. Gd shows a second-order phase transition with a Curie temperature of ∼294 K. As expected for materials with a second-order phase transition, there are no signs of hysteresis or irreversible behavior in our magnetocaloric experiments. The maxima of ΔT_{ad} are found to be 4.7 and 13 K for a field change of 2 and 6.5 T, respectively. Taking into account the effect of different sample quality, our results are in good agreement with reported literature data [70]. For the first time, we measured the MCE in a polycrystalline Gd in pulsed magnetic fields up to 70 T. We find a very large adiabatic temperature change of $\Delta T_{ad} \approx 60$ K. Unlike the low-field data, there is no sign of a pronounced maximum for a field change of 70 T. In addition, our ΔT_{max} data are found to follow perfectly a $H^{2/3}$ dependence even for magnetic fields as high as 70 T.

5 Magnetocaloric effect in Ni$_{50}$Mn$_{35}$In$_{15}$

5.1 Overview of the Ni-Mn-In Heusler alloys

Heusler alloys are named after Fritz Heusler, a 19th-century German mining engineer and chemist, who discovered the ferromagnetic alloy with composition Cu$_2$MnAl, while containing no ferromagnetic element [83, 84, 85]. Heusler alloys are ternary intermetallic compounds with the stoichiometry X$_2$YZ (2:1:1), known as "full-Heusler" compounds with L2$_1$ cubic crystal structure, and with the stoichiometry XYZ (1:1:1), known as "half-Heusler" materials with C1$_b$ cubic structure with one of the fcc lattices unoccupied [86] (see Fig. 5.1).

The recent discovery of room-temperature giant MCEs compounds has initiated tremendous efforts to develop magnetic refrigerators working close to ambient conditions further [11, 87]. Giant MCE materials own their high performance the strong coupling between the spin subsystem and the crystallographic structure. Therefore, a simultaneous change of magnetic and lattice entropies can be induced by applying a magnetic field [11, 15].

Among the most promising materials, Heusler-type Ni-Mn-In magnetic shape-memory alloys are attractive candidates for both fundamental research and application. These alloys have been shown to exhibit diverse functional properties such as shape memory [88, 89], magnetic superelasticity [44], magnetocaloric [15], and barocaloric effects [90], which originate from their strong magnetoelastic couplings.

Ni$_{50}$Mn$_{35}$In$_{15}$ exhibits on cooling a paramagnetic to ferromagnetic transition around 315 K, followed by a first-order structural transition from a cubic high-temperature phase to a low-temperature monoclinic phase at around 246 K,
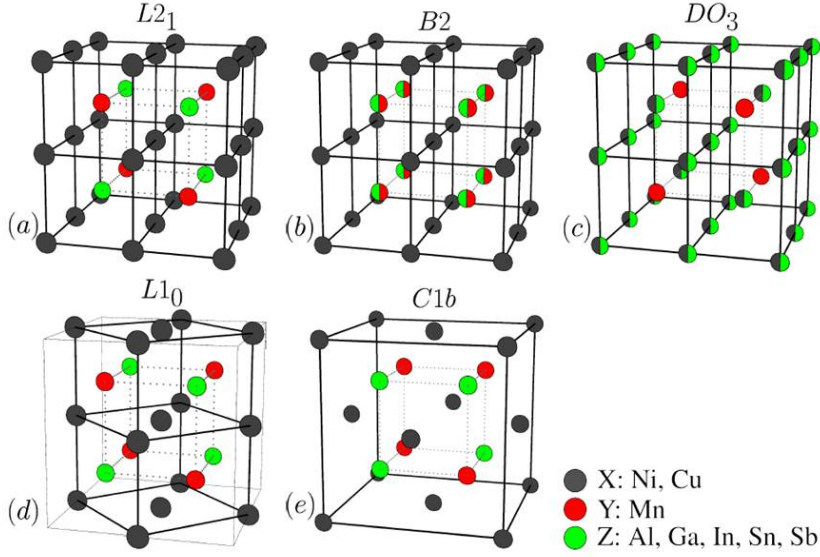
Figure 5.1: *Different types of Heusler austenite crystal structures: (a) $L2_1$ of Cu_2MnAl; (b) B2, CsCl-like; (c) DO_3, Fe_3Al-like; (d) full Heusler martensitic cell: two stacked $L1_0$ cells, AuCu-like and (e) half-Heusler alloy lattice $C1_b$, CaF_2-like. Taken from Ref. [91].*

the so-called martensitic transition. A conventional MCE is observed around the ferromagnetic transition in the austenitic phase. Here, under adiabatic conditions an increase in the sample temperature is observed upon application of a magnetic field. Additionally, an inverse MCE occurs around the martensitic first-order transition leading to a decrease in the sample temperature with increasing field. For this class of materials, the total adiabatic temperature change at the magnetic-field-induced martensitic transition can be decomposed as $\Delta T_{ad} = \Delta T_{ad}^{str} + \Delta T_{ad}^{mag}$, where ΔT_{ad}^{str} and ΔT_{ad}^{mag} denote the structural and magnetic contribution of the temperature change, respectively. When the field is applied adiabatically, the magnetic moments align and as a result the sample heats up $\Delta T_{ad}^{mag} > 0$ (Fig. 5.2, top row). At the same time, the structural transition from the low-magnetization and low-symmetry martensitic phase to the high-magnetization and high-symmetry austenitic phase leads to a very large cooling effect (Fig. 5.2, middle row). Since the total amount of heat absorption caused by the structural transformation exceeds the heat release from the magnetic subsystem, the sample temperature decreases under adiabatic conditions
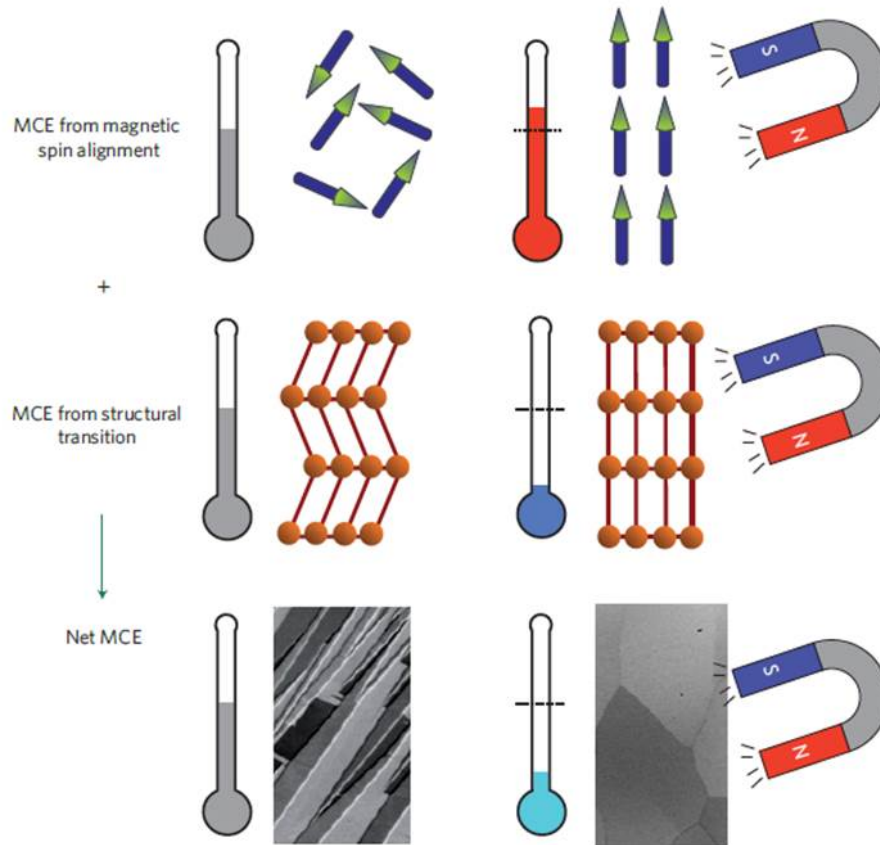
Figure 5.2: *Schematic sketches of the MCE contributions from the magnetic and structural part for a first-order magneto-structural transition. Taken from Ref. [15].*

upon application of a magnetic field $\Delta T_{ad} < 0$ (Fig. 5.2, bottom row) [15].

Polycrystalline ingots of Ni$_{50}$Mn$_{35}$In$_{15}$ were obtained by arc-melting stoichiometric amounts of the constituent elements under argon atmosphere. The ingots were remelted several times to assure a high homogeneity. Subsequently they were encapsulated in a quartz ampoule under argon atmosphere and annealed at 800 ℃ for 2 h and then quenched in ice water. The high quality of the samples was confirmed by powder X-ray diffraction.

In this chapter, we report on a detailed study of the MCE in a Ni$_{50}$Mn$_{35}$In$_{15}$ sample by direct magnetocaloric measurements in pulsed magnetic fields and by analyzing specific-heat data taken in static magnetic fields. Magnetization and specific-heat measurements were carried out in a physical property measurement system (Quantum Design). Direct measurements of ΔT_{ad} were performed in our home-built experimental setup in pulsed magnetic fields up to 50 T, as described in detail in chapter 3.

5.2 Magnetization

Figure 5.3(a) shows temperature-dependent magnetization curves, $M(T)$, of $Ni_{50}Mn_{35}In_{15}$ measured at 0.1 and 5 T, following FC (field-cooled) and FH (field-heated) protocols. The ferromagnetic transition in the austenitic phase takes place at $T_C \approx 315$ K, and the martensitic transition from the austenitic to the martensitic phase is observed on cooling at $T_M \approx 246$ K and on heating around $T_A \approx 257$ K. The applied field of 5 T shifts the martensitic transition temperature by about -7 K, which indicates that the magnetic field stabilizes the austenitic phase.

The field-dependent magnetization data in Fig. 5.3(b) indicate that it is possible to induce the reverse martensitic transition also by the application of a magnetic field; at 150 K, a field of 14 T is sufficient to observe a completed transition. For each $M(H)$ measurement the sample was cooled down from 350 K (austenitic phase) to 100 K (complete martensitic phase) in zero field and then heated up to the target temperature of the experiment. By this protocol we assure that the sample is always in the same, fully martensitic, initial state and that we can exclude any influence of hysteresis effects on the results. At 150 K, we determined from the inflection point in $M(H)$ a critical field of $H_A \approx 13$ T for inducing the transition from the martensitic to the austenitic state at a much lower field. When the field is removed again, the sample is transformed back to the martensitic state. Note, for temperatures close to the transition at T_A part of the sample remains in the austenitic phase after removing the magnetic field. We observe a hysteresis of $2 - 3$ T between the critical fields upon increasing and decreasing the magnetic field. Upon increasing the temperature toward T_A the critical field, $H_A(T)$, decreases.
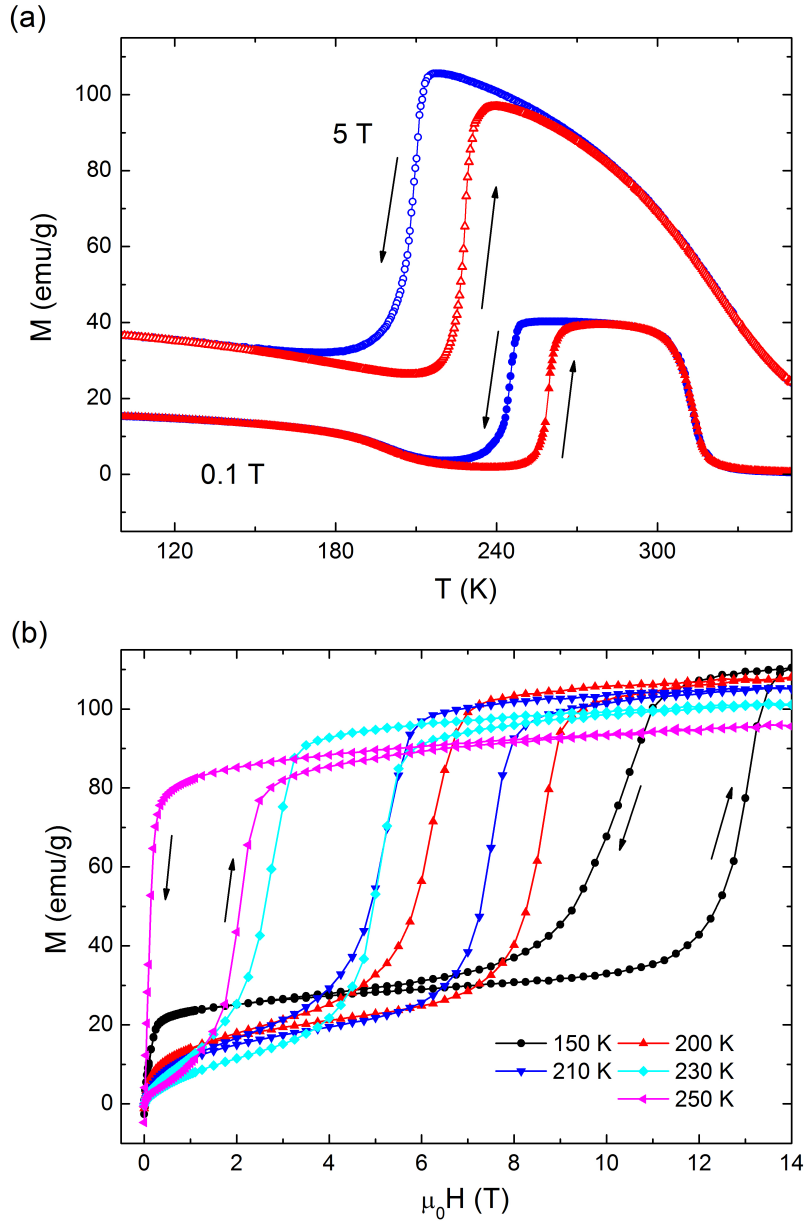
Figure 5.3: *(a) Field-cooled (circles) and field-heated (triangles) magnetization data measured in 0.1 (closed symbols) and 5 T (open symbols). (b) Isothermal-magnetization data measured in magnetic fields up to 14 T for different temperatures below T_A. Each measurement was preceded by heating up the sample to the fully austenitic state and then cooling down to the completely martensitic state (100 K) before approaching the measurement temperature. Data taken at the Max Planck Institute by C. Salazar Mejía [92].*

5.3 Magnetocaloric effect

The MCE, ΔT_{ad}, was measured by both direct and indirect methods. Figure 5.4 shows the time dependences ΔT_{ad}^t for selected temperatures recorded during the application of a pulsed field of (a) 6 and (b) 20 T together with the corresponding pulse profiles. For the pulsed-field measurements at temperatures below the martensitic first-order transition the sample was cooled down from 350 to 100 K in zero field and then heated up to the target temperature as in the case of the field-dependent magnetization measurements. Note, the little bumps observed at the beginning of the ΔT_{ad}^t curve in the 20 T experiments are contributions from the magnetization change in the sample. Unavoidable small open loops in the thermocouple wires act like magnetization pick-up coils and detect the metamagnetic transition [Fig. 5.3(b)] of the sample. The inset of Fig. 5.4(b) exemplifies how a reversal of the field polarity affects the sign and magnitude of the bump, confirming that it is not related to the MCE response. To minimize this effect at all temperatures two measurements taken on a positive and on a negative field pulse have been averaged.

Around the Curie temperature in the austenitic phase, $T_C \approx 315$ K, we observe a conventional MCE as expected (see the data at 300 and 340 K in Fig. 5.4). As the field is applied the magnetic moments in the austenite fully align with the field and the magnetic entropy decreases. Since the measurement is performed adiabatically, the decrease in the magnetic entropy is compensated by an increase of lattice entropy leading to an increase in the temperature of the sample. Furthermore, the effect is reversible, i.e., after the magnetic pulse the sample cools back to the starting temperature. We point out that the position of the maximum of the magnetic-field pulse roughly coincides with that of the maximum in ΔT_{ad}^t.

On the other hand, the ΔT_{ad}^t data at temperatures below the martensitic transition show a completely different behavior. When the field is applied, the structural transformation is induced and strongly negative ΔT_{ad}^t occur as shown in Fig. 5.4 (with the exception of the measurement at 200 K in the 6 T field range). This transformation leads to a strongly induced lattice entropy which results, in an adiabatically conducted experiment, to a negative temperature change (inverse MCE), $\Delta T_{ad}^{str} < 0$. Furthermore, the structural transforma-

tion involves a change in the magnetic state of the sample. The magnetization increases involving a negative entropy change (conventional MCE) corresponding to a positive temperature change, $\Delta T_{ad}^{mag} > 0$. As mentioned already, the structural contribution works against the magnetic contribution to the total MCE. As the structural contribution is dominant for temperatures close to the martensitic transition, an inverse MCE is observed, i.e., the sample cools upon application of the magnetic field, $\Delta T_{ad} = \Delta T_{ad}^{str} + \Delta T_{ad}^{mag} < 0$ [15]. Moreover, close to T_A the inverse effect is irreversible and the sample does not recover to the initial temperature after the magnetic field is removed and the maximum of the pulsed field does not coincide with the minimum in ΔT_{ad}^{t}.

For all measured temperatures below 300 K (except for 200 K and 6 T) the applied magnetic field is large enough to induce and observe a complete reverse martensitic transition (see Fig. 5.4). Thus, a pure austenitic state is reached at the end of the field-up sweep. As mentioned previously, a hysteresis of $2-3$ T is present between the induced transition in the up and down sweep. In more detail, as the magnetic field is reduced again, we first observe a conventional MCE due to the change of the magnetic entropy in the ferromagnetic austenitic phase and the sample continues to cool down further [15, 93, 94]. As the field continues to decrease, the sample transforms back to the martensitic phase at a lower critical field of the field-induced martensitic transition [Fig. 5.3(b)] leading to an increase in lattice entropy. As a consequence, the sample starts to heat up again, $\Delta T_{ad}^{str} > 0$. Depending on the temperature the material either recovers the martensitic phase completely [see for instance the data at 230 K with field pulse of 6 T in Fig. 5.4(a)], or a mixed martensitic/austenitic state is established (see the data at 240 and 250 K). In the latter case, only part of the sample transforms back and, therefore, a smaller change in temperature is observed in the down sweep compared to the up sweep. As a result, the final temperature of the sample is lower than the initial one. In particular, for the starting temperature 255 K with 6 T pulse the temperature of the sample after the field pulse remains below the starting temperature, consequently, the sample does not transform back to the martensite and no further heating is observed.
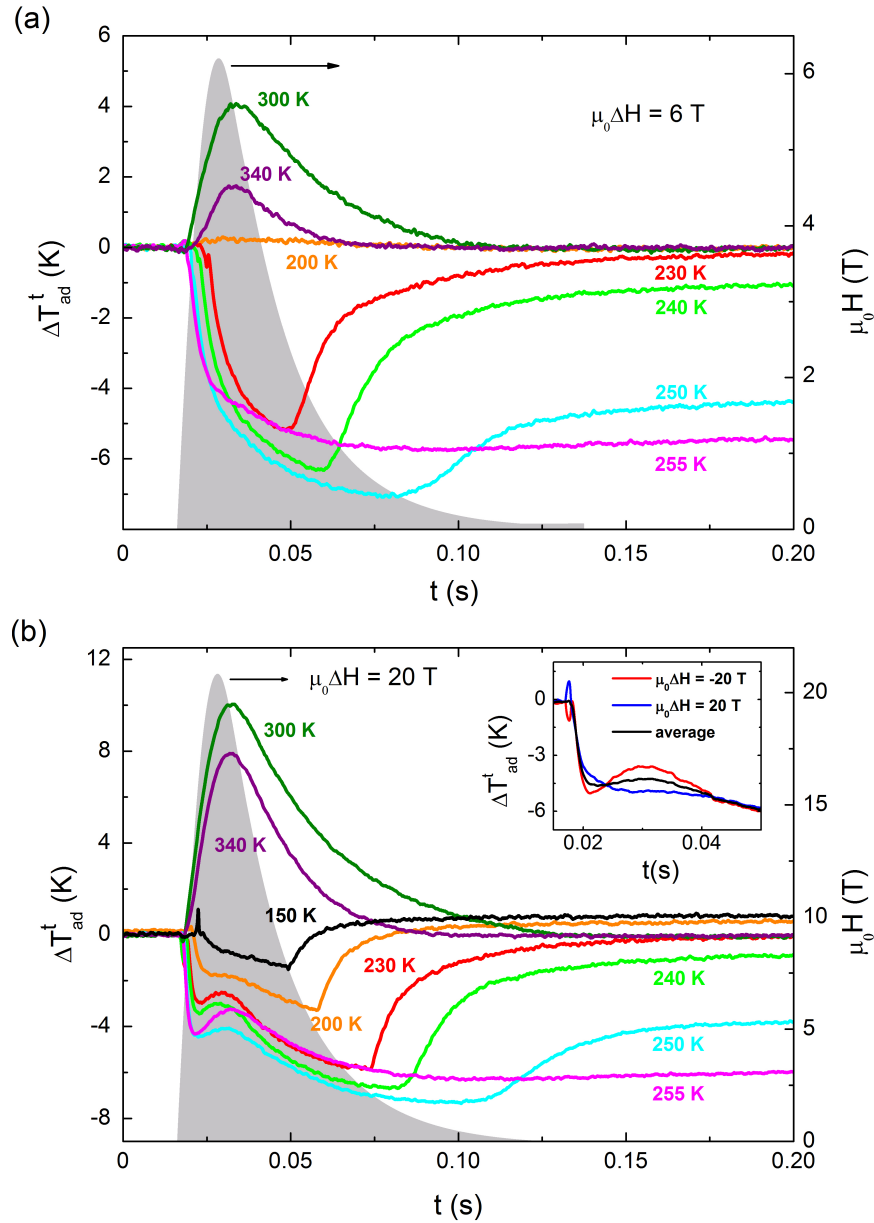
Figure 5.4: *Time dependences of the adiabatic temperature change at (a) 6 T and (b) 20 T, measured in pulsed magnetic fields. Each measurement was preceded by heating up the sample to the fully austenitic state and then cooling down to the completely martensitic state (100 K) before approaching the measurement temperature. The field profile is also indicated (right axis). The inset shows the temperature dependence of ΔT_{ad} with pulsed fields of -20 T and 20 T at 240 K and the average of the two [92].*

Additionally to the MCE experiments in pulsed magnetic fields, we carried out specific-heat measurements in zero field and in an applied field of 6 T. The specific-heat data are presented in Fig. 5.5(a). For the measurement in magnetic field the sample was cooled in zero field from the austenitic phase down to 2 K, then the magnetic field was applied, and the specific heat was recorded on heating from 2 to 380 K. At the first-order martensitic transition we carefully analyzed the slope of the temperature profile of a long heat pulse to obtain the specific heat [95]. This procedure avoids an underestimation of the specific heat due to the latent heat at the first-order phase transition [95, 96].

From these results we calculated the temperature dependence of the total entropy for 0 and 6 T and subsequently the adiabatic temperature change, ΔT_{ad} (see Eqs. (2.16) in chapter 2) [28]. ΔT_{ad} obtained from the specific-heat data is presented in Fig. 5.5(b) together with the results of the direct measurements. As mentioned before due to the finite response time of the thermocouple and the pick-up of a magnetic signal due to the change in magnetization at the metamagnetic transition, it is not possible to trace the time (field) dependence of ΔT_{ad}^t precisely, only the maximum/minimum in ΔT_{ad}^t is well defined and those values are plotted as ΔT_{ad} in Fig. 5.5(b). We find, as expected, an inverse MCE in the region below the martensitic transition and a conventional MCE around the ferromagnetic transition of the austenitic phase, i.e., in an adiabatic environment the sample cools down and warms up, respectively, upon increasing the magnetic field.

An important feature, which we want to point out is that the MCE just below the martensitic transition saturates already in small magnetic fields. ΔT_{ad} reaches a value of around -7 K at 6 T which does not change up to 20 T anymore. With a field change of 20 T, ΔT_{ad} displays a broader peak, since the reverse martensitic transition can be induced also at lower temperatures. Our findings confirm that the inverse MCE due to the first-order martensitic transition is limited by the latent heat of the transition [97]. We note that the martensitic transition can be induced by a field of 20 T even at 4 K [98]. With increasing temperature this critical field decreases and for 150 K the transition is already completed at 14 T, as visible in Fig. 5.3(b). However, the MCE measured at this temperature is only 20% of the maximum value at 250 K. This behavior is related to the decrease in the entropy change at the structural
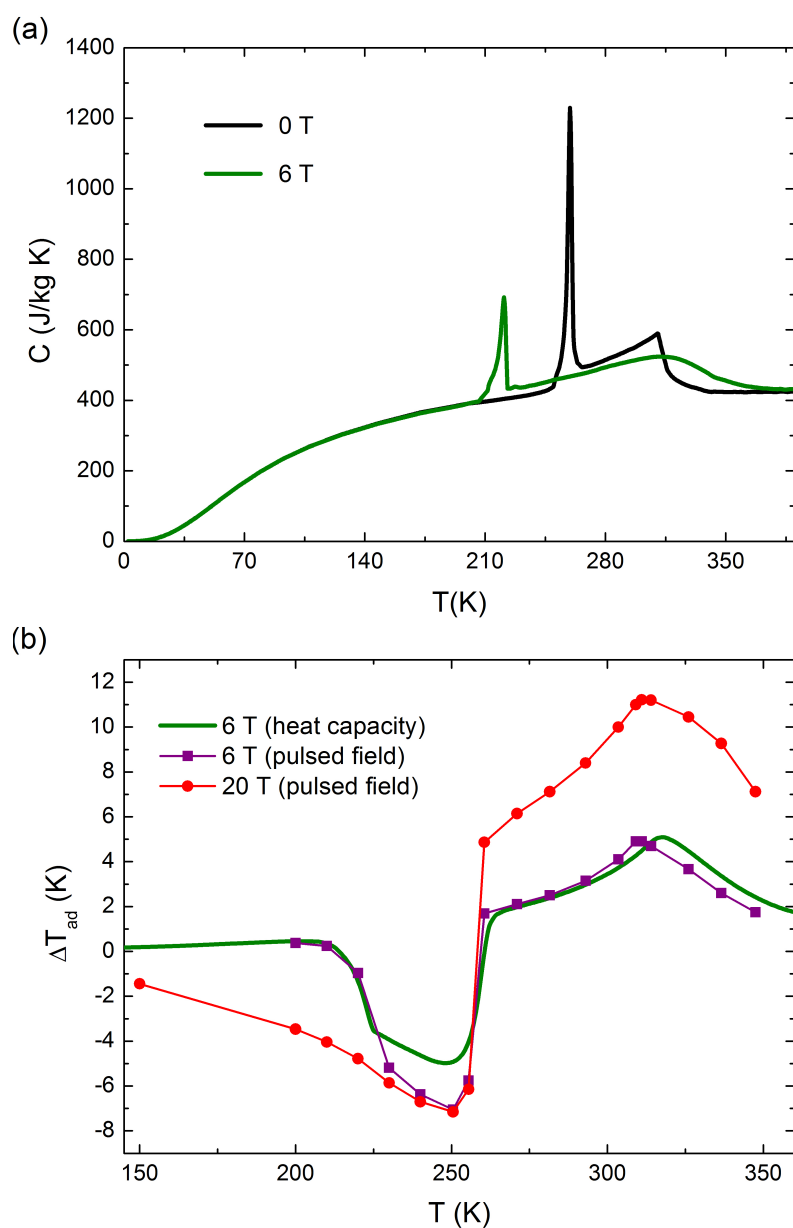
Figure 5.5: *(a) The temperature dependence of the specific heat at 0 and 6 T. (b) The adiabatic temperature change, ΔT_{ad}, as a function of temperature obtained from specific-heat data in a field of 6 T and magnetocaloric measurements in pulsed fields of 6 and 20 T. Specific-heat data taken at the Max Planck Institute by C. Salazar Mejía [92].*

transition with decreasing temperature [99].

Around the second-order ferromagnetic transition in the austenitic phase ($T_C \approx 315$ K) we find good agreement between the results obtained from the specific-heat and from the MCE measurements in pulsed fields, but there are distinct discrepancies below the first-order martensitic transition. At temperatures just below the martensitic transition the minimum in the time-depended temperature change, ΔT_{ad}^t, is observed for a magnetic field beyond the field-pulse maximum on the down sweep (Fig. 5.4). This maximum in $|\Delta T_{ad}^t|$ corresponds, therefore, not only to the MCE as it is generally defined. As we have discussed before, at these temperatures an inverse MCE is observed, i.e., the sample cools down due to a dominant structural contribution ($\Delta T_{ad}^{str} < 0$ and $\Delta T_{ad}^{mag} > 0$). This is the value of ΔT_{ad} extracted from the specific-heat experiments in static fields, but in case of the pulsed-field experiments decreasing the magnetic field leads to a further cooling of the sample, since $\Delta T_{ad}^{mag} < 0$ and, initially, $\Delta T_{ad}^{str} \approx 0$. Only once the field-induced structural transition takes place upon further lowering the magnetic field, ΔT_{ad}^{str} provides a positive contribution to $\Delta T_{ad}^t(t)$.

The observed irreversibility in the MCE is expected in shape-memory Heusler materials [93, 97]. It originates from the thermal/magnetic hysteresis at the first-order martensitic phase transition. Therefore, field cycling or repeated measurements at the same temperature without considering the magnetic and thermal history of the sample lead to undefined results in the MCE. To study the influence of the irreversibility of the transition on the MCE for temperatures close to T_A, we have measured M and ΔT_{ad}^t in two subsequent magnetic-field sweeps. The second pulse was applied after waiting one hour after the first pulse, which was performed following our standard protocol as mentioned above. Figure 5.6 displays the results at 250 K for (a) ΔT_{ad}^t and (b) M. The magnetization data indicate that pulse 1 induces the reverse martensitic transition and that the sample stays in the austenitic phase. After one hour, only a small part of the sample has transformed back to the martensitic phase. Thus, the entropy change due to the second pulse is much smaller and the maximum temperature change of the sample is less than $1/2$ of that observed in the first pulse, $|\Delta T_{ad}| \approx 6$ K [Fig. 5.6(a)]. This observation is consistent with the M data obtained during the second pulse, i.e., only part of the sample is in the marten-

sitic state and can still transform to the austenitic phase. Furthermore, ΔT^t_{ad} stays almost constant after the initial decrease; the temperature relaxes only very slowly towards the starting temperature. This behavior hampers the use of shape-memory alloys in possible applications since to have a maximum cooling effect the sample needs to be brought to the initial conditions before each cooling cycle.
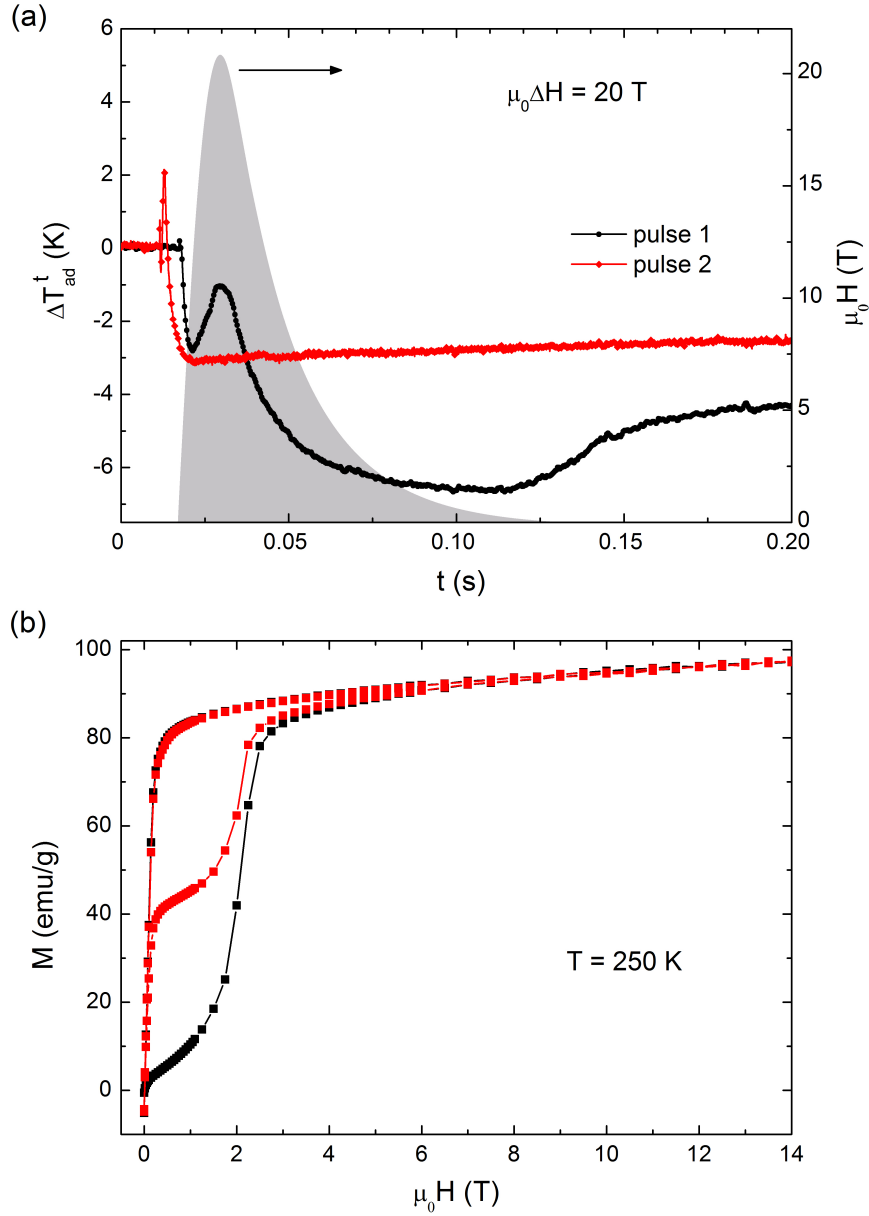
Figure 5.6: *(a) Time dependence of ΔT_{ad}^t measured at 250 K for a magnetic-field pulse of 20 T. Before measuring the initial curve (black circles) the sample was heated to the fully austenite state and then cooled down to the complete martensitic state (100 K). The second curve (red diamonds) was taken 1 hour after the first pulse. The field profile is also shown (right axis). (b) The corresponding field-dependent magnetization data following the same protocol. Magnetization data taken at the Max Planck Institute by C. Salazar Mejía [92].*

5.4 Summary

In summary, we have investigated the MCE in the shape-memory Heusler alloy $Ni_{50}Mn_{35}In_{15}$ by direct magnetocaloric measurements in pulsed magnetic fields and by specific-heat experiments in constant fields. The conventional MCE around the Curie temperature in the austenitic phase exhibits a strong magnetic-field dependence; for a field change of 20 T we find a maximum ΔT_{ad} of about 11 K. In this region of the phase diagram we do not find any hysteresis or irreversible behavior in the magnetocaloric experiments neither in static nor in pulsed-magnetic fields. Furthermore, ΔT_{ad} is in a good agreement with data from specific heat. This changes below the martensitic phase transition. Here, we observe an inverse MCE, which originates from structural and magnetic contributions. In the direct magnetocaloric experiments we find a saturating MCE with a maximum negative temperature change of $\Delta T_{ad} = -7$ K. This value is significantly larger than the calculated results from the specific heat suggest. The cause for this lies in the hysteresis observed at the martensitic phase transition which leads to a strongly irreversible time and field dependence of ΔT_{ad}^t below the martensitic phase transition. This irreversible behavior has to be carefully taken into consideration for using shape-memory Heusler alloys in magnetocaloric-cooling applications, especially, since the length of the magnetic-field pulse is comparable to the inverse of useful operation frequencies of cooling devices [92].

6 Magnetocaloric effect in La(Fe,Si,Co)$_{13}$

6.1 Overview of the La(Fe$_{13-x}$Si$_x$)-based compounds

La(Fe$_{13-x}$M$_x$) intermetallic compounds have been investigated since the late 1960s [100, 101] and their magnetic properties were originally described by Palstra *et al.* [102, 103] in the mid-1980s. Bulk LaFe$_{13}$ material does not exist due to a positive heat of formation between La and Fe, but adding small amounts of other elements, such as Si, Co, or Al stabilizes the intermetallic La(Fe$_{13-x}$M$_x$) phases. The La(Fe$_{13-x}$M$_x$) compounds have the cubic NaZn$_{13}$-type structure [36, 100, 101, 102, 103], which is illustrated in Fig. 6.1. The unit cell has 8 formula units, i.e., 112 atoms, with a large atom such as La or Na in the $8a$ positions (Wyckoff notation). The smaller atoms such as Zn, Fe, Co, Si, or Al are located either in the $8b$ positions or the $96i$ positions. In the $96i$ positions, the smallest atoms build ordered icosahedra[1] surrounding the $8b$ positions. Hence, for each formula unit of e.g. LaCo$_{13}$, one Co atom will sit in the center of an ordered icosahedron made up of other 12 Co atoms [20].

In 1999, Fujita *et al.* [104] reported for La(Fe$_{11.44}$Si$_{1.56}$) a large volume change, ~1.5%, above the Curie temperature, 195 K, as observed in measurements up to magnetic fields of 10 T. They suggested that because of the large volume change and sharp itinerant-electron metamagnetic transition (IEM), this alloy might have some interesting magnetocaloric behavior [36].

In 2001, a giant MCE in the La(Fe$_{13-x}$Si$_x$) compounds was first reported by Hu *et al.* [39] . They reported $\Delta S_M = -140$ mJ/cm^{3}K^{-1} for La(Fe$_{11.4}$Si$_{1.6}$) for

---

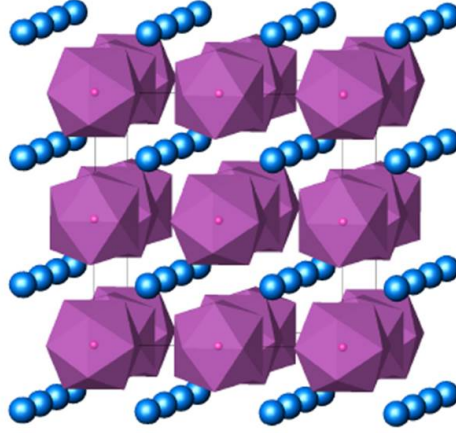[1] A polyhedron having 20 faces and 12 vertices.

Figure 6.1: *The cubic structure of NaZn$_{13}$. The large atoms (blue) sit interstitially in the 8a site between icosahedra (made out of 12 Co atoms) of smaller atoms in the 96i site (purple), which surround a central smaller atom in the 8b site. Taken from Ref. [20].*

a field change of 5 T at $T_C = 208$ K (for comparison with other MCE materials see Fig. 2.5). They also found that with an increase of Si content, the magnetic ordering temperature is raised and the MCE is considerably reduced [36].

Among the promising magnetocaloric materials, La(Fe,Si)$_{13}$-based compounds are most attractive candidates and have been widely studied from the point of view of fundamental research and practical applications [17, 18, 39, 53, 104, 105]. These alloys have shown a large MCE and have the advantage to consist of low-cost materials compared to other MCE alloys, e.g. Gd$_5$(Si,Ge)$_4$, because they mainly consist of Fe and light rare-earth elements. Further, the constituent elements are non-toxic unlike MnAs-based compounds [106, 107]. In addition, they demonstrate small thermal/magnetic hysteresis, large relative cooling power and high thermal conductivity [108, 109].

For all the magnetic NaZn$_{13}$-structured materials, the type of phase transition and the transition temperature are extremely sensitive to the composition. In the composition range $1.0 \leqslant x \leqslant 1.6$, LaFe$_{13-x}Si_x$, the compounds undergo a first-order magnetic phase transition from a high-temperature paramagnetic

(PM) to a low-temperature ferromagnetic (FM) state. Additionally, above the Curie temperature, a first-order IEM transition from PM to FM is induced by applying an external magnetic field [36, 104, 109, 110].

The IEM transition is related to a change in the band structure of the 3d electrons by applying a magnetic field. Therefore, the origin of the IEM transition is associated with a special 3d band structure which exhibits a sharp peak of the density of state (DOS) just below the Fermi level [111, 112]. This transition is connected with a structural transition, which, however, is only a volume change ($\sim$1.5%) without a change in symmetry.

As x increases, a transformation of the phase transition from first-order to second-order takes place. When $1.6 < x \leqslant 2.0$ a typical second-order transition occurs and the corresponding magnetic-entropy change and, therefore, ΔT_{ad} becomes smaller [113]. With a further increase of the Si content, a tetragonal structure is formed [109, 114].

Although the LaFe$_{13-x}$Si$_x$ compounds display a giant MCE, a maximum in ΔT_{ad} usually appears at low temperatures (< 210 K). For the purpose of practical applications, it is desired to have the maximum temperature change near ambient temperatures. Therefore, it is crucial to find out an effective approach to shift T_C to higher temperatures without remarkably affecting ΔT.

Hu *et al.* [39, 115] found that Co substitution for Fe significantly increases T_C from $\sim$185 to $\sim$330 K. However, Co additions weaken the nature of the first-order transition and decrease the value of ΔT_{ad}. As shown in Fig. 6.2, the ΔT versus T curves of low x are sharp and show large MCEs, which is typical for first-order transition. While for the second-order transitions the MCE peak is broader. Therefore, it is of great interest to investigate the MCE dependence on alloying LaFe$_{13-x}$Si$_x$ showing a change in the nature of the transition. From this point of view, we investigated two compositions of La(Fe,Co,Si)$_{13}$: LaFe$_{11.74}$Co$_{0.13}$Si$_{1.13}$ (LFCS1) with a first-order transition, and LaFe$_{11.21}$Co$_{0.65}$Si$_{1.11}$ (LFCS2) with a second-order transition. For simplicity we use in the following the abbreviations for each compound as indicated above.

The samples were produced and supplied by Vacuumschmelze GmbH [116], which has a long history of manufacturing and handling magnetic materials. Vacuumschmelze uses a powder-metallurgy method which makes industrial-scale production feasible.

In this chapter, we report on a detailed study of the magnetic and magnetocaloric properties of LFCS1 and LFCS2. Various experimental techniques have been used to obtain a more complete information on these compounds. The MCE is determined by means of direct measurements in pulsed magnetic and quasi-static fields as well as indirect measurements (from specific-heat data). In addition, adiabatic and isothermal magnetization data are presented. Finally, magnetostriction measurements in pulsed magnetic and in quasi-static fields are discussed in detail.
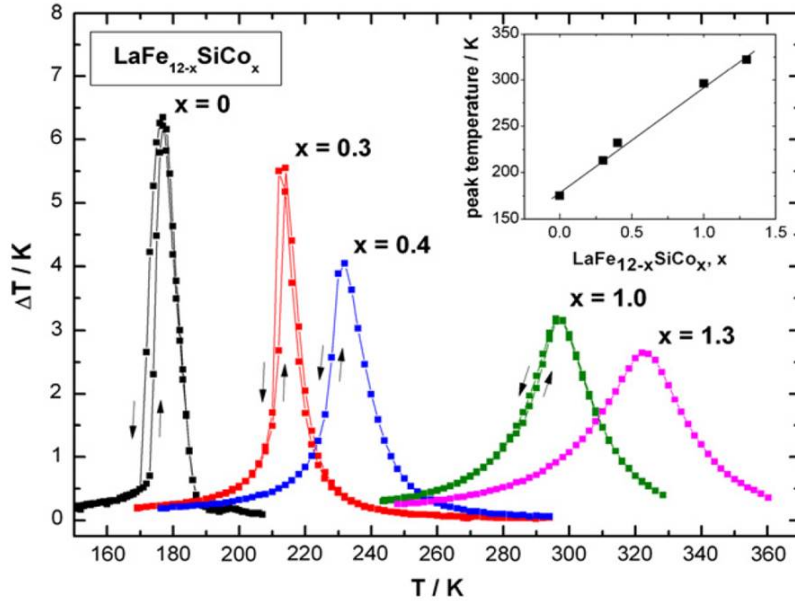

Figure 6.2: *Adiabatic temperature change as a function of temperature for*
LaFe₁₂₋ₓSiCoₓ, (x = 0−1.3) and for magnetic-field changes of 1.9 T. With
increasing Co content the magnetic transition changes from first to second
order, and the value of ΔT_{ad} decreases from 6.5 K to 2.7 K. The inset
shows the MCE maximum temperature as a function of Co content. A
small thermal hysteresis is visible in all samples except for x = 1.3. Taken
from Ref. [106].

6.2 Magnetization

Figure 6.3(a) shows the field dependence of the isothermal magnetization for LFCS1 measured in magnetic fields up to 14 T for different temperatures around T_C. Characteristic S-shaped curves accompanied with magnetic hysteresis are observed. This is caused by a field-induced IEM transition that takes place just above T_C ($\approx$ 198 K). Upon increasing the temperature, the sharp IEM transition is gradually broadened over a wide magnetic-field interval and the hysteresis reduces. Moreover, the transition field increases with an average slope of 0.2 T/K. Note, the IEM transition is accompanied by an abrupt change of magnetization near T_C, resulting in a large MCE in the LFCS1 compound.

The field-dependent magnetization for LFCS1 measured in pulsed magnetic fields up to 60 T for different temperatures around T_C are shown in Fig. 6.3(b). As mentioned in chapter 3, the up-sweep time of the pulsed field is about 7 ms, which is way too short to keep the sample at a temperature in equilibrium with the environment. Therefore, the measurement of the pulsed-field magnetization should be considered as an adiabatic process. Although the magnetization data above T_C exhibit an S-shaped field dependence with magnetic hysteresis, for the same starting temperature (e.g. 198 K), the overall shape of the curves do not coincide with the static-field data.

To show the difference between the isothermal and adiabatic magnetization data, one curve from the pulsed-field measurement set with initial temperature of $T_0 = 198$ K is shown in Fig. 6.3(a)(black curve). The black arrows indicate the mismatch between the pulsed-field magnetization and the corresponding isothermal magnetization taken in static fields. This mismatch can be explained as follows: at low fields, the magnetization data almost coincide. As the magnetic field reaches the critical value, the sample under adiabatic conditions starts heating due to the MCE, and the magnetization at a given field should match the value from the corresponding isotherm measured at $T_0 + \Delta T_{ad}$. From that we can estimate the expected magnetocaloric effect. For example, it should amount to about 15 K for a field change of 5 T at starting temperature 198 K.

Figure 6.4(a) displays the isothermal magnetization curves for different temperatures around T_C ($\approx$ 257 K) for LFCS2. The field-dependent magnetization
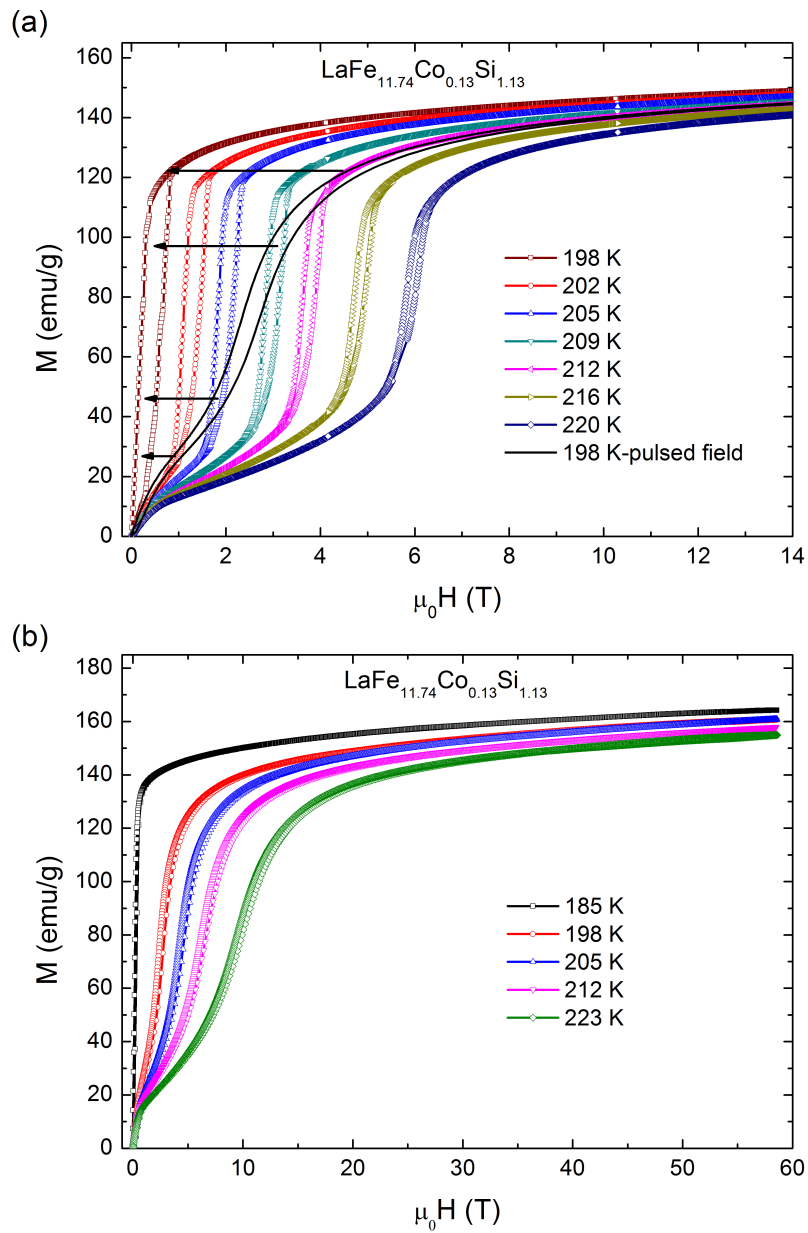
Figure 6.3: *(a) Isothermal magnetization data, M, of LFCS1 measured in magnetic fields up to 14 T for different temperatures around T_C, together with pulsed-field data at 198 K. Black arrows show the difference between adiabatic and isothermal magnetization. (b) Magnetization measured for different starting temperatures around T_C in pulsed magnetic fields up to 60 T. Isothermal magnetization data taken at TU Darmstadt by D. Yu. Karpenkov.*

evolves with increasing temperature as expected for a typical second-order transition. At low fields, a gradual decrease of the spontaneous magnetization with increasing temperature is observed. For high fields, the magnetization at all temperatures tends to saturate. The magnetization decreases with increasing temperature even at the highest field. The latter allows to expect some magnetocaloric effect also in high fields.

It is apparent from Figs. 6.4(a) and 6.3(a) that with increasing Co content, the nature of the phase transition changes from first to second order and the magnetic hysteresis and S-shaped field dependence of the magnetization disappear.

The field-dependent magnetization for some selected temperatures for the same compound measured in pulsed magnetic fields up to 60 T is shown in Fig. 6.4(b). Here, the magnetization evolves rather smoothly with increasing magnetic field without any clear feature signalling a phase transition.

The comparison of the magnetization data for pulsed-field and isothermal static-field measurement also indicates that the MCE affects the magnetization results which are measured under adiabatic conditions [Fig. 6.4(a)]. The discrepancy is designated with the black arrows for one curve from the pulsed-field measurement set with $T_0 = 257$ K and it can be understood as discussed for LFCS1.
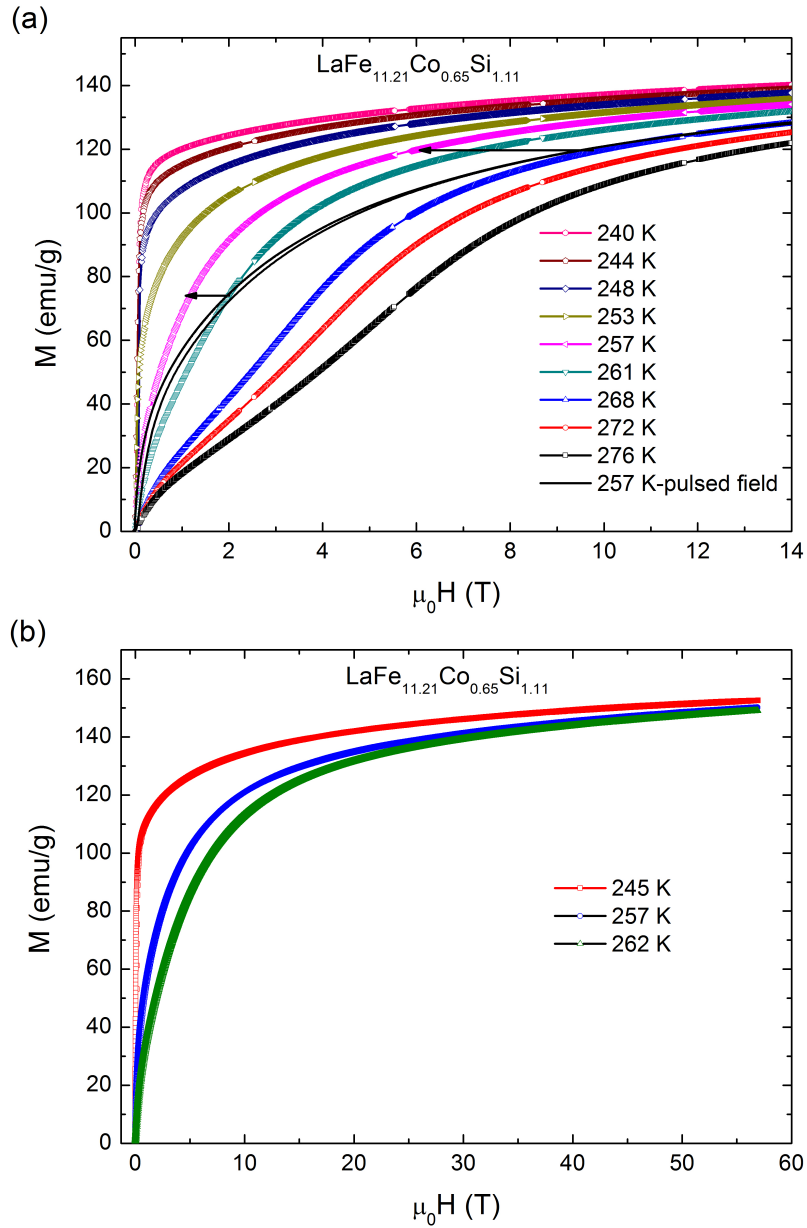
Figure 6.4: (a) Isothermal magnetization data, M, of LFCS2 measured in magnetic fields up to 14 T for different temperatures around T_C, together with pulsed-field data at 257 K. Black arrows show the difference between adiabatic and isothermal magnetization. (b) Magnetization measured for selected starting temperatures around T_C in pulsed magnetic fields up to 60 T. Isothermal magnetization data taken at TU Darmstadt by D. Yu. Karpenkov.

6.3 Magnetocaloric effect

The temperature dependence of the adiabatic temperature change, ΔT_{ad}, measured in pulsed magnetic fields of 2, 5, and 10.5 T for LFCS1 (with low cobalt concentration) are shown in Fig. 6.5(a). For a field change of 2 T, ΔT_{ad} shows a sharp maximum around T_C. When increasing the magnetic field up to 5 T, the observed peak broadens extending towards higher temperatures. This becomes even more pronounced at 10.5 T. This behavior can be explained as follows. At temperatures below $T_C = 198$ K, the sample is in a ferromagnetic state and applying a magnetic field only marginally changes the entropy of the system and so ΔT_{ad}. Since at T_C the magnetization changes rapidly because of the field-induced first-order transition, a MCE maximum is expected around T_C [according to the Maxwell relation: $\Delta S(T) = \int_0^H (\partial M/\partial T)_H \, dH$]. Above T_C an applied magnetic field can induce the transition (for temperatures not too high above T_C) resulting in an entropy jump. Depending on the field strength, the transition can be either complete or incomplete. In the case of an incomplete transition, the sample is transformed only partially and the observed ΔT_{ad} value is correspondingly lower. This is visible as a decrease in ΔT_{ad} above T_C [see e.g. the 2 T data in Fig. 6.5(a)]. According to the magnetization data shown in Fig. 6.3(a), a maximum field of 10 T is sufficient to complete the transition at any considered temperature. Thus, at 10.5 T the MCE maximum extends towards higher temperatures and ΔT_{ad} displays a broad maximum against T. The reduction of ΔT_{ad} above 215 K is due to the fact that the height of the magnetization jump, and thus the associated transition entropy is considerably decreasing. This broad maximum is also reported by Fujita *et al.* in the La(Fe,Si)$_{13}$ system [16].

The maximum values of ΔT_{ad} are found to be ∼5, ∼9, and ∼11 K for field changes of 2, 5, and 10.5 T, respectively.

In addition to the MCE experiments in pulsed magnetic fields, we carried out further MCE measurements in quasi-static fields. Figure 6.5(b) represents the temperature dependence of ΔT_{ad} for LFCS1 and for a magnetic field change of 1.9 T. This dependence is acquired from ΔT_{ad} versus magnetic-field measurements during cooling and heating. The maximum value of ΔT_{ad} is about 7 K at 198 K during the cooling process through the PM-FM transition, whereas on

heating ΔT_{ad}^{max} is only about 6.3 K.

For comparison, the results of the temperature dependence of ΔT_{ad} measured in pulsed magnetic fields is also plotted in Fig. 6.5(b) for the similar magnetic-field change of 2 T. Considering the largely different field-sweep rates in quasi-static ($\sim$1 T/s) and pulsed magnetic fields ($\sim$150 T/s), the general temperature dependence of ΔT_{ad} agrees well for the two methods. It is important to note that the pulsed-field data were collected only during the heating process.

As expected, for the first-order magnetic phase transition, the magnetocaloric effect in LFCS1 is characterized by a thermal hysteresis, in our case with a width of $\sim$1 K. A detailed explanation was suggested by Lyubina *et al.* [53]. According to theoretical considerations of first-order magnetic phase transitions [117, 118, 119], the spontaneous magnetization is produced by the exchange interactions, which are a function of interatomic distances and lattice deformation. As the system is transformed from the para- to the ferromagnetic state (during cooling or during the application of the magnetic field), the new interatomic distances will set the new energy minimum. In other words, the system will tend to expand by $\sim$1%. The volume expansion of every individual crystalline grain is hindered by the environment. As T_C is dependent on the actual interatomic distances, thus in case of the PM-FM transition, the observed T_C is lower as compared to a rigid system. However, the inverse FM-PM transition is connected to a volume shrinkage and the observed T_C is close to the "intrinsic" value for a hypothetical non-compressible lattice [117].

Figure 6.6(a) shows the magnetic-field dependence of ΔT_{ad} for LFCS1 in pulsed magnetic fields up to 50 T for various starting temperatures. The maximum value of ΔT_{ad} is found to be about 17 K at a starting temperature of 223 K.

However, in order to understand the physics behind this behavior, the data should be plotted as sample temperature vs applied magnetic field. Figure 6.6(b) displays such a diagram for LFCS1. The phase boundary separating the PM and FM states is plotted as dashed line. As shown previously in Fig. 6.6(a), depending on the starting temperature the magnetic field shifts T_C to higher temperatures. When the magnetic field is applied at temperatures above zero-field T_C (e.g. 212 K), the sample first is in the PM state and applying the magnetic field only slightly changes the entropy of the system. Thus, there is
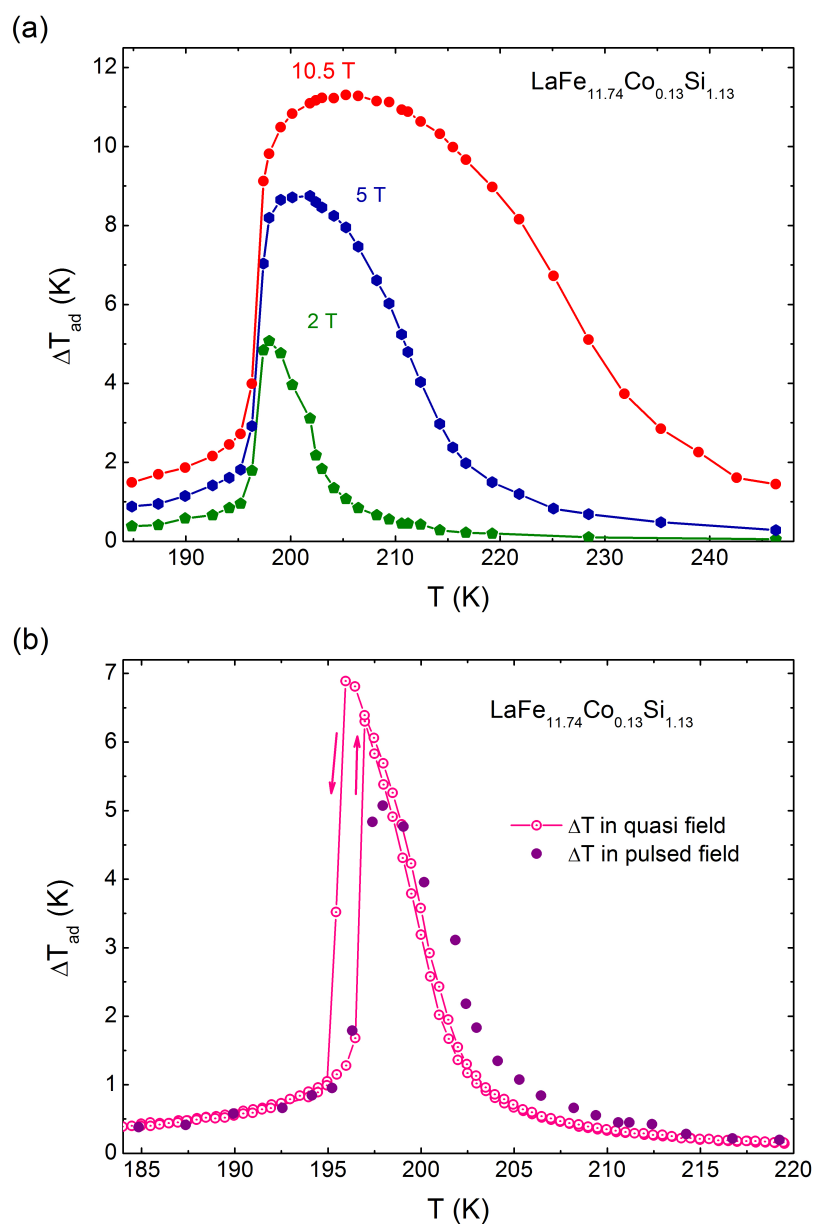
Figure 6.5: *The adiabatic temperature change, ΔT_{ad}, as a function of temperature for LFCS1 measured in (a) pulsed magnetic fields of 2, 5, and 10.5 T and (b) in quasi-static fields of $\sim$2 T together with pulsed-field data at the same field. Static fields data taken at TU Darmstadt by D. Yu. Karpenkov.*
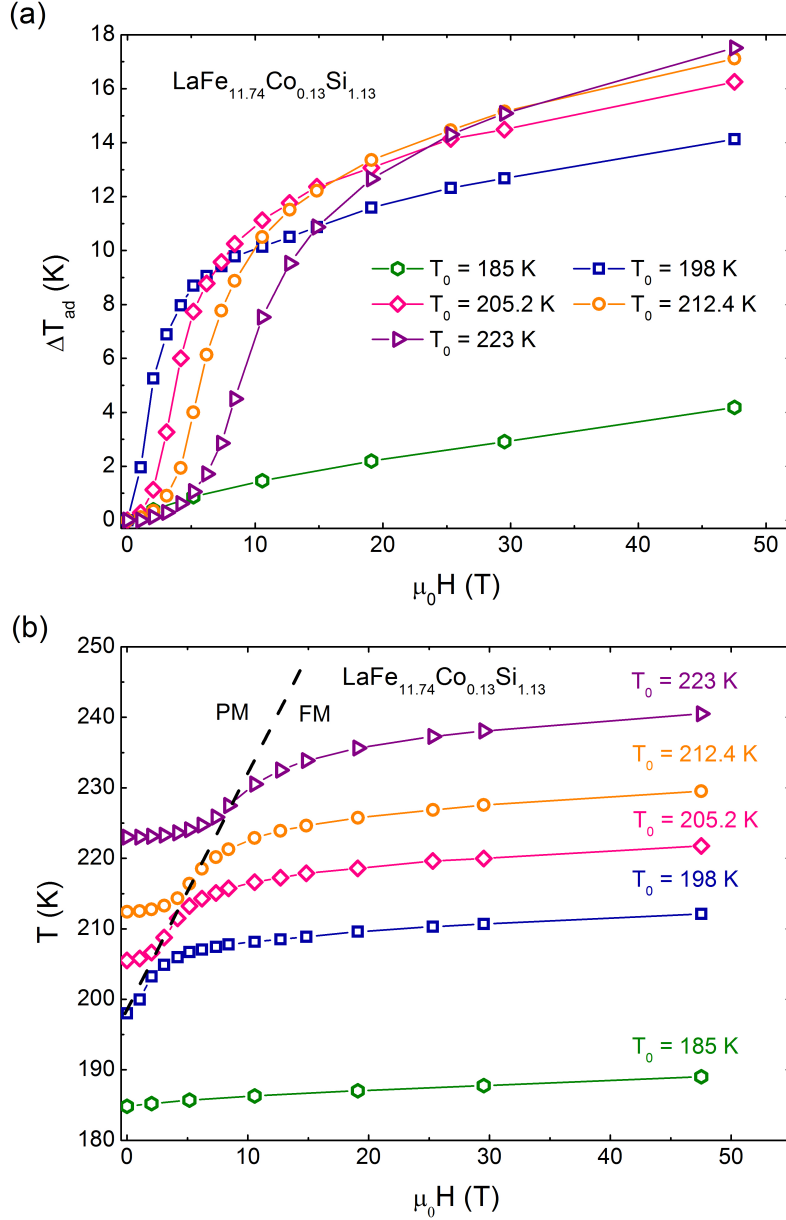
Figure 6.6: *(a) Field dependence of the adiabatic temperature change of LFCS1 measured in pulsed magnetic fields up to 50 T for various staring temperatures around T_C. (b) Field dependence of the sample temperature for different starting temperatures in pulsed fields.*

only a small temperature increase of the sample. Upon increasing the magnetic field the PM-FM transition happens and an entropy jump takes place which causes a significant sample heating. This heating process continues until the sample transforms completely to the FM state and again the increase of the sample temperature becomes small. For temperatures below the zero-field T_C (at 185 K), the sample is in the FM state and the MCE is small.

Figure 6.7(a) shows the temperature dependence of ΔT_{ad} measured in pulsed magnetic fields of 4 T for LFCS2. The MCE data exhibit a peak located in the transition region ($T_C \approx 257$ K) as expected for an SOMT [120]. Besides, the position of the MCE peak is hardly affected by increasing the magnetic field and only the value of ΔT_{ad} increases [see inset in Fig. 6.7(a)]. The maximum values of ΔT_{ad} are found to be about 5 and 7 K for a field change of 4 and 6 T, respectively.

In order to determine the maximum value for ΔT_{ad}, we have also performed MCE measurement in pulsed magnetic fields up to 50 T. The data is presented in Fig. 6.7(b) and ΔT_{ad}^{max} is about 16 K at a starting temperature of 257 K.

Interestingly, the maximum value of ΔT_{ad} measured at 50 T near the Curie temperatures of LFCS1 [Fig. 6.6(a)] and LFCS2 [Fig. 6.7(b)] are comparable. However, LFCS1 shows higher values already at smaller fields.
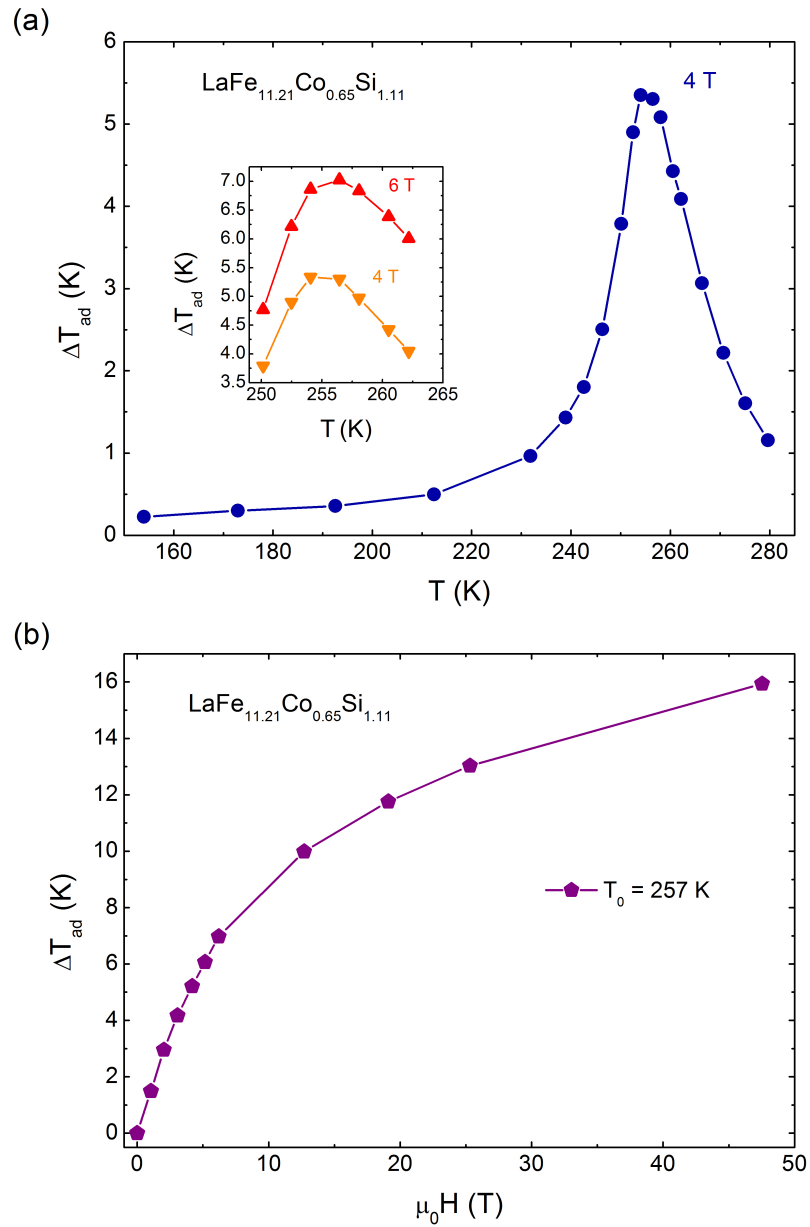
Figure 6.7: *The adiabatic temperature change, ΔT_{ad}, as a function of temperature for LFCS2 measured in pulsed magnetic fields of 4 T. The inset displays data for 4 and 6 T pulses. (b) ΔT_{ad} as a function of pulsed magnetic fields up to 50 T at a starting temperature of 257 K.*

6.4 Specific heat

As mentioned in chapter 2 in connection with the Maxwell relations, the MCE can be extracted from specific-heat data. Although indirect, this method can serve as benchmark as it is applicable for first-order transitions [16, 40, 121].

Figure 6.8(a) shows the temperature dependence of the specific heat of LFCS1 measured in the vicinity of T_C in zero field as well as 2 and 5 T. The peak-like data was obtained from the slope fitting of a long heat pulse, whereas the specific heat away from the transition was measured by the standard relaxation technique (see section 3.5 of this thesis). The measurements have been done following the heating protocol: the sample was cooled in zero field from the paramagnetic phase down to 170 K, and then the specific heat was recorded on heating from 170 to 280 K. From the sharp peak at zero field the Curie temperature $T_C \approx 198$ K is obtained. The application of magnetic fields shifts the peak to higher temperatures [40]. The appearance of the sharp specific-heat peaks is a typical characteristic of a FOMT, which is accompanied by large latent heat at T_C.

The entropy S_H can be calculated by integrating C/T. The resulting entropy at constant field of 0, 2, and 5 T are shown in Fig. 6.8(b). Sharp jumps in S are observed around T_C, originating from the latent heat of the FOMT. Upon increasing the magnetic field, the observed jumps shift to higher temperatures, which is consequence of the evaluation of the specific-heat peak.

The $S - T$ diagram can be used to determine ΔT_{ad}. For example, one determines S for $H = 0$ at the starting temperature and draws a horizontal line until it crosses the S data at $H \neq 0$. This line corresponds to an adiabatic process with constant entropy and, so, the temperature difference extracted gives ΔT_{ad} [shown by black arrows in Fig. 6.8(b)]. For a magnetic field change of 2 T, the expected ΔT_{ad}^{max} is about 6 K, which matches quite well with the corresponding experimental value in quasi-static fields ($\Delta T_{ad}^{max} = 6.3$ K). Upon increasing the field to 5 T, as expected, the effect increases and amounts to about a 15 K temperature change around T_C. Moreover, good agreement is observed between ΔT_{ad} obtained from the specific-heat and from the adiabatic and isothermal $M(H)$ data. For example, from the $M(H)$ data, the calculated values are $\sim$6 and $\sim$15 K for magnetic field changes of 2 and 5 T, respectively.
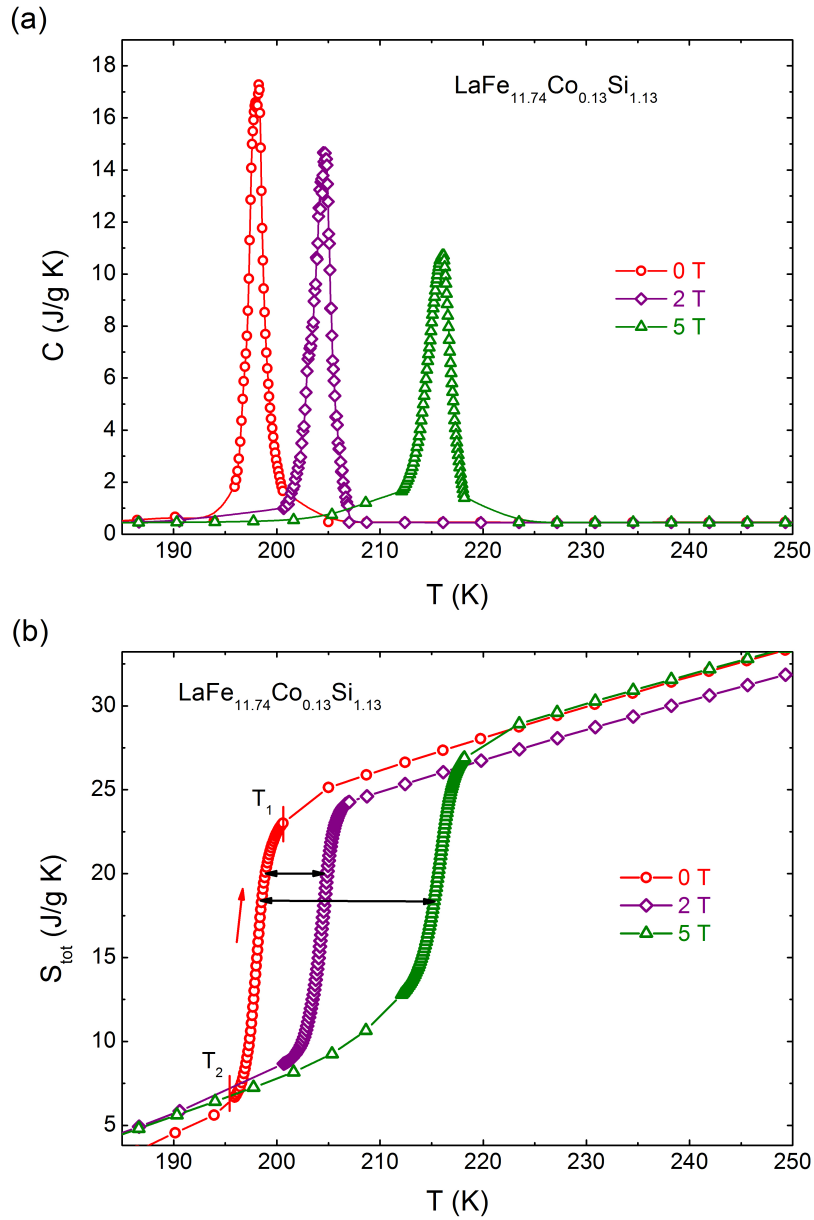
(a)

(b)

Figure 6.8: *Temperature dependence of (a) the specific heat C and (b) the total entropy S_{tot}, for LFCS1 in magnetic fields of 0, 2, and 5 T.*

6.5 Magnetostriction

The $LaFe_{13-x}Si_x$ intermetallic compounds have been shown to exhibit a large volume change of about 1.5% just above T_C. Using X-ray powder diffraction Fujita *et al.* [40] showed that during thermal expansion, the crystal structure does not change while a large volume change is observed.

The magnetostriction/thermal expansion measurements of LFCS1 and LFCS2 were performed in both quasi-static and pulsed magnetic fields. Note, as these compounds are known to show an isotropic expansion, only the length changes along one axis, parallel to the magnetic field, if applied, was measured.

Because of the large volume expansion, these compounds become very brittle and break into small grains when the volume change is performed frequently [19, 87]. In order to prevent the sample from cracking and to obtain the maximum effect, the quasi-static magnetostriction was derived from thermal expansion measurements at constant field. Figure 6.9(a) shows the temperature-dependent strain data of LFCS1 in zero (blue curve) and 1.9 T (red curve). It can be seen that the relative length change ($\Delta l/l_0$) drops sharply at T_C ($\approx$ 198 K) with increasing temperature. Moreover, as already known from the other data, T_C shifts towards higher temperatures with increasing the magnetic field to 1.9 T.

The difference between the two data sets gives the magnetostriction which is shown in Fig. 6.9(b). The data shows a sharp jump close to T_C followed by a plateau and then drops sharply at 205 K. The maximum of $\Delta l/l_0$ is found to be $\sim$0.49% around T_C. The extracted volume change, taken as three times $\Delta l/l_0$, is about 1.47% for the magnetic-field change of 1.9 T.

The magnetostriction measurement in pulsed field is a formidable task because the sample is subject to a fast field-sweep rate ($\sim$8500 T/s) and it tends to crack even after initial magnetization. Figure 6.10(a) shows field-dependent magnetostriction data of the best attempt measured in pulsed magnetic fields up to 60 T at $T_0 = 210$ K (above T_C). Alike the magnetization process, the strain shows a sharp increase corresponding to the first-order IEM transition. The abrupt steps occurring in the data are the result of the sample cracks. The real magnetostriction curve can be reconstructed by moving up the affected data blocks [shown by the green curve in Fig. 6.10(a)]. The saturation magnetostriction is estimated as about 0.35%. Repeating the measurement on the same
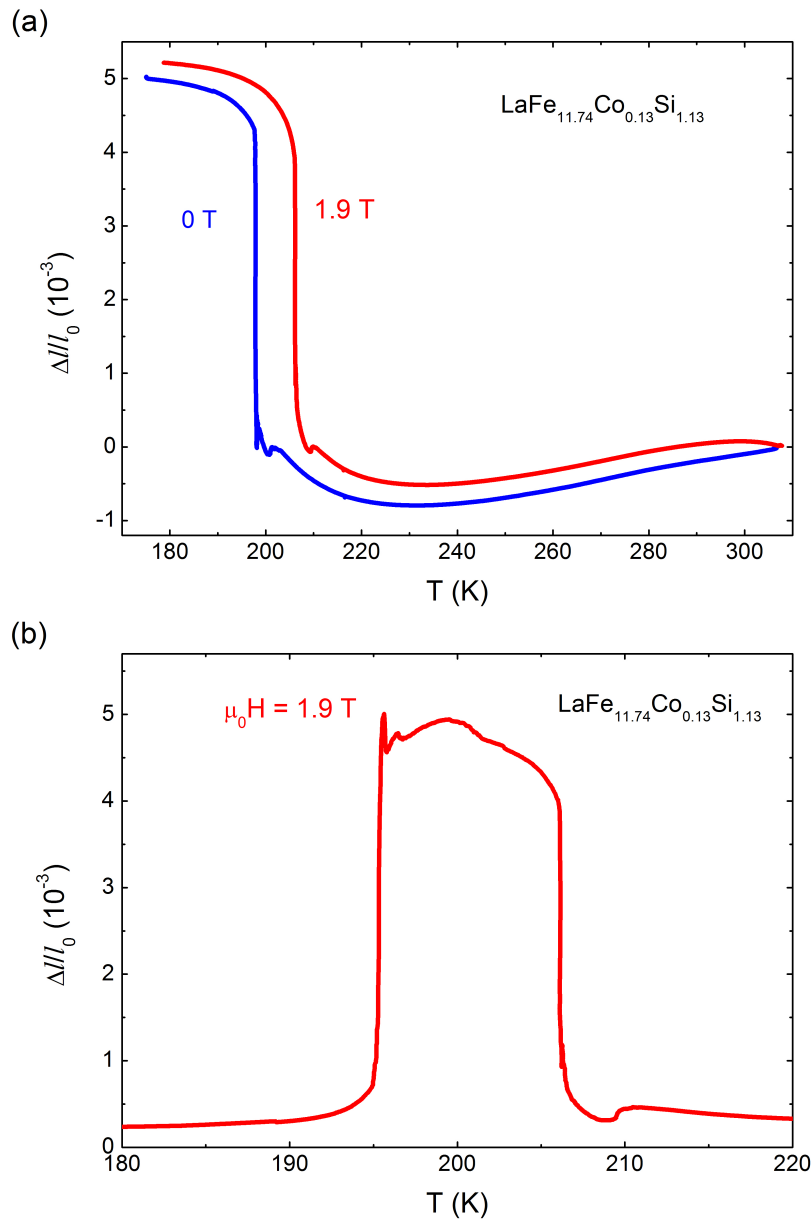
Figure 6.9: *Strain as a function of temperature for LFCS1 (a) measured at 0 T (blue curve) and 1.9 T (red curve) and (b) obtained from (a), by subtracting the strain data at 0 T from those of 1.9 T. Data taken at TU Darmstadt by D. Yu. Karpenkov.*
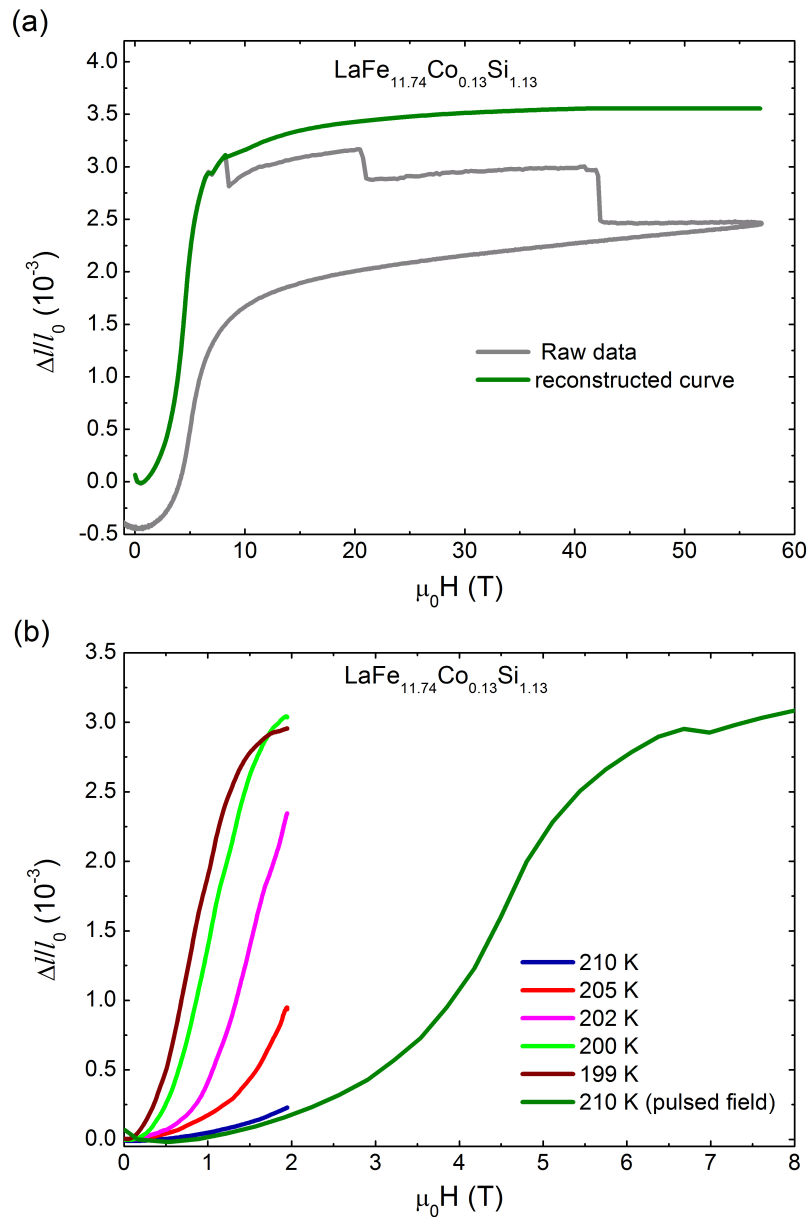
Figure 6.10: *Field-dependent longitudinal magnetostriction, $\Delta l/l_0$, of LFCS1 measured (a) in pulsed magnetic fields up to 60 T at 210 K and (b) in static-fields up to 2 T for some selected temperatures together with the pulsed-field data at 210 K. Static fields data taken at TU Darmstadt by D. Yu. Karpenkov.*

sample is impossible.

The magnetostriction measurements in quasi-static fields face similar difficulties, however, it is possible to complete one measurement without the sample being cracked. Figure 6.10(b) shows magnetostriction data measured in quasi-static fields up to 2 T for some selected temperatures, together with the pulsed-field data at 210 K shown only up to 8 T. The magnetostriction data at 210 K match quite well for the different measurements. Also in the quasi-static field measurements $\Delta l/l_0$ exhibits a tendency to saturate, e.g. at 199 K, $\Delta l/l_0 \approx 0.3\%$ when the field reaches 2 T. Before the first crack appears in the pulsed-field strain data at 210 K, $\Delta l/l_0$ has almost reached the value of 0.3% at $\sim$6 T, which agrees well with the saturation value measured in quasi-static fields and justify our reconstruction of the striction curve in pulsed magnetic fields [see Fig. 6.10(a)]. Taking into account the isotropic magneto-volume effect, one obtains about 1.0% of volume increase.

Figure 6.11(a) displays the temperature dependence of the strain of LFCS2 measured at 0 T (red curve) and 2 T (blue curve). The difference between the two curves is shown in Fig. 6.11(b). The magnetostriction rises smoothly with increasing temperature, passes through a maximum around $T_C = 257$ K and drops slowly. A maximum magnetostriction of $\sim$0.24% is reached for the magnetic field of 2 T. This value is approximately two times smaller than the peak strain obtained for LFCS1 at the same field. For LFCS2, the magnetostriction was also measured in pulsed magnetic fields up to 60 T for some selected temperatures around T_C [see Fig. 6.12(a)]. Note, due to the fact that the LFCS2 sample is more stable and does not crack in our pulse-field, we were able to measure the magnetostriction for several temperatures reliably. In contrast to LFCS1, the data show a smooth increase of the sample length in a similar way as the magnetization up to 60 T $\Delta l/l_0$ exhibits a maximum of 0.43% at 60 T being larger than $\sim$0.35% observed for LFCS1. $\Delta l(H)/l_0$ data for pulsed and static fields are presented in Fig. 6.12(b). The data exhibit fairly good agreement.

We can use the magnetostriction data to explain some similarities between the two seemingly very different compounds. Figure 6.13 shows $\Delta l/l_0$ versus M^2 for LFCS2 for two different starting temperatures, namely 257 and 245 K. Interestingly, one can clearly observe a linear dependence at 257 K [Fig. 6.13(a)], in contrast to the strong nonlinearity in the ferromagnetic region at 245 K [Fig.

6.13(b)]. The volume expansion is expressed by $\omega(T) = \kappa C_{mv}[M(T)^2 + \xi(T)^2]$, where κ, C_{mv}, and $\xi(T)$ are the compressibility, the magnetovolume-coupling constant, and the amplitude of spin fluctuations, receptively [122, 123]. Note, $\omega \cong 3\Delta l/l_0$, due to the isotropic magneto-volume effect.

As we know, for LFCS1 the IEM transition leads to an abrupt increase of the magnetization and sample volume which results in a fairly large heat release. For LFCS2 the linear behavior means that the magnetovolume-coupling factor is constant over the whole field range. The magnetization of the second-order sample in the paramagnetic state is tightly bound to the volume increase and, alike for the first-order sample, gives the main contribution to the entropy change.

That explains why the physics of the two compounds are substantially different in the low-to-medium field range, while in fields around 50 T the main thermodynamic parameters, i.e., volume, magnetization, and ΔT, reach similar values for these largely different systems (with and without a metamagnetic transition).
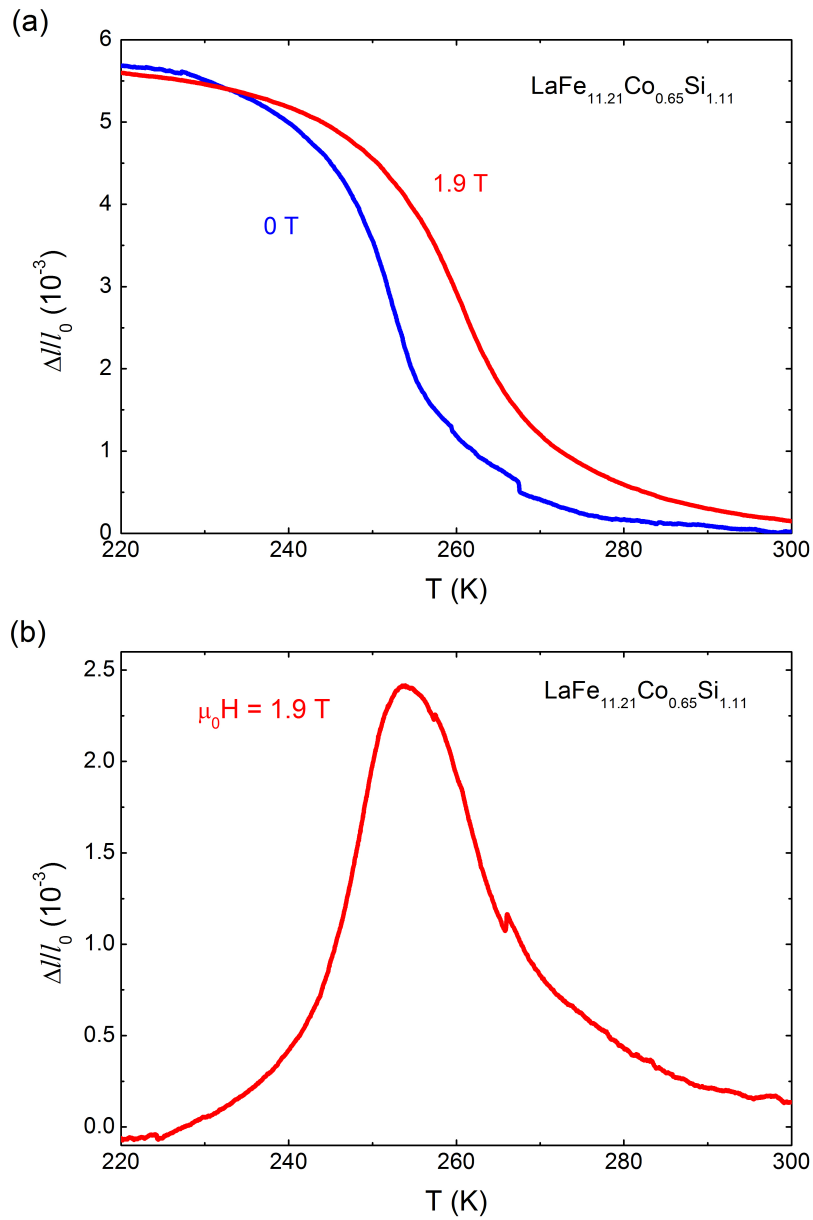
Figure 6.11: *Temperature dependence of the strain in LFCS2 parallel to the direction of applied field (a) at 0 T (red curve) and 2 T (blue curve) and (b) the difference between the strain data at 0 T and 1.9 T. Data taken at TU Darmstadt by D. Yu. Karpenkov.*
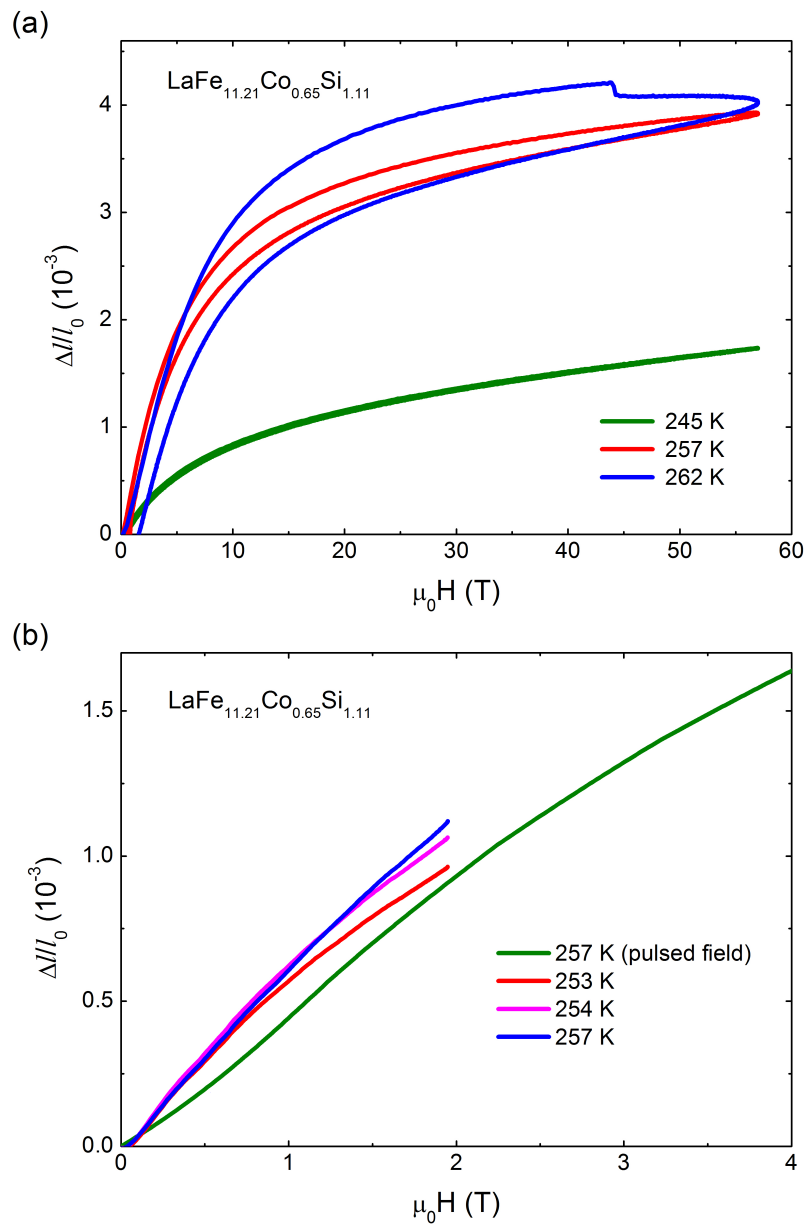
(a)

(b)

Figure 6.12: *Field dependence of the longitudinal magnetostriction, $\Delta l/l_0$, of LFCS2 measured (a) in pulsed magnetic fields up to 60 T for some selected temperatures around T_C and (b) in static-fields up to 2 T for some selected temperatures together with the pulsed-field data at 257 K. Static fields data taken at TU Darmstadt by D. Yu. Karpenkov.*
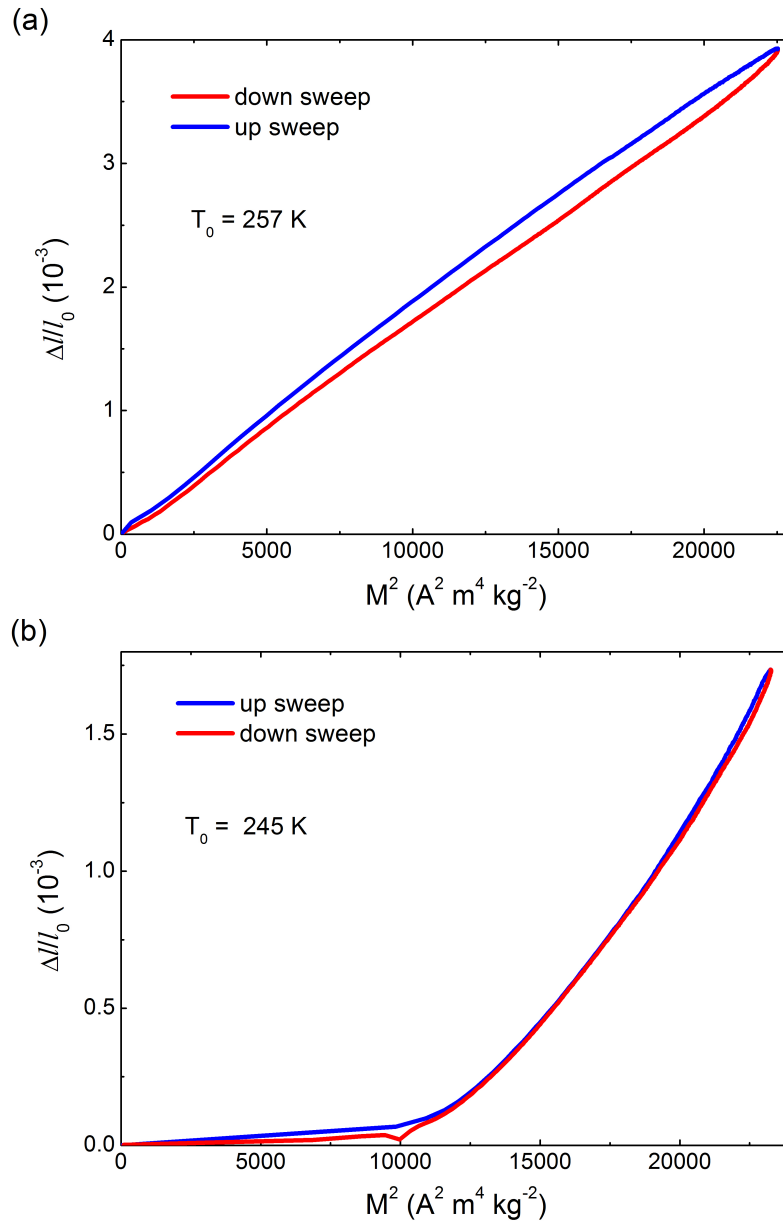
(a)

(b)

Figure 6.13: *Magnetization dependence of the longitudinal magnetostriction, $\Delta l/l_0$, of LFCS2 for (a) 257 K and (b) 245 K.*

6.6 Summary

We have performed a comparative study of the magnetic and magnetocaloric properties of two samples with the nominal compositions $LaFe_{11.74}Co_{0.13}Si_{1.13}$ (LFCS1) and $LaFe_{11.21}Co_{0.65}Si_{1.11}$ (LFCS2) by measuring the magnetization, the MCE, and the magnetostriction in both pulsed and static magnetic fields, and also the specific heat in constant fields.

- The pulsed-field magnetization of both compounds has been measured in fields up to 60 T under nearly adiabatic conditions. For LFCS1, the presence of S-shaped curves associated with magnetic hysteresis proves the occurrence of field-induced IEM transitions just above $T_C \approx 198$ K. However, the increasing Co content in LFCS2 changes the nature of the phase transition from first to second order and the magnetic hysteresis and S-shaped field dependence of the magnetization disappear. The pulsed-field results are compared with isothermal magnetization data in steady fields up to 14 T. We find, for the same staring temperature, that the overall shapes of the magnetization curves are different for each compound. This explains the different MCEs that can be extracted from the crossing points of the adiabatic with the isothermal magnetization.

- The MCE of the two samples has been measured in pulsed magnetic fields up to 50 T. For LFCS1 showing a first-order transition ($T_C = 198$ K), the abrupt change of the magnetization and subsequent release of latent heat leads to a substantial magnetocaloric effect in a moderate magnetic field. The maximum values of ΔT_{ad} are found to be about 5, 9, and 11 K for the field changes of 2, 5, and 10.5 T, respectively. Whereas the MCE of LFCS2 showing a second-order transition ($T_C = 257$ K) is maximal at the transition point and increases monotonically with magnetic field. The maxima obtained upon field changes of 4 and 6 T are $\Delta T_{ad}^{max} = \sim 5$ and ~ 7 K, respectively. Interestingly, the maximum value of ΔT_{ad} measured at 50 T near the Curie temperatures of LFCS1 and LFCS2 are comparable. However, LFCS1 shows a large MCE already at smaller fields ($2 - 10$ T). For LFCS1, the MCEs obtained from the specific heat and direct measurements in pulsed and quasi-static fields of 2 T are in good agreement

with each other.

- The magnetostriction measurements of LFCS1 and LFCS2 are performed in both quasi-static and pulsed magnetic fields. An irreversible magneto-volume effect of about 1% is observed for LFCS1 in a pulsed magnetic fields of 60 T. Whereas for LFCS2, the data show a smooth increase of the sample length up to 60 T, and $\Delta l/l_0$ exhibits a maximum of 0.43% being larger than $\sim$0.35% observed for LFCS1. We also find that magnetizing LFCS2 in the paramagnetic state is tightly bound to the volume increase and this, likewise for the first-order sample, gives the main contribution to the entropy change.

Although the physics of the two compounds is substantially different in the low-to-medium field range, in fields around 50 T the main thermodynamic parameters, i.e., volume, magnetization, and ΔT_{ad}, reach similar values.

7 Conclusion

This thesis was devoted to the investigation of the magnetocaloric effect (MCE) by measurements in pulsed and quasi-static magnetic fields as well as by analyzing specific-heat data taken in static magnetic fields. We established a new technique for the direct measurement of the MCE in pulsed fields. We studied the following materials: Gadolinium (Gd) with a second-order phase transition, $Ni_{50}Mn_{35}In_{15}$ with multiple magnetic transitions, and $La(Fe,Si,Co)_{13}$ compounds with first- and second-order transitions, depending on the Co concentration.

The main conclusions are as follows:

- We have investigated the magnetocaloric properties of a polycrystalline gadolinium sample by means of MCE measurements in pulsed and quasi-static magnetic fields, providing the temperature and field dependence of the adiabatic temperature change. Gd shows a second-order phase transition with a Curie temperature of $\sim$294 K. The maxima of ΔT_{ad} are found to be 4.7 and 13 K for a field change of 2 and 6.5 T, respectively. Taking into account the effect of different sample quality, our results are in good agreement with reported literature data [70]. For the first time, we measured the MCE in a polycrystalline Gd in pulsed magnetic fields up to 70 T. We find a very large adiabatic temperature change of $\Delta T_{ad} \approx 60$ K. Unlike the low-field data, there is no sign of a pronounced maximum for a field change of 70 T. In addition, our ΔT_{max} data are found to follow perfectly a $H^{2/3}$ dependence even for magnetic fields as high as 70 T.

- We have investigated the MCE in the shape-memory Heusler alloy $Ni_{50}Mn_{35}In_{15}$ by direct magnetocaloric measurements in pulsed magnetic fields and by specific-heat experiments in constant fields. The conventional MCE around the Curie temperature in the austenitic phase exhibits

93

a strong magnetic-field dependence; for a field change of 20 T we find a maximum ΔT_{ad} of about 11 K. In this region of the phase diagram we do not find any hysteresis or irreversible behavior in the magnetocaloric experiments neither in static nor in pulsed-magnetic fields. Furthermore, ΔT_{ad} is in a good agreement with data from specific heat. This changes below the martensitic phase transition. Here, we observe an inverse MCE, which originates from structural and magnetic contributions. In the direct magnetocaloric experiments we find a saturating MCE with a maximum negative temperature change of $\Delta T_{ad} = -7$ K. This value is significantly larger than the calculated results from the specific heat suggest. The cause for this lies in the hysteresis observed at the martensitic phase transition which leads to a strongly irreversible time and field dependence of ΔT_{ad}^{t} below the martensitic phase transition. This irreversible behavior has to be carefully taken into consideration for using shape-memory Heusler alloys in magnetocaloric-cooling applications, especially, since the length of the magnetic-field pulse is comparable to the inverse of useful operation frequencies of cooling devices.

- We have performed a comparative study of the magnetic and magnetocaloric properties of two La(Fe,Co,Si)$_{13}$ compounds with different Co concentrations (implementing two types of phase transitions). We measured the magnetization, magnetostriction, and MCE in both pulsed and F fields, as well as the specific heat in constant fields. LaFe$_{11.74}$Co$_{0.13}$Si$_{1.13}$ with low Co concentration shows a first-order IEM transition, accompanied by an abrupt increase of the magnetization and volume, and a release of latent heat. The latter leads to a substantial magnetocaloric effect in a moderate magnetic field. The maximum values of ΔT_{ad} are found to be about 5, 9, and 11 K for field changes of 2, 5, and 10.5 T, respectively. Furthermore, MCE results obtained in pulsed magnetic fields of 2 T are in good agreement with data from quasi-static field measurements and with data from specific heat. On the other hand, LaFe$_{11.21}$Co$_{0.65}$Si$_{1.11}$ with higher Co concentration exhibits a typical second-order phase transition and there is no sign of a metamagnetic transition. The magnetocaloric effect is maximal at the transition temperature, and increases monotoni-

cally with magnetic field. The maxima obtained upon field changes of 4 and 6 T are $\Delta T_{ad}^{max} = {\sim}5$ and ${\sim}7$ K. By magnetostriction measurements in pulsed magnetic fields for LFCS2, we find that the magnetization of this sample in the paramagnetic state is tightly bound to the volume increase and, alike for the first-order sample, gives the main contribution to the entropy change. That explains why the physics of the two compounds is substantially different in the low-to-medium field range, while in fields around 50 T the main thermodynamic parameters, i.e., volume, magnetization, and ΔT, reach similar values for such different systems (with and without metamagnetic transition).

Our results may stimulate some further studies. In the present work we touched three classes of magnetocaloric materials, which are maybe most important for possible applications, and, therefore, attract a lot of interest in both fundamental and applied research. Our experimental technique at present is restricted to temperatures above about 80 K. This limitation should be overcome, since many interesting MCE phenomena in solid-state physics occur at low and very low temperatures. We plan to extend our technique to lower temperatures, where measurement of the magnetocaloric effect can be used as a powerful tool for mapping phase diagrams, as well as a complementary technique to other pulsed-field measurements, where the temperature of the sample is poorly defined due to near-adiabatic conditions. We plan to continue our activity with R_2Fe_{17} and R_2Co_{17} materials, which high-field metamagnetic transitions are observed.

Bibliography

[1] P. Weiss and A. Piccard, J. Phys. (Paris) 5th Ser. **7**, 103 (1917).

[2] P. Weiss and A. Piccard, Comptes Rendus **166**, 352 (1918).

[3] P. Debye, Ann. Phys. **81**, 1154 (1926).

[4] W. F. Giauque, J. Amer. Chem. Soc. **49**, 1864 (1927).

[5] W. F. Giauque and D. P. MacDougall, Phys. Rev. **43**, 768 (1933).

[6] K. A. Gschneidner Jr. and V. K. Pecharsky, Rare Earths: Science, Technology and Applications III, ed. R. G. Bautista et al., (Warrendale, PA: The Minerals, Metals and Materials Society), p. 209 (1997).

[7] V. K. Pecharsky and K. A. Gschneidner Jr., J. Magn. Magn. Mater. **200**, 44 (1999).

[8] K. A. Gschneidner Jr. and V. K. Pecharsky, Annu. Rev. Mater. Sci. **30**, 387 (2000).

[9] K. A. Gschneidner Jr. and V. K. Pecharsky, Fundamentals of Advanced Materials for Energy Conversion, ed. D. Chandra and R. G. Bautista, (Warrendale, PA: The Minerals, Metals and Materials Society), p. 9 (2002).

[10] C. B. Zimm, A. Jastrab, A. Sternberg, V. K. Pecharsky, K. A. Gschneidner Jr., M. Osborne, and I. Anderson, Adv. Cryog. Eng. **43**, 1759 (1998).

[11] V. K. Pecharsky and K. A. Gschneidner Jr., Phys. Rev. Lett. **78**, 4494 (1997).

[12] V. K. Pecharsky and K. A. Gschneidner Jr., J. Appl. Phys. **85**, 5365 (1999).

[13] R. Niemann, O. Heczko, L. Schultz, and S. Fähler, Int. J. Refrig. **37**, 281 (2014).

[14] M. D. Kuz'min, Appl. Phys. Lett. **90**, 251916 (2007).

[15] J. Liu, T. Gottschall, K. P. Skokov, J. D. Moore, and O. Gutfleisch, Nat. Mater. **11**, 620 (2012).

[16] S. Fujieda, A. Fujita, and K. Fukamichi, Appl. Phys. Lett. **81**, 1276 (2002).

[17] O. Gutfleisch, A. Yan, and K. H. Müller, J. Appl. Phys. **97**, 10M305 (2005).

[18] J. Liu, J. D. Moore, K. P. Skokov,M. Krautz, L. Löwe, A. Barcza, M. Katter, and O. Gutfleisch, Scr. Mater. **67**, 584 (2012).

[19] G. F. Wang, Ph.D. thesis, University of Zaragoza (2012).

[20] B. R. Hansen, Ph.D. thesis, Technical University of Denmark (2010).

[21] A. M. Tishin, K. A. Gschneidner Jr., and V. K. Pecharsky, Phys. Rev. B **59**, 503 (1999).

[22] B. K. Ponomarev, Prib. Tekh. Eksp. **3**, 153 (1983).

[23] S. Y. Dan'kov, A. M. Tishin, V. K. Pecharsky, and K. A. Gschneidner Jr., Rev. Sci. Instrum. **68**, 2432 (1997).

[24] B. R. Gopal, R. Chahine, and T. K. Bose, Rev. Sci. Instrum. **68**, 1818 (1997).

[25] B. R. Gopal, R. Chahine, M. Foldeaki, and T. K. Bose, Rev. Sci. Instrum. **66**, 232 (1995).

[26] M. Foldeaki, R. Chahine, and T. K. Bose, J. Appl. Phys. **77**, 3528 (1995).

[27] M. W. Zemansky, *Heat and Thermodynamics*, 6th ed. (McGraw-Hill, New York, 1981).

[28] V. K. Pecharsky and K. A. Gschneidner Jr., J. Appl. Phys. **86**, 565 (1999).

[29] V. K. Pecharsky and K. A. Gschneidner Jr., Adv. Cryog. Eng. **42A**, 423 (1996).

[30] K. A. Gschneidner Jr. and V. K. Pecharsky, Int. J. Refrig. **31**, 945 (2008).

[31] O. Tegus, E. Brück, K. H. J. Buschow, and F. R. de Boer, Nature **415**, 150 (2002).

[32] http:// www.nist.gov/ncnr/refrigeration_012709.cfm

[33] A. Kitanovski, J. Tušek, U. Tomc, U. Plaznik, M. Ozbolt, and A. Poredoš, Magnetocaloric Energy Conversion: From Theory to Applications (Springer, London, 2015).

[34] A. Smith, C. R. H. Bahl, R. Bjork, K. Engelbrecht, K. K. Nielsen, and N. Pryds, Adv. Energy Mater. **2**, 1288 (2012).

[35] M. H. Phan and S. C. Yu, J. Magn. Magn. Mater. **308**, 325 (2007).

[36] K. A. Gschneidner Jr., V. K. Pecharsky, and A. O. Tsokol, Rep. Prog. Phys. **68**, 1479 (2005).

[37] N. T. Trung Ph.D. thesis, Technical University of Delft (2010).

[38] H. Wada and Y. Tanabe, Appl. Phys. Lett. **79**, 3302 (2001).

[39] F. X. Hu, B. G. Shen, J. R. Sun, Z. H. Cheng, G. H. Rao, and X. X. Zhang, Appl. Phys. Lett. **78**, 3675 (2001).

[40] A. Fujita, S. Fujieda, Y. Hasegawa, and K. Fukamichi, Phys. Rev. B **67**, 104416 (2003).

[41] N. T. Trung, Z. Q. Ou, T. J. Gortenmulder, O. Tegus, K. H. J. Buschow, and E. Brück, Appl. Phys. Lett. **94**, 102513 (2009).

[42] N. H. Dung, Z. Q. Ou, L. Caron, L. Zhang, D. T. C. Thanh, G. A. de Wijs, R. A. de Groot, K. H. J. Buschow, and E. Brück, Adv. Energy Mater. **1**, 1215 (2011).

[43] N. H. Dung, L. Zhang, Z. Q. Ou, and E. Brück, Appl. Phys. Lett. **99**, 092511 (2011).

[44] T. Krenke, E. Duman, M. Acet, E. F. Wassermann, X. Moya, L. Mañosa, and A. Planes, Nat. Mater. **4**, 450 (2005).

[45] E. K. Liu, W. H. Wang, L. Feng, W. Zhu, G. J. Li, J. L. Chen, H. W. Zhang, G. H. Wu, C. B. Jiang, H. B. Xu, and F. de Boer, Nat. Commun. **3**, 873 (2012).

[46] S. Zherlitsyn, T. Herrmannsdörfer, Y. Skourski, A. Sytcheva, and J. Wosnitza, J. Low Temp. Phys. **146**, 719 (2007).

[47] S. Zherlitsyn, B. Wustmann, T. Herrmannsdörfer, and J. Wosnitza, J. Low Temp. Phys. **170**, 447 (2013).

[48] S. Zherlitsyn, T. Herrmannsdörfer, B. Wustmann, and J. Wosnitza, IEEE Trans. Appl. Supercond. **20**, 672 (2010).

[49] S. Zherlitsyn, B. Wustmann, T. Herrmannsdörfer, and J. Wosnitza, IEEE Trans. Appl. Supercond. **22**, 4300603 (2012).

[50] A. Kirste, Ph.D. thesis, Technical University of Berlin (2003).

[51] T. Kihara, Y. Kohama, Y. Hashimoto, S. Katsumoto, and M. Tokunaga, Rev. Sci. Instrum. **84**, 074901 (2013).

[52] J. Liu, T. Gottschall, K. P. Skokov, J. D. Moore, and O. Gutfleisch, Nat. Mater. **11**, 620 (2012), Supplementary Information.

[53] J. Lyubina, R. Schäfer, N. Martin, L. Schultz, and O. Gutfleisch, Adv. Mater. **22**, 3735 (2010), Supplementary Information.

[54] Y. Skourski, M. D. Kuz'min, K. P. Skokov, A. V. Andreev, and J. Wosnitza, Phys. Rev. B **83**, 214420 (2011).

[55] H. Czichos, T. Saito, L. E. Smith, Handbook of Metrology and Testing, (Springer, Berlin, Heidelberg, 2011).

[56] Quantum Design vibrating sample magnetometer (VSM) Option, User's Manual (2011).

[57] R. Daou, F. Weickert, M. Nicklas, F. Steglich, A. Haase, and M. Doerr, Rev. Sci. Instrum. **81**, 033909 (2010).

[58] Quantum Design, Physical Property Measurement System, Heat Capacity Option, User's manual (2000).

[59] S. Das, Ph.D. thesis, Iowa State University (2010).

[60] Y. Wang, T. Plackowski, and A. Junod, Physica C **355**, 179 (2001).

[61] G. V. Brown, J. Appl. Phys. **47**, 3673 (1976).

[62] K. A. Gschneidner Jr., Y. Mudryk, and V. K. Pecharsky, Scr. Mater. **67**, 572 (2012).

[63] B. F. Yu, M. Liu, P. W. Egolf, and A. Kitanovski Int. J. Refrig. **33**, 1029 (2010).

[64] K. K. Nielsen, J. Tusek, K. Engelbrecht, S. Schopfer, A. Kitanovski, C. R. H. Bahl, A. Smith, N. Pryds, and A. Poredos, Int. J. Refrig. **34**, 603 (2011).

[65] R. Bjørk, C. R. H. Bahl, A. Smith, and N. Pryds, Int. J. Refrig. **33**, 437 (2010).

[66] C. R. H. Bahl and K. K. Nielsen, J. Appl. Phys. **105**, 013916 (2009).

[67] P. Strange, A. Svane, W. M. Temmerman, Z. Szotek, and H. Winter, Nature **399**, 756 (1999).

[68] M. Rotter, Habilitationsschrift, Technical University Dresden (2003).

[69] J. M. D. Coey, K. Gallagher, and V. Skumryev, J. Appl. Phys. **87**, 7028 (2000).

[70] S. Y. Dan'kov, A. M. Tishin, V. K. Pecharsky, and K. A. Gschneidner Jr., Phys. Rev. B **57**, 3478 (1998).

[71] Y. Kohama, C. Marcenat, T. Klein, and M. Jaime, Rev. Sci. Instrum. **81**, 104902 (2010).

[72] M. D. Kuz'min and A. M. Tishin, Cryogenics **33**, 868 (1993).

[73] A. M. Tishin and I. Y. Spichkin, The Magnetocaloric Effect and its Applications, (Inst. of Phys. Publishing, Bristol, Philadelphia, 2003).

[74] M. D. Kuz'min, K. P. Skokov, D. Yu. Karpenkov, J. D. Moore, M. Richter, and O. Gutfleisch, Appl. Phys. Lett. **99**, 012501 (2011).

[75] V. Franco, J. S. Blázquez, and A. Conde, Appl. Phys. Lett. **89**, 222512 (2006).

[76] V. Franco, A. Conde, J. M. Romero-Enrique, Y. I. Spichkin, V. I. Zverev, and A. M. Tishin, J. Appl. Phys. **106**, 103911 (2009).

[77] M. D. Kuz'min, M. Richter, and A. M. Tishin, J. Magn. Magn. Mater. **321**, L1 (2009).

[78] H. Oesterreicher and F. T. Parker, J. Appl. Phys. **55**, 4334 (1984).

[79] Q. Dong, H. Zhang, J. Shen, J. Sun, and B. Shen, J. Magn. Mater. **319**, 56 (2007).

[80] J. Lyubina, M. D. Kuz'min, K. Nenkov, O. Gutfleisch, M. Richter, D. L. Schlagel, T. A. Lograsso, and K. A. Gschneidner Jr., Phys. Rev. B **83**, 012403 (2011).

[81] A. Yu. Romanov and V. P. Silin, Phys. Met. Metallogr. **83**, 111 (1997).

[82] J. S. Amaral, P. B. Tavares, M. S. Reis, J. P. Araújo, T. M. Mendonça, V. S. Amaral, and J. M. Vieira, J. Non-Cryst. Solids **354**, 5301 (2008).

[83] F. Heusler, Verhandlungen der Deutschen Physikalischen Gesellschaft **5**, 219 (1903).

[84] F. Heusler, W. Starck, and E. Haupt, Verhandlungen der Deutschen Physikalischen Gesellschaft **5**, 220 (1903).

[85] O. Heusler, Annalen der Physik **411**, 155 (1934).

[86] S. Aksoy, PhD thesis, University of Duisburg-Essen (2010).

[87] E. Brück, J. Phys. D: Appl. Phys. **38**, R381 (2005).

102

[88] R. Kainuma, Y. Imano, W. Ito, Y. Sutou, H. Morito, S. Okamoto, O. Kitakami, K. Oikawa, A. Fujita, T. Kanomata, and K. Ishida, Nature **439**, 957 (2006).

[89] A. Planes, L. Mañosa, and M. Acet, J. Phys.: Condens. Matter **21**, 233201 (2009).

[90] L. Mañosa, D. Gonzalez-Alonso, A. Planes, E. Bonnot, M. Barrio, J.-L. Tamarit, S. Aksoy, and M. Acet, Nat. Mater. **9**, 478 (2010).

[91] I. Titov, PhD thesis, University of Duisburg-Essen (2014).

[92] M. Ghorbani-Zavareh, C. Salazar Mejia, A. K. Nayak, Y. Skourski, J. Wosnitza, C. Felser, and M. Nicklas, Appl. Phys. Lett. **106**, 071904 (2015).

[93] V. V. Khovaylo, K. P. Skokov, O. Gutfleisch, H. Miki, R. Kainuma, and T. Kanomata, Appl. Phys. Lett. **97**, 052503 (2010).

[94] I. Titov, M. Acet, M. Farle, D. Gonzalez-Alonso, L. Mañosa, A. Planes, and T. Krenke, J. Appl. Phys. **112**, 073914 (2012).

[95] J. C. Lashley, M. F. Hundley, A. Migliori, J. L. Sarrao, P. G. Pagliuso, T. W. Darling, M. Jaime, J. C. Cooley, W. L. Hults, L. Morales, D. J. Thoma, J. L. Smith, J. Boerio-Goates, B. F. Woodfield, G. R. Stewart, R. A. Fisher, and N. E. Phillips, Cryogenics **43**, 369 (2003).

[96] V. Hardy, Y. Bréard, and C. Martin, J. Phys.: Condens. Matter **21**, 075403 (2009).

[97] B. Emre, S. Yuce, E. Stern-Taulats, A. Planes, S. Fabbrici, F. Albertini, and L. Mañosa, J. Appl. Phys. **113**, 213905 (2013).

[98] A. K. Nayak, C. Salazar Mejía, S. W. D´Souza, S. Chadov, Y. Skourski, C. Felser, and M. Nicklas, Phys. Rev. B **90**, 220408 (2014).

[99] C. Salazar Mejía, M. Ghorbani Zavareh, A. K. Nayak, Y. Skourski, J. Wosnitza, C. Felser, and M. Nicklas, J. Appl. Phys. **117**, 17E710 (2015).

[100] P. I. Kripyakevich, O. S. Zarechnyuk, E. I. Gladushevsky, and O. I. Bodak, Z. Anorg. Chem. **90**, 358 (1968).

[101] O. I. Bodak and E. I . Gladyshevskii, Dopov. Akad. Nauk Ukr. RSR, Ser. A **12**, 1125 (1969).

[102] T. T. M. Palstra , J. A. Mydosh, G. J. Nieuwenhuys, A. M. van der Kraan, and K. H. J. Buschow J. Magn. Magn. Mater. **36**, 290 (1983).

[103] T. T. M. Palstra, H. G. C. Werij, G. J. Nieuwenhuys, J. A. Mydosh, F. R. de Boer, and K. H. J. Buschow. J. Phys. F: Met. Phys. **14**, 1961 (1984).

[104] A. Fujita, Y. Akamatsu, and K. Fukamichi, J. Appl. Phys. **85**, 4756 (1999).

[105] A. Fujita, S. Fujieda, and K. Fukamichi, Phys. Rev. B **65**, 014410 (2001).

[106] L. Löwe, J. Liu, K. P. Skokov, J. Moore, H. Sepehri-Amin, K. Hono, M. Katter, and O. Gutfleisch, Acta. Mater. **60**, 4268 (2012).

[107] O. Gutfleisch, M. A. Willard, E. Brück, C. H. Chen, S. G. Sankar, and J. P. Liu, Adv. Mater. **23**, 821 (2011).

[108] J. Lyubina, O. Gutfleisch, M. D. Kuz'min, and M. Richter, J. Magn. Magn. Mater. **320**, 3571 (2008).

[109] J. Liu, M. Krautz, K. P. Skokov, T. G. Woodcock, and O. Gutfleisch, Acta Mater. **59**, 3602 (2011).

[110] M. D. Kuz'min and M. Richter, Phys. Rev. B **76**, 092401 (2007).

[111] H. Yamada, J. Inoue, and M. Shimizu, J. Phys. F: Met. Phys. **15**, 169 (1985).

[112] S. Fujieda, A. Fujita, K. Fukamichi, Y. Yamazaki, and Y. Iijima, Appl. Phys. Lett. **79**, 653 (2001).

[113] B. G. Shen, J. R. Sun, F. X. Hu, H. W. Zhang, and Z. H. Cheng, Adv. Mater. **21**, 4545 (2009).

[114] W. H. Tang, J. K. Liang, G. H. Rao, and X. Yan, Phys. Stat. Sol. **141**, 217 (1994).

[115] F. X. Hu, B. G. Shen, J. R. Sun, and X. X. Zhang, Chin. Phys. **9**, 550 (2000).

[116] http://www.vacuumschmelze.de/en

[117] C. P. Bean and D. S. Rodbell, Phys. Rev. **126**, 104 (1962).

[118] N. P. Grazhdankina, Sov. Phys. Usp. **11**, 727 (1969).

[119] H. Yamada, Phys. Rev. B **47**, 11211 (1993).

[120] G. H. Wen, R. K. Zheng, X. X. Zhang, W. H. Wang, J. L. Chen, and G. H. Wu, J. Appl. Phys. **91**, 8537 (2002).

[121] K. P. Skokov, K. H. Müller, J. Moore, J. Liu, A. Karpenkov, M. Krautz, and O. Gutfleisch, J. Alloys Compd. **552**, 310 (2013).

[122] A. Fujita, K. Fukamichi, M. Yamada, and T. Goto, J. Appl. Phys. **93**, 7263 (2003).

[123] A. Fujita, K. Fukamichi, J.-T. Wang, and Y. Kawazoe, Phys. Rev. B **68**, 104431 (2003).

List of publications

o Direct measurements of the magnetocaloric effect in pulsed magnetic fields:
The example of the Heusler alloy $Ni_{50}Mn_{35}In_{15}$
<u>M. Ghorbani-Zavareh</u>, C. Salazar Mejia, A. K. Nayak, Y. Skourski, J.
Wosnitza, C. Felser, M. Nicklas
Applied Physics Letters **106**, 071904 (2015).

o Dependence of the inverse magnetocaloric effect on the field-change rate
in Mn_3GaC and its relationship to the kinetics of the phase transition
F. Scheibel, T. Gottschall, K. P. Skokov, O. Gutfleisch,
<u>M. Ghorbani-Zavareh</u>, Y. Skourski, J. Wosnitza, ö. Cakir, M. Farle, and
M. Acet
Journal of Applied Physics **117**, 233902 (2015).

o Pulsed high-magnetic-field experiments: New insights into the magnetocaloric effect in Ni-Mn-In Heusler alloys
C. Salazar Mejia, <u>M. Ghorbani-Zavareh</u>, A. K. Nayak, Y. Skourski, J.
Wosnitza, C. Felser, M. Nicklas
Journal of Applied Physics **117**, 17E710 (2015).

o Dynamic effects of the martensitic transition in magnetocaloric Heusler
alloys by direct ΔT_{ad} measurements in different magnetic field rates
T. Gottschall, K. P. Skokov, F. Scheibel, M. Acet, <u>M. Ghorbani-Zavareh</u>,
Y. Skourski, J. Wosnitza, M. Farle, and O. Gutfleisch
submitted to Physical Review Applied.

Acknowledgment

This Dissertation would not have been possible without the goodwill and synchronized efforts of many people. It is a pleasure to thank everyone who has helped me reach this milestone of my life.

❖ First and foremost, I would like to express my gratitude to Prof. Dr. Joachim Wosnitza, my supervisor, for giving me the opportunity to work in his group, for his permanent interest in the progress of this work and supports of my research.

❖ I am deeply grateful to my scientific advisor, Dr. Yurii Skourski, who is always very patient and enthusiastic in training me experimental skills. His almost daily support and encouragement throughout my time as a Ph.D.-student has been invaluable and, at times, vital.

❖ I would like to thank Dr. Thomas Herrmannsdörfer, for his enormous support and friendship.

❖ Thank you Prof. Dr. Oliver Gutfleisch for agreeing to be a part of my Dissertation committee and for taking time out of your schedule to read my Dissertation.

❖ My collaborators in this research, Dr. Konstantin Skokov, Dr. Michael Nicklas and Dr. Catalina Salazar Mejia, deserve special mention for providing excellent quality samples that used in this Dissertation and for their willingness to discuss relevant scientific material whenever necessary. Thank you for your time and guidance.

❖ Dr. Elizabeth Lauren Green deserves a special thank you for being a great friend to me and has given me immense professional as well as emotional support.

Versicherung

Hiermit versichere ich, dass ich die vorliegende Arbeit mit dem Titel "Direct Measurements of the Magnetocaloric Effect in Pulsed Magnetic Fields" ohne unzulässige Hilfe Dritter und ohne Benutzung anderer als der angegebenen Hilfsmittel angefertigt habe. Die aus fremden Quellen direkt oder indirekt übernommenen Gedanken sind als solche kenntlich gemacht. Die Arbeit wurde bisher weder im Inland noch im Ausland in gleicher oder ähnlicher Form einer anderen Prüfungsbehörde vorgelegt.

Die vorliegende Dissertation wurde am Hochfeld-Magnetlabor im Helmholtz-Zentrum Dresden-Rossendorf unter der wissenschaftlichen Betreuung von Herrn Prof. Dr. Joachim Wosnitza angefertigt.

Ich erkenne die Promotionsordnung der Fakultät Mathematik und Naturwissenschaften der Technischen Universität Dresden an.

Mahdiyeh Ghorbani-Zavareh
Dresden, January 2016